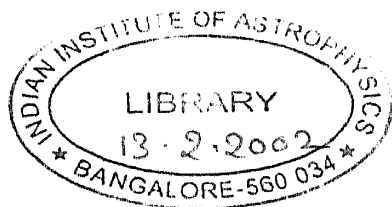


15393

ATMOSPHERES OF COOL STARS

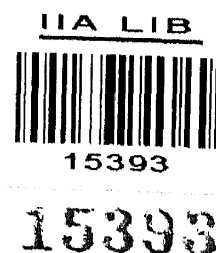


A Thesis
Submitted For The Degree Of
DOCTOR OF PHILOSOPHY
In The Faculty Of Science
BANGALORE UNIVERSITY

by
PRABHJOT SINGH


INDIAN INSTITUTE OF ASTROPHYSICS
BANGALORE 560 056
INDIA

DECEMBER 1995



DECLARATION

I hereby declare that the matter embodied in this thesis is the result of the investigations carried out by me in the Indian Institute of Astrophysics, Bangalore, India, under the supervision of Professor A. Peraiah. This work has not been submitted for the award of any degree, diploma, associateship, fellowship etc. of any university or institute.


PRABHJOT SINGH
(Candidate)



A. PERAIAH
(Supervisor)

Senior Professor,
Indian Institute of Astrophysics,
Bangalore 560 034.

Date: 27 Dec '95

To my parents, wife & daughter



Abstract

In this study I use partial frequency redistribution (PRD) functions to examine their effects on spectral line formation in spherically symmetric and expanding atmospheres of cool giant and supergiant stars. Primary aim of this investigation is to bring out the differences between the emergent spectral line profiles resulting from PRD and complete redistribution (CRD) under the influence of various physical parameters characterizing the atmospheres of cool giants and supergiants. The appreciation of this aspect will be important for quantitative analysis of stellar spectra and for computing model atmospheres of such stars.

In a scattering process, both the direction and the frequency of a photon may change. These changes are described by partial frequency redistribution functions. There are following four categories of redistribution functions: **Case I**, *zero line width*, denoted by R_I . It does not apply to any real line; demonstrates the effects of Doppler redistribution alone to an observer in the laboratory frame. **Case II**, *radiation damping in the upper state and coherence in the atom's rest frame*, denoted by R_{II} . It applies to resonance lines in low density media. **Case III**, *complete redistribution in the atom's frame*, denoted by R_{III} . **Case IV**, *subordinate line redistribution between two broadened states*, denoted by R_V . It applies to non-coherent subordinate line scattering. Complete redistribution is a limiting approximation which implies that there is a complete reshuffling of atoms in their excited state in such a way that there is no correlation between the frequencies of the incoming and the scattered photons.

The assumption of CRD has been widely used in earlier works on line transfer because it not only simplifies the numerical solution of the transfer equation but also provides a good approximation to reality in those media which are dense enough to support high collision rates. However, in the extended and tenuous atmospheres of cool giants and supergiants where low densities (and hence low collision rates) prevail, CRD is not expected to yield accurate emergent spectral line profiles. Moreover, in the wings of strong resonance lines, the scattering is nearly coherent. This leads to a deviation of the line profiles from those calculated in accordance with the assumption of CRD. Therefore, a natural recourse to the application of partial frequency redistribution can lead to more accurate line profiles.

Over the last two decades, considerable progress has been made in using partial frequency redistribution functions to study the spectral line formation in idealized stellar atmospheres. Most of these studies are limited to the assumption of plane-parallel geometry and/or the absence of velocity fields. These assumptions are unrealistic because the real atmospheres of cool giants and supergiants expand and are geometrically extended. There are only few papers in literature which have taken into account *both* the spherical geometry and the expansion effects to study PRD effects on emergent line profiles in idealized atmospheres. These studies employ either R_I or R_{II} . R_{III} has usually been represented by CRD. Some studies have been done to model the spectral lines formed in the expanding chromospheres of red giants using R_{II} . So far, the *combined effects* of sphericity and velocity fields on the differences between the solutions resulting from R_V and the CRD have not been explored. As an important feature of the present work I make a detailed comparative study of the PRD effects of R_{II} ,

R_{III} and R_V on the spectral line formation in the atmospheres of cool giants and supergiants taking into account both the sphericity and the expansion effects.

In order to achieve the above mentioned goals, I adopt a two-pronged approach. In the first approach, I consider parameterized stellar atmospheres to explore the influence of different physical parameters on the differences between the solutions due to PRD and CRD. These include the atmospheric extent, expansion velocity and the thermalization parameter (which gives the probability of collisional destruction of photons). The solutions considering idealized models serve as a preliminary step to solutions of actual stellar atmospheric problems by providing an insight into the basic physical phenomena.

In the second approach, I adopt computed model atmospheres (temperature and electron number density distributions) of red giants and supergiants. From these models, the line optical depth and the thermalization parameter is computed at each depth point in the atmosphere to study the frequency redistribution effects on some actually observed spectral lines from the stars of the same type. This is an important study as it brings out the model dependence of the differences between the partial frequency redistribution and complete redistribution solutions.

For all cases, I solve the equation of transfer in the frame work of discrete space theory of radiative transfer using Peraiah-Grant method.

In the first parametric study I examine the effects of angle-averaged R_V and R_{II} on emergent flux profiles in static spherically symmetric stellar envelopes. I write the equation of transfer for spherical symmetry in the rest frame for a two-level atom. Initially, to bring out the effects of geometrical extension alone, I neglect velocity fields. I assume a constant value of the thermalization parameter and set Planck's function equal to unity throughout the atmosphere. I neglect the background continuum. In this study I show that the effect of spherical extension is much more on the emergent flux profiles resulting from R_{II} than on those resulting from R_V when the damping parameters of the lower and upper levels of an atom are comparable. The effect of R_V (as compared to CRD) on emergent flux profiles increases by making the lower level sharper than the upper level. This effect is further enhanced by increasing the spherical extension.

In the second parametric study I go a step further to include the effects of expansion velocity in order to explore the *combined* effects of sphericity and expansion on the emergent flux profiles resulting from R_{II} and R_V , as compared to CRD. I consider an atmosphere having geometrical extension and small velocity of expansion which is characteristic of the atmospheres of cool giants and supergiants. I assume that there is no background continuum; set Planck's function equal to unity and choose a constant value of the thermalization parameter at all depths in the atmosphere. In this study I show that there are substantial differences between the emergent flux profiles resulting from PRD (R_{II} and R_V) and CRD.

In the third parametric study I investigate the PRD effects of R_{III} alone on the emergent line profiles in an expanding spherically symmetric stellar atmosphere. This is because, the limiting case of complete redistribution is usually taken to be an adequate representation of R_{III} in radiative transfer problems to study the spectral line formation in stellar atmospheres.

However, the combined effect of sphericity and macroscopic velocity cannot be estimated a priori. I consider only low velocity regime which is appropriate for the atmospheres of cool giants and supergiants. I treat this problem in the rest frame formalism. In this work I established that the differences between the emergent mean intensity profiles resulting from CRD and R_{III} are much smaller in expanding spherically symmetric stellar atmospheres than reported previously for plane-parallel atmospheres.

As a next important step in this investigation, I adopt computed model atmospheres of red giants and supergiants to explore the PRD effects (as compared to CRD) on some observed lines (e.g. Si II). I use the temperature structure and the electron & hydrogen number densities from the given models to compute the line optical depth and the thermalization parameter at each depth point in the atmosphere. Model values of the radii and the atmospheric extensions are used. I solve the line transfer equation using R_{II} and CRD to compute the emergent spectral line profiles. This study shows that the differences between the results due to PRD and CRD are highly model dependent. The results of non-chromospheric models show a departure of $\approx 10\%$; where as the results of chromospheric model of α -Orionis show enormous departures of PRD results from those of CRD.

Finally, I summarize the results of this study along with its achievements and limitations.

ACKNOWLEDGEMENT

I am indebted to Professor A. Peraiah for suggesting this problem and for allowing me to use his basic radiative transfer code. Stimulating discussions with him and freedom of experimentation which he allowed, made me an independent worker during the course of present investigation. His systematic style of working made me a disciplined researcher. I feel myself privileged to have been closely associated with him.

I express a deep sense of gratitude and profound appreciation to Drs. D. Mohan Rao and K.E. Rangarajan for spending a great deal of their time in many thought provoking discussions, continuous encouragement and help throughout the work. I have immense appreciation for the help extended by Mr. B. A. Varghese in setting right some of the intricate computational mazes.

I am grateful to Professor R. Cowsik, Director IIA, Dr. R. Srinivasan, Dean IIA and Professor J.C. Bhattacharya ex-Director IIA, for providing excellent research facilities. I thank our library staff, and in particular Ms. A. Vagiswari and Ms. Christina Louis, for providing efficient cross referencing from oceans of existing literature and prompt procurement of requested literature from other libraries and abroad. I am grateful to Mr. A.V. Ananth and Mr. J.S. Nathan for providing fast & modern computing facilities round-the-clock. I also thank Professor S.S. Hasan for getting me an account on CONVEX computer at CMMACS, NAL Bangalore, where part of this work was done.

I express my sincere thanks to Dr. Sunetra Giridhar, Professor. M. Parthasarathy, and Dr. P.K. Raju for supplementing the spectral line data used in this study. I profusely thank Professor Bhaskar Datta, not only for allowing me to use his PC486 which expedited the completion of this work, but also for his constant encouragement and good humour throughout this work. I am extremely thankful to Dr. S. Chatterjee for influencing me with his incorrigible optimism and enthusiasm in all circumstances. I also thank Mr. M.S. Rao for his help and encouragement.

I sincerely appreciate all my friends in particular Tejinder S. Birdie, Ripudaman Singh, N.D.N. Prasad & Anil Sharma who always provided cheer whenever I was in need of it.

Finally, I am at loss of words to acknowledge all the affection and care I received from my parents, and especially from my wife, Simran Kaur, who is the person behind my success.

Contents

1	Introduction	1
1.1	Motivation	1
1.2	Brief definitions of partial frequency redistribution functions	2
1.3	Objective	2
1.4	Review of the related work	2
1.5	Layout of the presentation	6
2	Solution of the line transfer equation using Discrete Space Theory	8
2.1	Introduction	8
2.2	Discrete Space Theory of Radiative Transfer	8
2.2.1	Interaction Principle	10
2.2.2	Star Products	12
2.2.3	Calculation of Radiation Field at Internal Points	15
2.3	Solution of the line transfer equation	18
3	Effects of angle-averaged R_V and R_{II} on emergent flux profiles in a static spherically symmetric stellar atmosphere	24
3.1	Introduction	24
3.2	Equations and computational procedure	25
3.2.1	Angle-averaged redistribution functions	26
3.2.2	Choice of depth points N	29
3.2.3	Optical depth laws	33
3.3	Results	36
3.4	Conclusions	47

4	Partial frequency redistribution effects of R_V and R_{II} in expanding spherically symmetric stellar atmospheres	48
4.1	Introduction	48
4.2	Equations and computational procedure	49
4.3	Results	55
4.4	Conclusion	55
5	Effects of angle-averaged R_{III} on spectral line formation in expanding spherically symmetric stellar atmospheres	56
5.1	Introduction	56
5.2	Basic equations and computational procedure	57
5.3	Results	60
5.4	Conclusion	64
6	Partial frequency redistribution effects on observed resonance lines using model atmospheres of cool stars	65
6.1	Introduction	65
6.2	Adopted model atmospheres	66
6.3	Calculation of thermalization parameter ϵ	70
6.4	Calculation of line center optical depth τ_0	73
6.5	The equation of line transfer	74
6.6	Results	79
6.7	Conclusion	84
7	Concluding Remarks	85
7.1	In retrospect	85
7.2	In prospect	88

List of Figures

2.1	Schematic diagram showing a spherical shell with incident and emergent intensities; E^- or E^+ denotes contribution from internal sources.	11
2.2	Description of the diffuse radiation field in a spherically symmetric atmosphere.	16
3.1	Plot of the emission probability ($R_{II}(x', x)/\phi(x')$) at frequency x per absorption, when the absorption is at frequency x' . Damping parameter $a = 2.0 \times 10^{-3}$. D.Mihalas, Stellar Atmospheres, Chapter 13, p429.	28
3.2	Plot of the emission probability ($R_V(x', x)/\phi(x')$) at frequency x per absorption, when the absorption is at frequency x' . Damping parameter $a = 2.0 \times 10^{-3}$. See P.Heinzel, 1981, JQSRT, 25, 483.	30
3.3	Sensitivity of emergent flux profiles to the number of depth points N using exponential opacity distribution.	31
3.4	Sensitivity of emergent flux profiles to the number of depth points N using r^{-2} opacity distribution.	32
3.5	Optical depth variation versus depth points in a spherically symmetric atmosphere having $R = 50$. $n = 75$ denotes the innermost boundary and $n = 1$ denotes the boundary of the outermost layer of the atmosphere.	35
3.6	Emergent line source functions for the parameters shown in the figure.	37
3.7	Emergent flux profiles corresponding to the source functions of fig.3.6.	38
3.8	Same as fig. 4a but for $a_j/a_i = 10$	40
3.9	Emergent flux profiles corresponding to the line source functions of fig.3.8.	41
3.10	Same as fig.3.6 but for r^{-2} opacity distribution.	42
3.11	Emergent flux profiles corresponding to the line source functions of fig.3.10.	43
3.12	Same as fig.3.10 but for $a_j/a_i = 10$, $a = 1.1 \times 10^{-3}$	44
3.13	Emergent flux profiles corresponding to the line source functions of fig.3.12.	45
4.1	Emergent flux from an expanding atmosphere having the velocity of expansion $V = 1$ in units of thermal velocity; $R = 1$ denotes plane-parallel case and $R = 30$ denotes the extended atmosphere having an extension 30 times the stellar radius (set equal to 1).	51

4.2	The effect of expansion velocity $V = 1$ in comparison to static case $V = 0$ for an extended atmosphere $R = 30$	52
4.3	The effect of increasing the atmospheric extension from $R = 30$ to $R = 100$ for an atmosphere with constant velocity of expansion $V = 1$	53
5.1	Source function S versus optical depth τ through spherically symmetric and differentially expanding envelope having $b/a = 5, 50$; $V_b = 0, 1$; and $T = 10^3$. Corresponding CRD results are shown by dotted (....) lines.	59
5.2	Emergent mean intensities J_x in the line versus x , corresponding to source functions of figure 1. $x = (\nu - \nu_0)/w$; w being standard Doppler width.	60
5.3	Emergent line flux F_x versus x at $V_b = 1$; $\epsilon = \beta = 10^{-6}$; $b/a = 1$ (plane-parallel atmosphere), 5, 50 and $T = 10^3$	61
5.4	Emergent mean intensity profiles J_x versus x for a spherically symmetric envelope having extension $b/a = 50$; expansion velocity $V_b = 0$ (static case) and 1; and $\epsilon = \beta = 10^{-2}$	62
5.5	$\text{Log}(F_x)$ versus x for $b/a = 10$, at $V_b = 0, 1, 2$ for different values of $\epsilon = \beta = 0, 10^{-6}, 10^{-2}$. . .	63
6.1	Model1: Variation of the gas pressure P_g , the electron pressure P_e and the temperature T inside the adopted model atmosphere (Plez (1992)).	67
6.2	Model2: Variation of the gas pressure P_g , the electron pressure P_e and the temperature T inside the adopted model atmosphere (Plez (1992)).	68
6.3	Model3: Chromospheric model of α -Orionis (Hartmann & Avrett (1984)).	69
6.4	Variation of thermalization parameter ϵ versus depth point counter n for Ba II λ 4554, plotted for model1 ($T_{eff} = 3000$ K) and for model2 ($T_{eff} = 4000$ K).	71
6.5	Variation of thermalization parameter ϵ versus the atmospheric extent z for C II λ 1335 and Si II λ 1818, plotted for model3 (α -Orionis).	72
6.6	Variation of line center optical depth of Ba II λ 4554 versus the depth point counter n in the atmospheres of model1 ($T_{eff} = 3000$ K) and model2 ($T_{eff} = 4000$ K).	75
6.7	Variation of line center optical depths of C II λ 1335 & Si II λ 1818 versus the atmospheric extension z in the chromospheric atmosphere of α -Orionis (model3).	76
6.8	Emergent flux profiles of Ba II λ 4554 for model1.	80
6.9	Emergent flux profiles of Ba II λ 4554 for model2.	81
6.10	Emergent flux profile of Si II λ 1818 from the chromospheric atmosphere of α -Orionis, model3, due to PRD and CRD.	82
6.11	Emergent flux profile of C II λ 1335 from the chromospheric atmosphere of α -Orionis, model3, due to PRD and CRD.	83

List of Tables

3.1	Flux ratios showing the departures between the emergent fluxes due to PRD and CRD at $x = 4$, for different values of atmospheric extension R . $R = 1$ represents plane-parallel approximation, whereas $R > 1$ represents an extended and spherically symmetric atmosphere. These results are for $a_j/a_i = 1, 10$	46
3.2	Same as above but for $x = 6$	46
3.3	Same as above but for $x = 8$	47

Chapter 1

Introduction

The title **Atmospheres of Cool Stars** is very broad. No single study can cover all its aspects. This investigation focuses on one of the most important aspects of the subject : **effects of partial frequency redistribution functions on the spectral line formation**. Spectral lines carry a wealth of information concerning the medium in which they form. The line spectrum can be used to obtain accurate empirical models of stellar atmospheres, complete with such quantities as temperature, gas pressure, chemical composition, gravitational acceleration, velocity fields. With the advent of observations from balloons, rockets and satellites, great improvements have been made in the quantity and quality of stellar spectroscopic data. The availability of highly accurate line profiles has enhanced the importance of *partial frequency redistribution* in the process of spectral line formation.

1.1 Motivation

In the process of scattering in spectral line formation, an atom is excited from one bound level to another by absorbing a photon, and then decays back radiatively to the original state, with the emission of a photon. Very often, in the works on line transfer, it is assumed that the photons are *completely redistributed* over the line profile. This assumption has been widely used because, it not only simplifies the numerical solution of the transfer equation but also provides a good approximation to reality in those media which are dense enough to support high collision rates. **However, in the extended and tenuous atmospheres of cool giant and supergiant stars where low densities (and hence low collision rates) prevail, CRD is not expected to yield accurate emergent spectral line profiles.** Thus, it is necessary to consider the redistribution of photons by employing *partial frequency redistribution* functions, which describe the scattering process precisely. Moreover, in the wings of strong resonance lines, the scattering is nearly coherent. This leads to a deviation of the line profiles from those

calculated in accordance with the assumption of CRD. Therefore, a natural recourse to the application of partial frequency redistribution (PRD) can lead to more accurate line profiles.

1.2 Brief definitions of partial frequency redistribution functions

In a scattering process, both the direction and the frequency of a photon may change. These changes are described by partial frequency redistribution functions. There are following four categories of redistribution functions: **Case I**, *zero line width*, denoted by R_I . It does not apply to any real line; demonstrates the effects of Doppler redistribution alone to an observer in the laboratory frame. **Case II**, *radiation damping in the upper state and coherence in the atom's rest frame*, denoted by R_{II} . It applies to resonance lines in low density media. **Case III**, *complete redistribution in the atom's frame*, denoted by R_{III} . **Case IV**, *subordinate line redistribution between two broadened states*, denoted by R_V . It applies to non-coherent subordinate line scattering. Complete redistribution is a limiting approximation which implies that there is a complete reshuffling of atoms in their excited state in such a way that there is no correlation between the frequencies of the incoming and the scattered photons.

1.3 Objective

This study investigates the effects of partial frequency redistribution (PRD) functions R_{II} , R_{III} and R_V on spectral line formation in spherically symmetric and expanding atmospheres of cool giant and supergiant stars. Primary objective of this investigation is to bring out the differences between the emergent spectral line profiles resulting from PRD and complete redistribution (CRD) under the influence of various physical parameters characterizing the atmospheres of cool giants and supergiants. As an important feature of this work a detailed comparative study is made of the PRD effects of R_{II} , R_{III} and R_V on the spectral line formation in the atmospheres of cool giants and supergiants taking into account both the sphericity and the expansion effects. The appreciation of this aspect will be important for quantitative analysis of stellar spectra and for computing model atmospheres of such stars.

1.4 Review of the related work

Five decades have passed since Heney [27] discussed about the frequency redistribution of radiation including both the natural broadening and the Doppler motions of the radiating atom. Other early discussions on this subject are found in the works of Holstein [28], Unno

[69], Sobolev [67] and Warwick [76]. It was Hummer [31] who derived the redistribution functions for two level atomic model. He defined the term redistribution function $R(\nu', \vec{n}'; \nu, \vec{n})$ as the probability that a photon having initial frequency ν' and direction \vec{n}' will be absorbed, leading to the re-emission in the line of a (ν, \vec{n}) photon. He then defined the following four redistribution functions :

1. For the cases of zero line width in the atom's frame; denoted by R_I .
2. For radiative damping of the upper level only; denoted by R_{II} .
3. For radiative *and* collisional damping of the upper level only; denoted by R_{III} .
4. For radiative damping of both levels; denoted by R_{IV} .

Hummer derived angle-independent redistribution functions for the cases of isotropic and dipole phase functions. He also discussed the symmetry properties of redistribution functions. In subsequent radiative transfer calculations, isotropic angle-independent redistribution functions have found maximum use. At this point it is worth mentioning that, Heinzel [23] pointed out that Hummer's [31] R_{IV} function is erroneous because it is derived from an incorrect expression for scattering in the atomic frame. In the same paper Heinzel [23] derived a new redistribution function R_V for resonance scattering of subordinate lines assuming that both levels are radiatively broadened. Later, Heinzel and Hubený [24] generalized this redistribution function to include collisional broadening of both the upper and lower levels of the atom. Jefferies and White [33] examined the validity of the CRD approximation and found that in the line core the photons are completely redistributed whereas in the wings scattering is nearly coherent. On this basis they proposed an approximation known as *partially coherent scattering*. Kneer [35] pointed out that this approximation is neither normalized nor symmetric, and he proposed a modified form of the *partially coherent scattering* redistribution function. Subsequently, Basri [9] found that *partially coherent scattering* cannot account for Doppler diffusion in the line wings, which can be important for low density atmospheres. Therefore, he argued that it is required to use exact forms of redistribution functions in order to achieve accurate radiative transfer solutions. Ayres [5] proposed a revised form of *partially coherent scattering* which includes the role of Doppler diffusion. Jefferies and White also called attention to the lowering of the line profile in the inner wing which occurs as the scattering in the wing is taken to be nearly coherent. They noted that this lowering can be caused in isothermal atmospheres by taking scattering to be coherent in the line wing, or in a chromosphere if the whole line is formed in CRD. Therefore, a *proper understanding and treatment of spectral line formation in the line wings is essential for determining the temperature structure in a stellar atmosphere*.

Hummer [32] presented the first detailed solutions of the radiative transfer equation including PRD to go beyond the schematic partially coherent scattering approximation of Jefferies and White [33]. He used planar geometry, constant properties of the medium, two-level atomic model and angle-averaged R_I and R_{II} for isotropic phase function. He showed that the emergent intensity due to R_{II} in the line wings can be substantially lower than the CRD solutions. Vardavas [71, 72, 73] studied the effects of angle-averaged and angle-dependent R_I , R_{II} and

R_{II} on spectral line formation in planar geometry for static and moving media. Peraiah [51] described the numerical solution of the transfer equation in spherical geometry based on the *discrete-space theory* of radiative transfer. He presented a computer code and the solutions of transfer equation in the rest frame using PRD functions R_I and R_{II} . Peraiah [52] used R_{II} to investigate its effects on spectral line formation in spherically symmetric and expanding stellar atmospheres. Rangarajan et al. [60] studied the effects of stimulated emission on radiative transfer with PRD functions R_{II} and R_{III} in plane-parallel geometry. The combined effect of R_{II} and non-coherent electron scattering on polarized resonance line transfer in plane-parallel geometry was examined by Nagendra et al. [46]. Mohan Rao et al. [44] employed Domke-Hubeny redistribution matrix and used a combination of R_{II} and R_{III} to study the polarized line transfer with collisional redistribution in a plane-parallel atmosphere. Nagendra [47] also used Domke-Hubeny redistribution matrix to study PRD effects on resonance line polarization in spherical atmospheres. Collisional redistribution effects on line polarization in spherical atmospheres were investigated by Nagendra [48]. Mohan Rao et al. [45] explored the effects of R_{II} , R_{III} and R_V on source functions (S_L) for plane-parallel and isothermal stellar atmospheres and showed, that, for a purely scattering medium with frequency independent incident radiation, the frequency dependent source function $S_L(R_V)$ lies below $S_L(R_{III})$ but above $S_L(R_{II})$ in the line wings. Singh [65] examined the combined effect of sphericity and expansion velocity on the differences between the emergent mean intensity profiles resulting from R_{III} and CRD.

Vernazza [74] showed that the flux and shape of the solar $L\alpha$ line could be matched by a parameterized PRD calculation in which the core is computed with CRD assumption and the scattering in the wings was taken to be 93% coherent and 7% CRD. Omont, Smith and Cooper [49] made quantum mechanical calculations to derive the redistribution function for resonance lines. These results led Milkey and Mihalas [40] to propose a PRD computational scheme in which they solved the coupled equations of radiative transfer and statistical equilibrium using the Vernazza, Avrett, and Loeser (VAL) [75] solar model. They arrived at three important results: 1) A fully self-consistent PRD calculation using depth-dependent coherence fractions computed from the broadening rates is feasible; 2) The computed line wings lie between the CRD and pure coherent scattering limits and are similar to the 93% coherency calculations of Vernazza [74]; and 3) A proper inclusion of PRD effects in the wings of $L\alpha$ is needed to compute electron density properly. In a subsequent paper Milkey and Mihalas [41] were able to match the shape of the observed $L\alpha$ profile by including a depth-dependent line profile function. Roussel-Dupré [62] pointed out a major problems in the method of Milkey and Mihalas [40, 41]: the Omont et al. [49] redistribution function used by them is not valid for the $L\alpha$ wings. Next, Milkey and Mihalas [42] applied their PRD method to the resonance line of MgII treating each transition as a two-level atom. They showed that the line source function behaves like pure coherent scattering case, while in the line core it is independent of frequency and slightly above the CRD case. Milkey, Ayres, and Shine [39] examined the effect of gravity on the shapes of MgII lines. They found that $\tau_{MgII}(\tau_{5000})$ increases systematically with decreasing gravity. Ayres, Linsky and Shine [6] and Ayres [4] used this result in trying to explain the Wilson-Bappu effect.

Shine, Milkey and Mihalas [64] applied cross-redistribution formulation to a five-level, five-transition CaII ion. They assumed HSRA model and several microturbulent velocity distributions. Their results provided strong evidence that the PRD approach includes much of the essential physics of the scattering processes, and in principle, PRD effects can account for many discrepancies between the line profiles calculated assuming CRD and the observations. Shine, Milkey and Mihalas [64] also considered the gravity dependence of the CaII lines with results in qualitative agreement with the results of Milkey, Ayres, and Shine [39]. Milkey, Shine and Mihalas [43] then included the full angle and frequency dependence of redistribution during the scattering processes in an observer's frame formulation. They found that angle-dependent effects are negligible for the CaII line in a homogeneous solar chromospheric model, but these effects could be important for an inhomogeneous medium like the real solar chromosphere.

Parallel with solar modeling, the development of chromospheric models for *late-type* stars based on the matching of observed and computed PRD profiles has taken place. Ayres and Linsky [7] constructed first such model to match CaII K line of α Boo (Arcturus, K2 III). They could obtain a good agreement to the shape of the inner wing and flux of the profile. In subsequent papers various authors who extended this work to derive atmospheric models for *giant and supergiant cool stars* are: Kelch et al [34] fitted K line of CaII and h & k lines of MgII using plane-parallel geometry, static medium for α Aur (G5 III), β Gem (K0 III) and α Tau (K5 III); Baliunas et al [8] using plane-parallel geometry, static medium fitted the same line as Kelch et al. [34] for λ And (G8 III-IV) and α Aur (G5 III); Eriksson et al. [15] used plane-parallel geometry, static medium and fitted MgII K line for β Cet (G9.5 III) star; Basri et al. [10] fitted CaII K, MgII K lines using plane-parallel static medium for β Dra (G2 II-Ib), ϵ Gem (G8 Ib) and α Ori (M2 Iab) stars; Basri et al. [10] fitted the same lines using plane-parallel geometry and circulation pattern for β Dra (G2 II-Ib); Avrett and Johnson [3] used plane-parallel geometry, static medium to fit MgII K line for N-type Carbon stars; Drake [14] used spherical geometry with winds to fit MgII K line for α Boo (K2 III) star. In this list, except Basri [9], all other papers have neglected velocity fields and atmospheric extension.

As appears evident from the review presented above, considerable progress has been made in using partial frequency redistribution functions to study the spectral line formation in idealized stellar atmospheres. But, most of these studies are limited to the assumption of plane-parallel geometry and/or the absence of velocity fields. These assumptions are unrealistic because the real atmospheres of cool giants and supergiants expand and are geometrically extended. Moreover, these studies employ either R_I or R_{II} . R_{III} has usually been represented by CRD. So far, the combined effects of sphericity and velocity fields on the differences between the solutions resulting from R_{II}, R_V and the CRD have not been explored in a comparative way. It is this gap which this study tries to fill up.

1.5 Layout of the presentation

In order to achieve the above mentioned goals, we adopt a two-pronged approach. In the **first approach**, we consider parameterized stellar atmospheres to explore the influence of different physical parameters on the differences between the solutions due to PRD and CRD. These include the atmospheric extent, expansion velocity and the thermalization parameter (which gives the probability of collisional destruction of photons) . The solutions considering idealized models serve as a preliminary step to solutions of actual stellar atmospheric problems by providing an insight into the basic physical phenomena.

In the **second approach**, we adopt computed model atmospheres (temperature and electron number density distributions) of red giants and supergiants. From these models, the line optical depth and the thermalization parameter is computed at each depth point in the atmosphere to study the frequency redistribution effects on some actually observed spectral lines from the stars of the same type. This is an important study as it brings out the model dependence of the differences between the partial frequency redistribution and complete redistribution solutions.

The work is presented in seven chapters.

- In **chapter one**, the need to study the partial frequency redistribution effects on the spectral line formation in the *atmospheres of cool stars* is discussed. Against this background, relevant literature on the use of various partial frequency redistribution functions to study the spectral line formation in stellar atmospheres is reviewed. The chapter is concluded with the layout of the presentation.
- In **chapter two**, the solution of equation of radiative transfer in the frame-work of the discrete space theory of radiative transfer using Peraiah-Grant formalism is described.
- In **chapter three**, the effects of angle-averaged R_V and R_{II} on emergent flux profiles in static spherically symmetric stellar envelopes is examined. The equation of transfer for spherical symmetry in the rest frame is solved for a two-level atom. Initially, to bring out the effects of geometrical extension alone, velocity fields are neglected. A constant value of the thermalization parameter is assumed and the Planck's function is set equal to unity throughout the atmosphere. The background continuum is neglected. This study establishes that sphericity enhances PRD effects. It is also shown that the effect of spherical extension is much more on the emergent flux profiles resulting from R_{II} than on those resulting from R_V when the damping parameters of the lower and upper levels of an atom are comparable. The effect of R_V (as compared to CRD) on emergent flux profiles increases by making the lower level sharper than the upper level. This effect is further enhanced by increasing the spherical extension.
- In **chapter four**, a step further is taken to include the effects of expansion velocity in order to explore the *combined* effects of sphericity and expansion on the emergent flux profiles resulting from R_{II} and R_V , as compared to CRD. An atmosphere having geometrical extension and small velocity of expansion is considered which is characteristic of the

atmospheres of cool giants and supergiants. It is assumed that there is no background continuum; Planck's function is set equal to unity and a constant value of the thermalization parameter is chosen at all depths in the atmosphere. This study shows that there are substantial differences between the emergent flux profiles resulting from PRD (R_{II} and R_V) and CRD.

- In chapter five, the PRD effects of R_{III} alone on the emergent line profiles in an expanding spherically symmetric stellar atmosphere are explored. This is because, the limiting case of complete redistribution is usually taken to be an adequate representation of R_{III} in radiative transfer problems to study the spectral line formation in stellar atmospheres. However, the combined effect of sphericity and macroscopic velocity cannot be estimated a priori. Only low velocity regime is considered which is appropriate for the *atmospheres of cool giants and supergiants*. This problem is treated in the rest frame formalism. In this work it is established that the differences between the emergent mean intensity profiles resulting from CRD and R_{III} are much smaller in expanding spherically symmetric stellar atmospheres than reported previously for plane-parallel atmospheres.
- In chapter six, as a next important step in this investigation, computed model atmospheres of red giants and supergiants are adopted to explore the PRD effects (as compared to CRD) on some observed lines (e.g. Si II). The temperature structure and the electron number density from the given models is used to compute the line optical depth and the thermalization parameter at each depth point in the atmosphere. Realistic values of the radii and the atmospheric extensions of cool giants are used. The line transfer equation is solved using R_{II} and CRD to compute the emergent spectral line profiles. This study aims at examining the model dependence of the differences between the results of PRD and CRD.
- Finally, in chapter seven the highlights of the present work are summarized and possible directions for further study using partial frequency redistribution functions are indicated.

Chapter 2

Solution of the line transfer equation using Discrete Space Theory

2.1 Introduction

The equation of radiative transfer, which describes the transport of radiation through a medium, is one of the essential equations in the stellar atmospheric research. This equation incorporates the physical properties of the medium and its solution provides insight into the behavior of the internal and emergent radiation field. It is an integro-differential equation and this feature increases the complexity of obtaining the solution depending upon the physics of the problem. It is not possible to solve this equation analytically for numerous astrophysical problems and so there exist several numerical methods to obtain the solution of the transfer equation. Amongst the notable methods, and the one used in this investigation is based on the Discrete Space Theory of Radiative Transfer. This method has two-fold advantages:

1. The solution obtained can be subjected to rigorous numerical analysis to enable one to predict in advance the most economic finite difference mesh for a problem.
2. The abstract mathematical structure is capable of generalization to other geometries.

This chapter describes the basics of the Discrete Space Theory and the solution of line transfer equation based on this theory.

2.2 Discrete Space Theory of Radiative Transfer

The earliest reference to the Principle of Invariance, which is a special case of the Interaction Principle, is found in a paper by Stokes [68] in which he obtained difference equations for reflection by a pile of identical glass plates. However, it was Ambartzumian [2] who introduced

the Principle of Invariance into the radiative transfer theory. Chandrasekhar [13] extensively used these principles to calculate the reflection and transmission functions. The classical statement of the Principle of Invariance can be stated as: *The law of diffuse reflection of an infinitely homogeneous plane-parallel scattering medium is invariant with respect to the addition or subtraction of layers of arbitrary finite optical thickness to or from the medium.* The Principle of Invariance is a consequence of the Interaction Principle and is essentially a statement of energy conservation in any medium. Redheffer [61] and Preisendorfer [59] wrote the Interaction Principle *without the internal source terms*. Grant and Hunt [19, 20] *included the internal source terms* and developed a numerical method to solve the transfer equation in inhomogeneous plane-parallel media. Grant and Peraiah [21] developed the solution of radiative transfer in spherical systems in the frame work of the Discrete Space Theory. This method has been applied to several case of extended and expanding stellar envelopes.

Peraiah and Grant [57] presented a numerical method to obtain diffuse radiation in the extended atmospheres of supergiant stars. This method is an extension of the discrete space theory of Grant and Hunt [19, 20] and has been widely used to study the spectral line formation in moving and extended atmospheres of supergiant stars. It has the following distinct merits:

- It is a highly accurate method for computing the internal as well as emergent radiation in the presence or absence of the internal radiation sources.
- It offers great flexibility to include a large number of physical processes that occur in stellar atmospheres.
- It is numerically stable and gives physically meaningful solutions.

In general the following steps are taken to obtain the solution

1. The medium is divided into a number of *cells* whose thickness is less than or equal to the critical thickness (τ_{crit}). The critical thickness is determined on the basis of the physical characteristics of the medium. τ_{crit} ensures stability and uniqueness of the solution.
2. The integration of the transfer equation is performed on the *cell* which is a two-dimensional grid bounded by $[r_n, r_{n+1}] \times [\mu_{j-1/2}, \mu_{j+1/2}]$, where

$$\mu_{j+1/2} = \sum_{k=1}^j c_k, \quad j = 1, 2, \dots, J$$

where c_k are the weights of Gauss Legendre quadrature formula.

3. These discrete equations are compared with the canonical equations of the interaction principle and to obtain the transmission and reflection operators of the *cell*.
4. Lastly, all the cells are combined by star algorithm and obtain the radiation field.

The medium can be divided into shells whose thicknesses are larger than τ_{crit} but integration is done only on *cell* and star algorithm is used to obtain the transmission and reflection operators of the shells by *adding* the cells (star product).

Further, a closer look at the *Interaction Principle*, the *Star Product* and the *Calculation of radiation field at internal points* is presented, following Peraiah [56].

2.2.1 Interaction Principle

The interaction principle relates the incident and emergent radiation field from a medium of given optical thickness. It permits us to set up exact difference equations for both reflection and transmission coefficients for radiation field. These coefficients are exact and can be used in the calculation of radiation field in the finite layers.

Figure 2.1 shows a shell of optical thickness, with incident and emergent intensities. It is assumed that specific intensities U_n^+ and U_{n+1}^- are incident at the boundaries n and $n+1$ respectively of the shell with optical thickness τ . The symbols with signs $+$ and $-$ represent specific intensities of the rays travelling in opposite directions. If μ represents the cosine of the angle made by a ray relative to the common normal (in the spherical case, μ is the angle made by the ray direction with the radius vector) to the stratification in the direction in which n increases. That is,

$$U_n^+ \{ U_n(\mu) : 0 < \mu \leq 1 \quad (2.1)$$

and

$$U_n^- \{ U_n(-\mu) : 0 < \mu \leq 1 \quad (2.2)$$

U_n^+ represents the specific intensity of the ray travelling in the direction μ and U_n^- represents the specific intensity of the ray travelling in the opposite direction. A finite set of values of $\mu(\mu_j : 1 \leq j \leq m; 0 < \mu_1 < \mu_2 < \mu_3 \dots \mu_m < 1)$ is selected

or

$$U_n^+ = \begin{pmatrix} U_n(\mu_1) \\ U_n(\mu_2) \\ \vdots \\ U_n(\mu_m) \end{pmatrix} \quad (2.3)$$

and

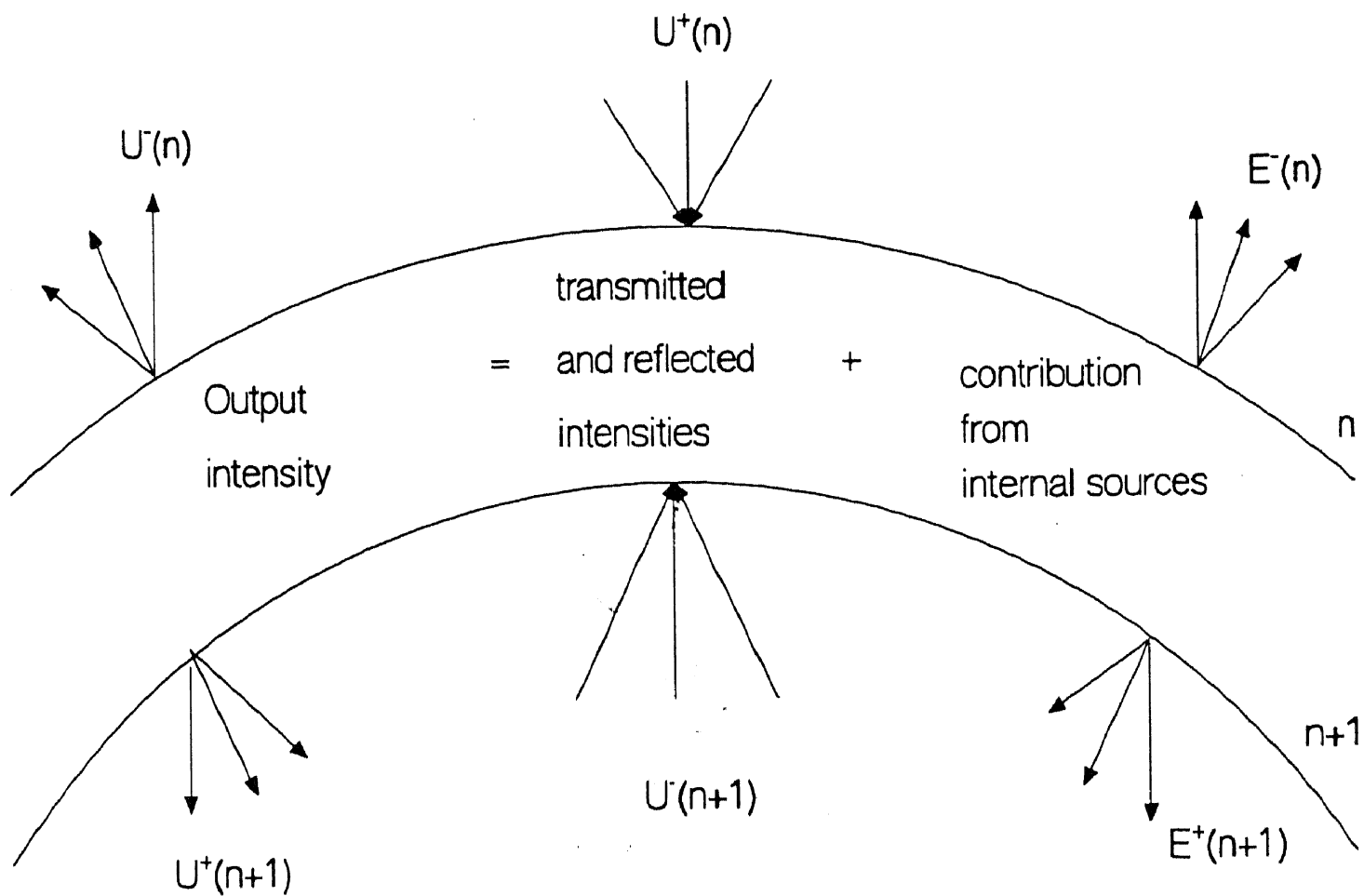


Figure 2.1: Schematic diagram showing a spherical shell with incident and emergent intensities; E^- or E^+ denotes contribution from internal sources.

$$U_n^+ = \begin{pmatrix} U_n(-\mu_1) \\ U_n(-\mu_2) \\ \vdots \\ U_n(-\mu_m) \end{pmatrix} \quad (2.4)$$

are m - dimensional vectors on Euclidean space.

- The incident intensity vectors are U_n^+ and U_{n+1}^- .
- The emergent intensity vectors are U_n^- and U_{n+1}^+ .

The emergent radiation field will have the contributions from the internal sources say, $\Sigma^+(n+1, n)$ and $\Sigma^-(n, n+1)$ corresponding to the output intensity vectors U_{n+1}^+ and U_n^- respectively.

Certain linear operators are assumed which reflect and transmit the incident radiation namely, $t(n+1, n)$, $r(n, n+1)$ and $r(n+1, n)$. These operators are calculated based on the physics of the medium. Then the output intensities are written in terms of the transmitted and reflected input intensities together with the internal sources as

$$U_{n+1}^+ = t(n+1, n)U_n^+ + r(n, n+1)U_{n+1}^- + \Sigma^+(n+1, n) \quad (2.5)$$

$$U_n^- = r(n+1, n)U_n^+ + t(n, n+1)U_{n+1}^- + \Sigma^-(n, n+1) \quad (2.6)$$

The introduction of the internal source terms namely, $\Sigma^+(n+1, n)$ and $\Sigma^-(n, n+1)$ is due to Grant and Hunt [19]. The relationship given by equations 2.5 and 2.6 is called the **Interaction Principle**. This can also be written concisely as

$$\begin{pmatrix} U_{n+1}^+ \\ U_{n+1}^- \end{pmatrix} = S(n, n+1) \begin{pmatrix} U_n^+ \\ U_{n+1}^- \end{pmatrix} + \Sigma(n, n+1) \quad (2.7)$$

where

$$S(n, n+1) = \begin{pmatrix} t(n+1, n) & r(n, n+1) \\ r(n+1, n) & t(n, n+1) \end{pmatrix} \quad (2.8)$$

2.2.2 Star Products

If there is another shell with boundaries $(n+1, n+2)$ adjacent to $(n, n+1)$, interaction principle for this shell can be written as

$$\begin{pmatrix} U_{n+2}^+ \\ U_{n+1}^- \end{pmatrix} = S(n+1, n+2) \begin{pmatrix} U_{n+1}^+ \\ U_{n+2}^- \end{pmatrix} + \Sigma(n+1, n+2) \quad (2.9)$$

where $S(n+1, n+2)$ is similarly defined as in equation 2.8. If one combines the two shells $(n, n+1)$ and $(n+1, n+2)$ then the interaction principle for the combined shell is written as, (for the thickness is arbitrarily defined)

$$\begin{pmatrix} U_{n+2}^+ \\ U_n^- \end{pmatrix} = S(n, n+2) \begin{pmatrix} U_n^+ \\ U_{n+2}^- \end{pmatrix} + \Sigma(n+1, n+2) \quad (2.10)$$

Redheffer [61] calls $S(n, n+2)$ the star product of the two S-matrices $S(n, n+1)$ and $S(n+1, n+2)$; and $S(n, n+2)$ written as

$$S(n, n+2) = S(n, n+1) \star S(n+1, n+2) \quad (2.11)$$

Equation 2.11 is obtained by elimination U_{n+1}^+ and U_{n+1}^- from equations 2.9 and 2.10. The r and t operators for the composite cell are written as

$$t(n+2, n) = t(n+2, n+1)[I - r(n+2, n+1)r(n, n+1)]^{-1}t(n+1, n) \quad (2.12)$$

$$t(n, n+2) = t(n, n+1)[I - r(n, n+1)r(n+2, n+1)]^{-1}t(n+1, n+2) \quad (2.13)$$

$$r(n+2, n) = r(n+1, n) + t(n, n+1)[I - r(n+2, n+1)r(n, n+1)]^{-1}r(n+2, n+1) \quad (2.14)$$

$$r(n, n+2) = r(n+1, n+2) + t(n+2, n+1)[I - r(n, n+1)r(n+2, n+1)]^{-1}r(n, n+1) \quad (2.15)$$

and

$$\Sigma(n, n+2) = \Lambda(n, n+1; n+2)\Sigma(n, n+1) + \Lambda'(n; n+1, n+2)\Sigma(n+1, n+2) \quad (2.16)$$

where I the identity matrix and

$$\Lambda(n, n+1; n+2) = \begin{pmatrix} t(n+2, n+1)[I - r(n, n+1)r(n+2, n+1)]^{-1} & 0 \\ t(n, n+1)r(n+2, n+1)[I - r(n, n+1)r(n+2, n+1)]^{-1} & I \end{pmatrix} \quad (2.17)$$

$$\Lambda'(n; n+1, n+2) = \begin{pmatrix} I & t(n+2, n+1)r(n, n+1)[I - r(n+2, n+1)r(n, n+1)]^{-1} \\ 0 & t(n, n+1)[I - r(n+2, n+1)r(n, n+1)]^{-1} \end{pmatrix} \quad (2.18)$$

and

$$\Sigma(n, n+1) = \begin{pmatrix} \Sigma^+(n+1, n+2) \\ \Sigma^-(n, n+1) \end{pmatrix} \quad (2.19)$$

Similarly, $\Sigma(n+1, n+2)$ is defined.

To obtain physical interpretation of 2.12 the operator inverse is expanded in a power series. For example,

$$t(n+2, n) = \sum_{k=0}^{\infty} t_k(n+2, n) \quad (2.20)$$

$$t_k(n+2, n) = t(n+2, n+1)[r(n, n+1) \times \quad (2.21)$$

$$r(n+2, n+1)]^k t(n+1, n) \quad (2.22)$$

This operator acts on intensities to the right and gives the contribution to U_{n+2}^+ from U_n^+ . The k^{th} term, $t_k(n+2, n)$ may be recognized as diffuse transmission from n to $n+1$, diffuse reflection from the layer $(n, n+1)$, k times in succession and finally diffuse transmission through $(n+1, n+2)$. Thus $t(n+2, n)$ is the sum of contributions involving scattering of all orders $k = 0, 1, 2, \dots \infty$. A similar interpretation can be given for other operators.

If $S(\alpha)$ is written to designate the cell, then

$$S(\alpha \star \beta) = S(\alpha) \star S(\beta) \quad (2.23)$$

where $\alpha \star \beta$ denotes the region obtained by putting the two cells α and β together. If the cells are homogeneous and plane parallel then

$$\alpha \star \beta = \beta \star \alpha \quad (2.24)$$

In general, the star multiplication is non-commutative. However, star multiplication is associative. For adding several layers $\alpha, \beta, \gamma \dots$

$$S[(\alpha \star (\beta \star \gamma) \star \dots)] = S[(\alpha \star \beta) \star \gamma \star \dots] \quad (2.25)$$

If the medium is homogeneous and very thick then one can use what is known as *doubling method* (see van de Hulst [30]). For example,

$$S(2^P d) = S(2^{P-1} d) \star S(2^{P-1} d), (P = 1, 2, 3, \dots) \quad (2.26)$$

which means that we can generate the S-matrix for a layer of thickness $2^P d$ in P cycles starting with $S(d)$ rather than in 2^P cycles of adding the $S(d)$'s one by one. If $P = 10$, then only a fraction $10/2^{10} \simeq 10^{-2}$ of the computational work is needed to add 2^{10} layers of thickness d .

2.2.3 Calculation of Radiation Field at Internal Points

One expects the reflection and transmission operators to be non-negative on the physical grounds that intensities are always non-negative. This condition will be satisfied only when the optical thickness of the shell is less than certain value called the *critical size* or τ_{crit} . If the optical thickness τ of the shell in question is larger than the τ_{crit} then we can divide the shell into several subshells whose τ is less than the τ_{crit} and then star algorithm is used to calculate combined response from the subshells whose total thickness is T . If, for example one need the radiation field at internal points in the atmosphere, one will have to divide the entire medium into as many shells as needed and calculate the radiation field at the N points in the medium. One can write down the interaction principle for each shell and solve the whole system of equations (see Grant and Hunt [18]).

Figure 2.2 shows the atmosphere in which to calculate the internal radiation field. The atmosphere is divided into N shells (homogeneous or inhomogeneous) with A and B as the inner and outer radii. The solution U_{n+1}^+ and U_n^- (for any shell between shell 1 (at B) and shell N at A) are obtained from the relations

$$U_{n+1}^+ = r(1, n+1)U_{n+1}^- + V_{n+1/2}^+ \quad (2.27)$$

$$U_n^- = t(n, n+1)U_{n+1}^- + V_{n+1/2}^- \quad (2.28)$$

with the boundary conditions $U_{N+1}^- = U^-(A)$.

The quantities $r(1, n+1)$, $V_{n+1/2}^+$ and $V_{n+1/2}^-$ are calculated by employing the initial conditions $r(1, 1) = 0$ and $V_{1/2}^+ = U^+(b)$. The computation is done by the following recursive relation

$$r(1, n+1) = r(n, n+1) + t(n+1, n)r(1, n)[I - r(n+1, n)r(1, n)]^{-1}t(n, n+1) \quad (2.29)$$

$$V_{n+1/2}^+ = t(n+1, n)V_{n-1/2}^+ + \Sigma^+(n+1, n) + R_{n+1/2}\Sigma^-(n, n+1) \quad (2.30)$$

$$V_{n+1/2}^- = r(n+1, n)V_{n-1/2}^+ + T_{n+1/2}\Sigma^-(n, n+1) \quad (2.31)$$

where

$$t(n+1, n) = t(n+1, n)[I - r(1, n)r(n+1, n)]^{-1} \quad (2.32)$$

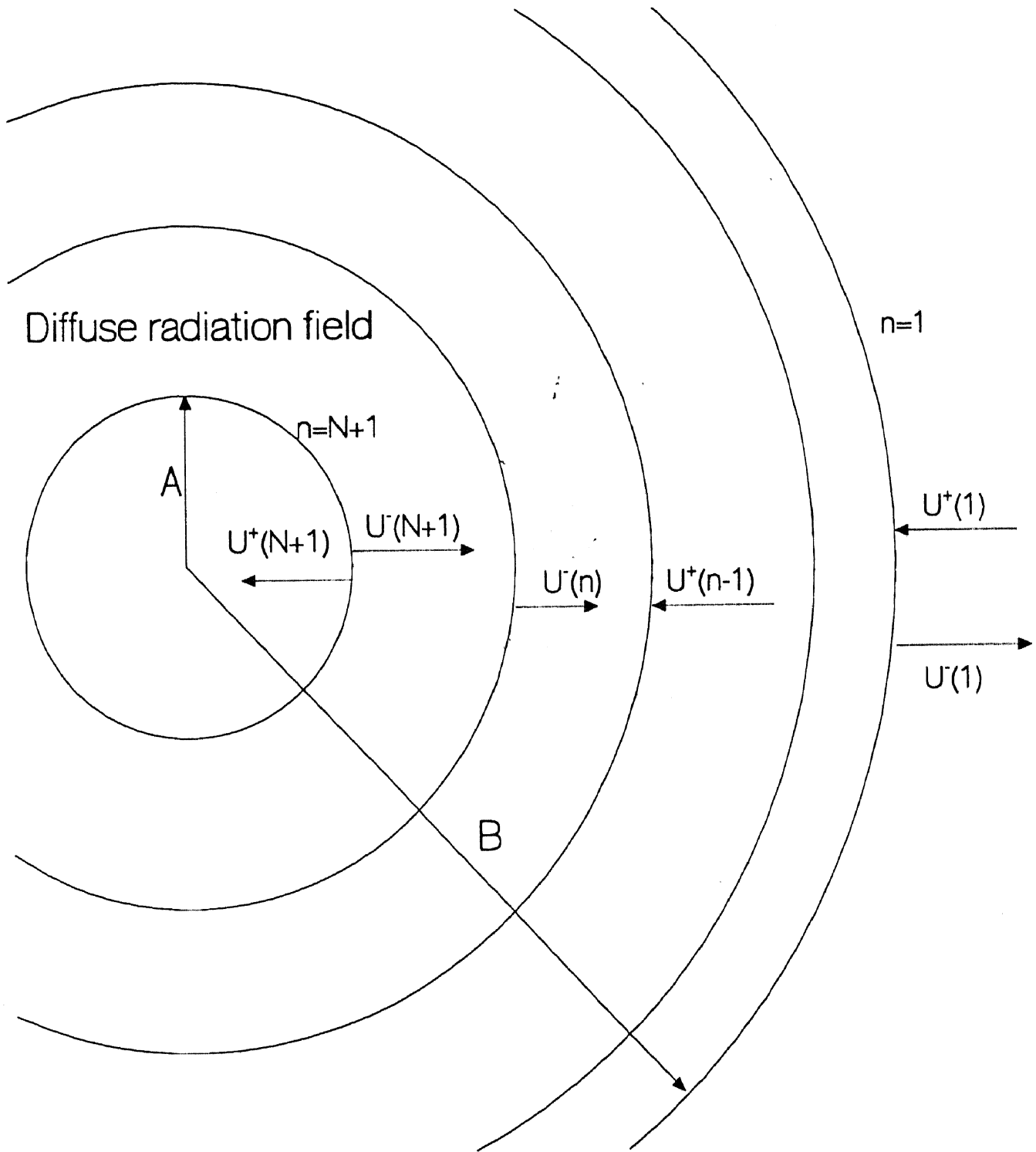


Figure 2.2: Description of the diffuse radiation field in a spherically symmetric atmosphere.

$$r(n+1, n) = r(n+1, n)[I - r(1, n)r(n+1, n)]^{-1} \quad (2.33)$$

$$R_{n+1/2} = t(n+1, n)r(1, n) \quad (2.34)$$

$$T_{n+1/2} = [I - r(n+1, n)r(1, n)]^{-1} \quad (2.35)$$

and

$$t(n, n+1) = T_{n+1/2}t(n, n+1) \quad (2.36)$$

To calculate the radiation field at the internal points one proceeds as follows:

1. Divide the medium into a number of shells (say N) with $N+1$ boundaries as mentioned earlier.
2. Start calculating the two pairs of reflection and transmission operators $r(n+1, n)$, $r(n, n+1)$, $t(n+1, n)$ and $t(n, n+1)$ in each shell (if the optical thickness in each shell is larger than τ_{crit} then apply star algorithm to use doubling procedure if the medium is homogeneous).
3. With the boundary condition that $r(1, 1) = 0$ and $V_{1/2}^+ = u^+(b)$ and the r and t operators mentioned in subsection 2.2.2, compute recursively $r(1, n+1)$, $V_{1/2}^+$ and $t(n, n+1)$ given in equations 2.29 to 2.30 from shell 1 to shell N (i.e. from B to A in figure 2.2).
4. Next one sweeps back from A to B (see figure 2.2) calculating the radiation field given in equations 2.27 & 2.28 with the boundary condition $U_{n+1}^- = U^-(a)$.

One has to retain the operators $r(1, n+1)$, $t(n, n+1)$, $V_{n+1/2}^+$ and $V_{n+1/2}^-$ for each shell that are calculated in the steps 2 and 3 above until one starts calculating the radiation field from A. (The storage of these operators will not increase the memory of the machine required for computations. The operators can be stored on a magnetic disc and can be recalled whenever necessary. The operators can be removed from the disc or tape so that the disc or tape can be used to store fresh data).

If the surface at A is reflecting, we can write

$$U_{N+1}^- = r_G U_{N+1}^+ \quad (2.37)$$

where r_G is the reflection operator. For a totally reflecting surface $r_G = I$. Therefore, we have

$$U_{N+1}^+ = [I - r(1, N+1)r_G]^{-1} V_{N+1/2}^+ \quad (2.38)$$

from which one can calculate U_{N+1}^- from equation 2.37. Rest of the calculations follow equations 2.27 and 2.28.

2.3 Solution of the line transfer equation

This section deals with the method to calculate the spectral line profiles using the Discrete Space Theory technique. The description given here follows from Peraiah [52, 53, 54].

In order to describe the method to solve the line transfer equation with partial frequency redistribution functions and velocity fields, a two-level line transfer problem in non-LTE case in an extended spherical medium is considered. The equation of line transfer in such medium is given by

$$\mu \frac{\partial I(x, \mu, r)}{\partial r} + \frac{1 - \mu^2}{r} \frac{\partial I(x, \mu, r)}{\partial \mu} = K_l [\beta + \phi(x, \mu, r)] [S(x, \mu, r) - I(x, \mu, r)] \quad (2.39)$$

and for the oppositely directed beam,

$$-\mu \frac{\partial I(x, -\mu, r)}{\partial r} + \frac{1 - \mu^2}{r} \frac{\partial I(x, -\mu, r)}{\partial \mu} = K_l [\beta + \phi(x, -\mu, r)] [S(x, -\mu, r) - I(x, -\mu, r)] \quad (2.40)$$

where $I(x, \mu, r)$ is the specific intensity at an angle $\cos^{-1}\mu$ ($\mu \in (0, 1)$) at the radial point r and frequency $x = (\nu - \nu_0)/\Delta_s$, where Δ_s is some standard frequency interval). β is the ratio κ_c/κ_l of opacity due to continuous absorption per unit interval of x to that in the line. The source function $S(x, \pm\mu, r)$ is given by,

$$S(x, \pm\mu, r) = \frac{\phi(x, \pm\mu, r)S_l(x, \pm\mu, r) + \beta S_c(r)}{\beta + \phi(x, \pm\mu, r)} \quad (2.41)$$

where $S_l(x, \pm\mu, r)$ and $S_c(r)$ refer to the source function in the line and in the continuum respectively. The line source function is given by

$$S_l(x, \pm\mu, r) = \frac{(1 - \epsilon)}{\phi(x, \pm\mu, r)} \int_{-\infty}^{\infty} dx' \int_{-1}^{+1} R(x, \pm\mu; x', \mu') I(x', \mu') d\mu' + \epsilon B(r) \quad (2.42)$$

where ϵ is the probability per scatter that a photon will be destroyed by collisional de-excitation; S_c and B are the continuum source function and Planck function, respectively; and $\phi(x, \pm\mu, r)$ and $R(x, \pm\mu; x', \mu')$ are the profile and partial redistribution functions. The profile function ϕ is given by

$$4\pi \int \int R(\nu, \vec{n}; \nu', \vec{n}') d\nu' d\Omega' = \phi(\nu) \quad (2.43)$$

Equations 2.39 and 2.40 are solved by using the source functions defined in equations 2.41 and 2.42 together with the appropriate redistribution function and following the procedure of integration described in Peraiah & Grant [57] and Grant & Peraiah [21]. This gives

$$M_m(U_{i,n+1}^+ - U_{i,n}^+) + \rho_c[\Lambda_m^+ U_{i,n+1/2}^+ + \Lambda_m^- U_{i,n+1/2}^-] + \tau_{n+1/2}(\beta + \phi_i)_{n+1/2} U_{i,n+1/2}^+ = \\ \tau_{n+1/2}(\rho\beta + \epsilon\phi_i)_{n+1/2} B'_{n+1/2} h + \frac{1}{2} \tau_{n+1/2} \sigma_{n+1/2} \phi_{i,n+1/2} \sum_{i'=-1}^I a_{i,n+1/2} (hh)^T b [U^+ + U^-]_{i,n+1/2} \quad (2.44)$$

Similarly, for the opposite-directed beam,

$$M_m(U_{i,n+1}^- - U_{i,n}^-) + \rho_c[\Lambda_m^+ U_{i,n+1/2}^- + \Lambda_m^- U_{i,n+1/2}^+] + \tau_{n+1/2}(\beta + \phi_i)_{n+1/2} U_{i,n+1/2}^- = \\ \tau_{n+1/2}(\rho\beta + \epsilon\phi_i)_{n+1/2} B'_{n+1/2} h + \frac{1}{2} \tau_{n+1/2} \sigma_{n+1/2} \phi_{i,n+1/2} \sum_{i'=-1}^I a_{i,n+1/2} (hh)^T b [U^+ + U^-]_{i,n+1/2} \quad (2.45)$$

where

$$U_{i,n+1}^+ = 4\pi r_{n+1}^2 \dot{I}(x_i, +\mu_m, r_{n+1}), \\ \phi_{m,i,n+1/2}^+ = \phi(x_i, +\mu_m, r_{n+1/2}), \\ R_{j,i',n+1/2}^{++} = R(x_i, +\mu_m; x_{i'}, x_{i'}, +\mu'_m; r_{n+1/2});$$

the Λ 's are the curvature matrices; ρ_c is the curvature factor; and

$$B'_{n+1/2} = 4\pi r_{n+1/2}^2 B_\nu, \\ c = [C_m \delta_{mk}], \\ M_m = [\mu_m \delta_{mk}]; \quad (2.46)$$

in which the μ 's and c 's are the roots and weights of the angle quadrature. The quantities ϕ^- , R^+ , etc. are to be similarly understood. The index $n+1/2$ refers the average over the shell with boundaries r_n and r_{n+1} , and i and i' are the indices corresponding to the frequencies of the incident and scattered photons.

We can define coefficients $W_{k;n+1/2}$ as

$$(\phi_i W_k) = a_{i,n+1/2} c_j \quad (2.47)$$

where the subscript k is

$$(i, j) \equiv k \equiv j + (i-1)J, 1 \leq k \leq K = IJ$$

with I and J being the total number of frequency and angle points, respectively.

Let

$$\begin{aligned} U_n^+ &= [U_{1,n}^+, U_{2,n}^+, U_{3,n}^+, \dots, U_{I,n}^+]^T, \\ \Phi_{n+1/2}^- &= [\Phi_{kk'}^+]_{n+1/2} = (\beta + \phi_k^+)_{n+1/2} \delta_{kk'}, \\ s_{n+1/2}^+ &= (\rho\beta + \epsilon\phi_k^+)_{n+1/2} B'_{n+1/2} \delta_{kk'}, \end{aligned}$$

where T denotes transpose, and rewrite equations 2.44 and 2.45 as

$$\begin{aligned} M[U_{n+1}^+ - U_n^+] + \rho_c[\Lambda^+ U_{n+1/2}^+ + \Lambda^- U_{n+1/2}^-] + \tau_{n+1/2} \phi_{n+1/2} U_{n+1/2}^+ = \\ \tau_{n+1/2} s_{n+1/2} + \frac{1}{2} [\tau \sigma \phi \phi^T W]_{n+1/2} [U^+ + U^+(R) + U^- + U^-]_{n+1/2} \end{aligned} \quad (2.48)$$

and

$$\begin{aligned} M[U_n^- - U_{n+1/2}^-] - \rho_c[\Lambda^+ U_{n+1/2}^- + \Lambda^- U_{n+1/2}^+] + \tau_{n+1/2} \phi_{n+1/2} U_{n+1/2}^- = \\ \tau_{n+1/2} s_{n+1/2} + \frac{1}{2} [\tau \sigma \phi \phi^T W]_{n+1/2} [U^+ + U^+ + U^- + U^-]_{n+1/2} \end{aligned} \quad (2.49)$$

The average intensities $U_{n+1/2}^-$ in the above equations are replaced by the following relations (Grant and Hunt [18])

$$(I - X_{n+1/2})U_n^+ + X_{n+1/2}U_{n+1}^+ = U_{n+1/2}^+ \quad (2.50)$$

$$(I - X_{n+1/2})U_n^- + X_{n+1/2}U_{n+1}^- = U_{n+1/2}^- \quad (2.51)$$

with $X = \frac{1}{2}I$ for diamond scheme. Then by comparing the resulting set of equations with those in the canonical form of Peraiah & Grant [57]

$$\begin{pmatrix} U_{n+1}^+ \\ U_n^- \end{pmatrix} = \begin{pmatrix} t(n+1, n) & r(n, n+1) \\ r(n+1, n) & t(n, n+1) \end{pmatrix} \times \begin{pmatrix} U_n^+ \\ U_{n+1}^- \end{pmatrix} + \begin{pmatrix} \Sigma_{n+1/2}^+ \\ \Sigma_{n+1/2}^- \end{pmatrix} \quad (2.52)$$

we obtain two pairs of reflection and transmission operators, namely, $t(n+1, n)$, $r(n, n+1)$, $r(n+1, n)$ and $t(n, n+1)$. The expressions for these operators are given below.

The cell operators are:

$$\begin{aligned} t(n+1, n) &= G^{+-}[\Delta^+ A + g^{+-} g^{-+}], \\ t(n, n+1) &= G^{-+}[A^- D + g^{-+} g^{+-}], \\ r(n+1, n) &= G^{-+} g^{-+}[I + \Delta^+ A], \\ r(n, n+1) &= G^{+-} g^{+-}[I + \Delta^- D] \end{aligned} \quad (2.53)$$

and the cell source vectors are:

$$\begin{aligned} \Sigma_{n+1/2}^+ &= G^{+-}[\Delta^+ s_{n+1/2}^+ + g^{+-} \Delta^- s_{n+1/2}^-] \tau_{n+1/2} \\ \Sigma_{n+1/2}^- &= G^{-+}[\Delta^- s_{n+1/2}^- + g^{-+} \Delta^+ s_{n+1/2}^+] \tau_{n+1/2} \end{aligned}$$

where

$$\begin{aligned}
G^{+-} &= [I - g^{+-}g^{-+}]^{-1}, \\
G^{-+} &= [I - g^{-+}g^{+-}]^{-1}, \\
g^{+-} &= \frac{1}{2}\tau_{n+1/2}\Delta^+Y_-, \\
g^{-+} &= \frac{1}{2}\tau_{n+1/2}\Delta^-Y_+, \\
D &= M - \frac{1}{2}\tau_{n+1/2}Z_-, \\
A &= M - \frac{1}{2}\tau_{n+1/2}Z_+, \\
\Delta^+ &= [M + \frac{1}{2}\tau_{n+1/2}Z_+]^{-1}, \\
\Delta^- &= [M + \frac{1}{2}\tau_{n+1/2}Z_-]^{-1}, \\
Z_+ &= \Phi_{n+1/2}^+ - \frac{1}{2}\sigma(R^{++}W^{++})_{n+1/2} + \rho\Lambda^+/\tau_{n+1/2}, \\
Z_- &= \Phi_{n+1/2}^- - \frac{1}{2}\sigma(R^{--}W^{--})_{n+1/2} - \rho\Lambda^+/\tau_{n+1/2}, \\
Y_+ &= (\rho\Lambda^+/\tau_{n+1/2}) + \frac{1}{2}\sigma(R^{-+}W^{-+})_{n+1/2}, \\
Y_- &= -(\rho\Lambda^-/\tau_{n+1/2}) + \frac{1}{2}\sigma(R^{+-}W^{+-})_{n+1/2}, \\
\sigma &= 1 - \epsilon
\end{aligned}$$

and I is the unitary matrix.

These operators describe the radiation field in a moving medium and, therefore, all four redistribution functions

$$\begin{aligned}
R(x, +\mu; x', \mu') & \quad (= R^{++}), \\
R(x, +\mu; x', -\mu') & \quad (= R^{+-}), \\
R(x, -\mu; x', \mu') & \quad (= R^{-+}), \\
R(x, -\mu; x', -\mu') & \quad (= R^{--})
\end{aligned}$$

are not equal and have to be calculated at each radial point of the medium. However, if the medium is static and partial redistribution is considered, then, by the symmetry relations (Hummer [31]), we have

$$\begin{aligned}
R(x, +\mu; x', +\mu') &= R(x, -\mu; x', -\mu'); R^{++} = R^{--} \\
R(x, +\mu; x', -\mu') &= R(x, -\mu; x', +\mu'); R^{+-} = R^{-+}
\end{aligned}$$

Furthermore, if one considers a static medium with complete redistribution, then all four redistribution functions that evaluate the scattering integral reduce to approximately $\phi\phi^T$,

where ϕ is the profile function and T is the transpose of the vector. Consequently, the form of the quantities Z_+, Z_-, Y_+, Y_- , etc., given above will be reduced to those given in Grant & Peraiah [21].

To obtain a stable solution one must choose an optical depth $\tau_{n+1/2}$ in each cell, given by

$$\tau_{n+1/2} \leq \tau_{crit} = \min_k \left| \frac{\mu_k \pm \frac{1}{2} \rho \Lambda_{kk}^+}{\frac{1}{2} (\Phi_k^+ - \frac{\sigma}{2} R_{kk}^{++} W_{kk}^{++})} \right| \quad (2.54)$$

for the diagonal elements of the matrices Δ^+ and Δ^- , and for the off-diagonal elements we must have

$$(\rho/\tau)_{n+1/2} < \min_k \left[\min_{k=k'+1} \left| \frac{\frac{1}{2} \sigma R_{kk'} W_{kk'}}{\Lambda_{kk'}^+} \right| \right] \quad (2.55)$$

Condition 2.56 is difficult to satisfy, which imposes a severe restriction on the size of the curvature factor to be used in each cell to obtain non-negative r and t matrices. From the inequalities set out in 2.55 and 2.56 above, it is clear that the medium of interest should be divided into a number of shells and relations (5.1) to (5.4) of Peraiah & Grant [57] should be used to calculate the diffuse radiation field at any point in the medium. However, it is time consuming to use a large number of shells and subdivide each shell so that the curvature factor ρ is small enough to facilitate the use of the doubling algorithm described in Peraiah [50] and the star algorithm of Grant & Hunt [19, 20].

If the shell is halved p times, the star algorithm is repeated p times, and in this event the curvature factor ρ_{ss} and the optical depth τ_{ss} for the subshell are given in terms of ρ_s and τ_s of the shell

$$\begin{aligned} \rho_{ss} &\approx \rho_s 2^{-p} / [1 - \rho_s (2^{-1} - 2^{-p})], \\ \tau_{ss} &= \tau_s 2^{-p}, \\ r^2 &= R^2 [1 - \rho_s (K + \frac{1}{2}) + \frac{1}{3} \rho_s^2 (K^2 + \frac{1}{2} K + \frac{1}{4})] \end{aligned} \quad (2.56)$$

where ρ_{ss} corresponds to a subshell approximately midway in the shell and ρ_s is the curvature factor for the whole shell, defined as

$$\rho_s = \Delta r / r_{out} \quad (2.57)$$

τ_{ss} being derived on the assumption that the optical depth in the whole shell is uniform. ρ_{ss} is taken to be the mean value for all subshells, which introduces error, and to reduce this error one must divide the shell into finer subshells that are small enough not to introduce serious errors. \bar{r} is the mean radius of the subshell; R is the outer radius of the shell in terms of the

inner radius of the medium; and $K = 2^{-1} - 2^{-p}$. The relations set out in 5.57 are derived on the basis of equation (30) of Grant [17].

To conserve flux, one must ensure that the scattering integral given in equation 2.42, and the corresponding discrete equivalent given in the last brackets of equations 2.44, 2.45, 2.48 and 2.49 are calculated exactly. For this purpose, the redistribution functions R^{++} , R^{+-} , etc., must be normalized to the machine accuracy so that, when there is pure scattering in the medium, conservation of flux can be checked easily (see Peraiah & Grant [57]). This can be achieved through the identity

$$\frac{1}{2} \sum_{P=1}^K \sum_{Q=1}^K (R_{PQ}^{++} W_P^{++} W_Q^{++} + R_{PQ}^{-+} W_P^{-+} W_Q^{-+}) = 1 \quad (2.58)$$

where

$$W_{P,Q} = a_i c_j, a_i = \frac{A_i R_{PQ}}{\sum_{P,Q=1}^K R_{PQ} A_i c_j}$$

and

$$(P, Q) \equiv j + (i + i)J$$

and also by relation (4.3) of Peraiah & Grant [57].

The method described above has been used to solve the line transfer equation in the following chapters.

Chapter 3

Effects of angle-averaged R_V and R_{II} on emergent flux profiles in a static spherically symmetric stellar atmosphere

3.1 Introduction

The influence of partial frequency redistribution (PRD) is expected to become more pronounced in the extended atmospheres of supergiant stars because of low densities. *Therefore, in this chapter, the dependence of the emergent flux profiles on the form of the angle-averaged partial redistribution functions R_V and R_{II} is examined for spherically symmetric stellar atmospheres in a comparative way.*

Scattering by a resonance line, that is broadened by radiation damping is described by the partial frequency redistribution function R_{II} derived by Hummer [31]. This redistribution function is strongly coherent in the line wings leading to the lowering of line profile outside the Doppler core (Hummer [32], Vardavas [73]). Vardavas [71, 72, 73] studied the effects of angle-averaged and angle-dependent R_I , R_{II} and R_{III} on spectral line formation in planar geometry for both static and moving media. Peraiah([51, 52]) studied the effects of partial frequency redistribution on spectral line formation in both static and expanding spherically symmetric stellar atmospheres using angle-averaged R_I and R_{II} . Rangarajan et al. [60] studied the effects of stimulated emission on radiative transfer with PRD functions R_{II} and R_{III} in plane-parallel geometry. Milkey & Mihalas [41] used a combination of R_{II} and R_{III} to study Solar Lyman- α line profile.

Redistribution of photons in angle and frequency due to scattering in subordinate lines is given by $R_V(x', \vec{n}'; x, \vec{n})$ in the notation of Heinzl. Here x' and x represent the frequency displace-

ment from line center (in units of Doppler width) of the incident and the scattered photons respectively; \vec{n}' and \vec{n} give the directions of the incident and the scattered photons respectively. Heinzel [23] derived the correct form of angle-dependent laboratory frame redistribution function (LFR), R_V , for radiatively broadened upper and lower levels of the atom. This LFR was extended to include collisional broadening of the levels by Heinzel and Hubeny [24]. Hubeny and Heinzel [29] solved the transfer problem using R_V for isothermal plane-parallel (both finite and semi-infinite) atmospheres. Mohan Rao et al. [44] examined the effects of R_{II} , R_{III} and R_V on source functions (S_L) for plane-parallel and isothermal stellar atmospheres and showed, that, for a purely scattering medium with frequency independent incident radiation, the frequency dependent source function $S_L(R_V)$ lies below $S_L(R_{III})$ but above $S_L(R_{II})$ in the line wings.

All the works cited above (except Peraiah [51, 52, 55, 56]) are limited to planar geometry. The assumption of a plane-parallel atmosphere holds good only when the density scale-height in the atmosphere is small compared to the radius of the star. But, many stars, in particular the supergiants are known to have extended atmospheres; in the first approximation it is assumed that such stars are spherically symmetric. These stars are known to have low gravities leading to low densities in their extended outer layers where the PRD effects are expected to be more pronounced (Basri [9]). *In this study it is shown, the effects of R_V on emergent flux profiles are shown for the first time in comparison to the effects of R_{II} and R_V considering spherically symmetric stellar atmospheres.* The appreciation of these effects will be of relevance to the problems of spectral line modeling in stellar atmospheres and also to the modellers of stellar atmospheres.

3.2 Equations and computational procedure

The line transfer equation for a two-level atom in spherical symmetry is written as follows (Peraiah [52], Singh [65])

$$\pm\mu\frac{\partial I(x, \pm\mu, r)}{\partial r} \pm \frac{1-\mu^2}{r}\frac{\partial I(x, \pm\mu, r)}{\partial \mu} = \kappa_l[\beta + \phi(x)][S(x, r) - I(x, \pm\mu, r)] \quad (3.1)$$

where \pm stands for the oppositely directed beams of radiation, $I(x, \pm\mu, r)$ represents specific intensity of the ray making an angle $\cos^{-1}\mu$ ($\mu \in [0, 1]$) with the radius vector. $\beta = \kappa_c/\kappa_l$ (continuum to line opacity). $\phi(x)$ represents the profile function, given as

$$\phi(x) = \int_{-\infty}^{+\infty} R_{II,V}(x', x) dx' \quad (3.2)$$

where $R_{II}(x', x)$ and $R_V(x', x)$ are the angle-averaged partial frequency redistribution functions. Here, x' and x represent the frequency displacement from line center in units of Doppler

width of the incident and scattered photons respectively. The profile is normalized as

$$\int_{-\infty}^{+\infty} dx \phi(x) = 1 \quad (3.3)$$

In the transfer equation (equation 3.1), $S(x, r)$ is the total (line plus continuum) source function which is written as

$$S(x, r) = \frac{\phi(x)S_l(x, r) + \beta S_c(r)}{\phi(x) + \beta} \quad (3.4)$$

where S_c is the continuum source function set equal to 1 in this computation. $S_l(x, r)$ represents the line source function, which, for a two-level atomic model, is given by the following expression

$$S_l(x, r) = \frac{1 - \epsilon}{\phi(x)} \int_{-\infty}^{+\infty} R_{II,V}(x', x) J(x') dx' + \epsilon B(r) \quad (3.5)$$

where $J(x')$ denotes the frequency-dependent mean intensity and ϵ is the probability per scatter that a photon is destroyed by collisional de-excitation written as

$$\epsilon = \frac{C_{21}}{C_{21} + A_{21}[1 - \exp(-\frac{h\nu}{k\Theta})]^{-1}} \quad (3.6)$$

where C_{21} is the rate of collisional de-excitation from level 2 to 1, A_{21} is Einstein's spontaneous emission probability for transition $2 \rightarrow 1$, h is the Planck's constant, ν is the photon frequency, k is the Boltzmann's constant and Θ is the temperature.

Under the assumption of complete redistribution, the line source function is written as

$$S_l(r) = (1 - \epsilon) \int_{-\infty}^{+\infty} \phi(x') J(x') dx' + \epsilon B(r) \quad (3.7)$$

where $\phi(x)$ is taken to be a Voigt profile with damping parameter a .

The line source functions written above for PRD (equation 3.5) and for CRD (equation 3.7) are valid for a two-level atomic model; whereas the simplest model needed to study subordinate line formation is a three-level atomic model. The reason for using a simplified two-level atomic model in this study is that, since we are interested in a *comparison* between radiative transfer solutions with three redistribution functions rather than in solving any specific transfer problem, we neglect the transition $3 \leftrightarrow 1$ (which provides an extra channel for destroying and creating photons in the subordinate line $3 \leftrightarrow 2$). Although this is a rather unphysical assumption that amounts to neglecting the terms A_{31} , C_{31} and Q_E (rate of elastic collisions), it is suitable for our purposes. Under this assumption the line source function for a three-level atomic model reduces to a line source function for a two-level atomic model.

3.2.1 Angle-averaged redistribution functions

In this study, an idealized stellar atmosphere is considered assuming it to be isothermal, static, spherically symmetric and extended. The outer layers of this extended atmosphere will be

tenuous, where the scattering processes will be important. Also, the radiation field will be anisotropic and one should ideally use angle-dependent form of redistribution functions. However, in the present study, the angle-independent (or angle-averaged) redistribution functions have been used. Although, by doing so, one loses information about the angular effects on emergent flux profiles, still, one is fully accounting for the frequency redistribution effects, which affect crucially the photon escape-probability, and hence the thermalization process. Therefore, by using angle-averaged redistribution functions, one accounts for critical aspects of redistribution process and sacrifices information only in an area of secondary importance.

The angle-averaged R_{II} has the following form (Mihalas [38])

$$R_{II}(x', x) = \pi^{-3/2} \int_{\frac{|x'-x|}{2}}^{\infty} e^{-u^2} [\tan^{-1}(\frac{\underline{x}+u}{a}) - \tan^{-1}(\frac{\bar{x}-u}{a})] du \quad (3.8)$$

where $\bar{x} = \max(|x|, |x'|)$ and $\underline{x} = \min(|x|, |x'|)$; a is the damping parameter.

R_{II} envisions an atom having a sharp lower level and a radiatively broadened upper level. The above expression has been derived assuming isotropic phase function. Figure 3.1 gives the plot of the emission probability ($R_{II}(x', x)/\phi(x')$) at frequency x per absorption, when the absorption is at frequency x' . Damping parameter $a = 2.0 \times 10^{-3}$.

It is seen that a photon incident in the line wing has a high probability of being re-emitted in the line wing. Thus R_{II} is strongly coherent outside the line core. This property has implication on the line wing emissions from strong resonance lines.

The angle-dependent R_V is given by the following expression (Heinzel [23])

$$R_V(x', \vec{n}'; x, \vec{n}) = \frac{1}{4\pi^2 \sin \theta} [H(a_i \sec \frac{\theta}{2}, \frac{x+x'}{2} \sec \frac{\theta}{2}) \times H(a_j \csc \frac{\theta}{2}, \frac{x-x'}{2} \csc \frac{\theta}{2}) + E_V(x', x, \theta)] \quad (3.9)$$

where θ is the angle between the incident (\vec{n}') and the scattered (\vec{n}) photon directions. a_i and a_j are the damping parameters of the lower and upper levels of an atom respectively. The function E_V is given by

$$E_V(x', x, \theta) = \frac{\sin(\theta/2)}{\pi^{1/2}} \text{Re} \int_0^\infty e^{-t^2} (e^{-2wt} + e^{-2w't}) \Delta(t) dt \quad (3.10)$$

where

$$\Delta(t) = D(z + t \cos \frac{\theta}{2} + a_i \sec \frac{\theta}{2}) - D(z + t \cos \frac{\theta}{2}) \quad (3.11)$$

$$z = (a_j - i \frac{x+x'}{2}) \sec \frac{\theta}{2} \quad (3.12)$$

$$w = a_i + a_j - ix \quad (3.13)$$

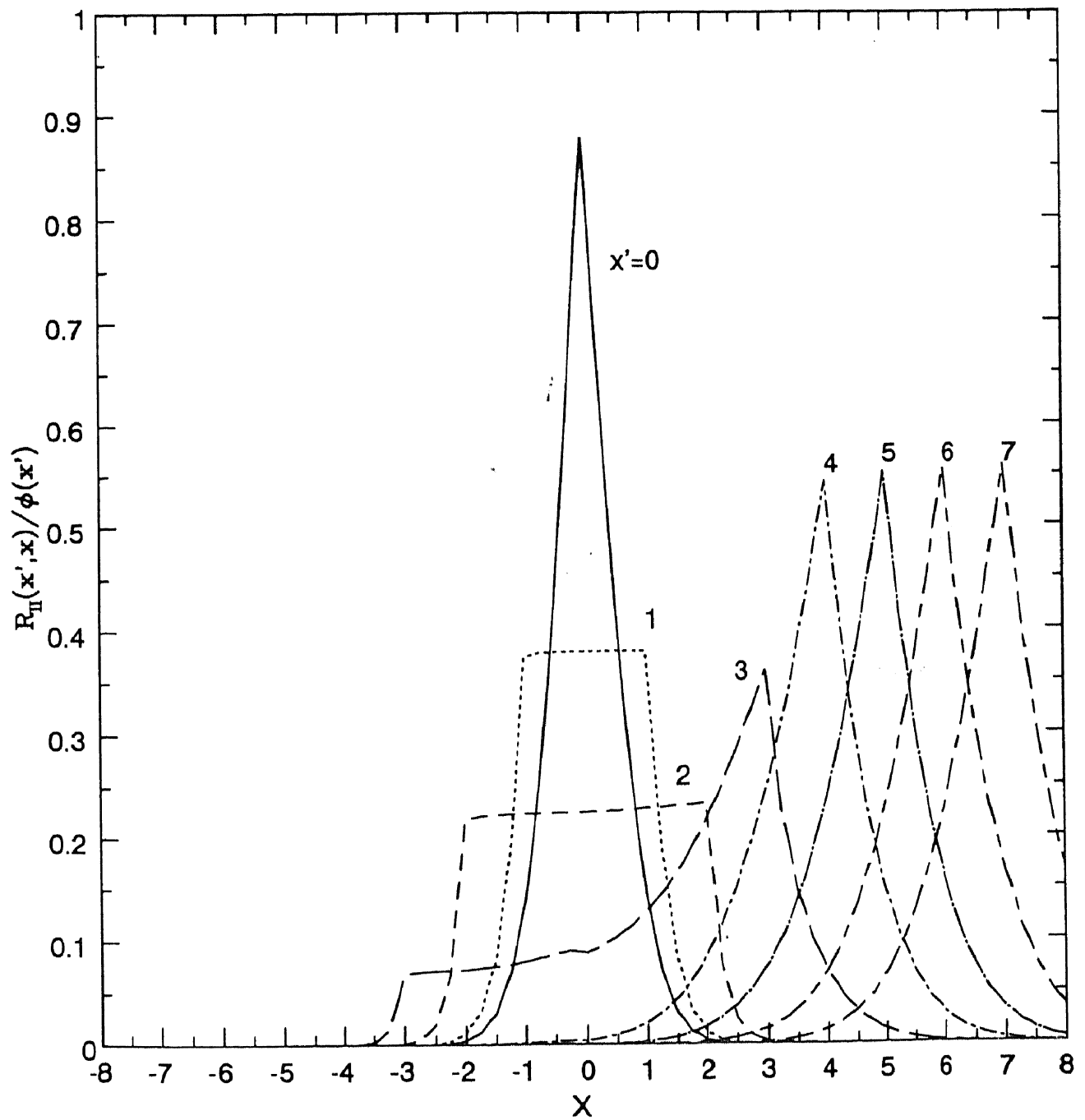


Figure 3.1: Plot of the emission probability ($R_{II}(x', x)/\phi(x')$) at frequency x per absorption, when the absorption is at frequency x' . Damping parameter $a = 2.0 \times 10^{-3}$. D.Mihalas, Stellar Atmospheres, Chapter 13, p429.

$$w' = a_i + a_j - ix' \quad (3.14)$$

$$D(\omega) = H(p, q) + iK(p, q) \quad (3.15)$$

$$\omega = p - iq \quad (3.16)$$

Here $H(p, q)$ and $K(p, q)$ are the Voigt functions which are computed using the method of Matta & Reichel [37]. The angle-averaged expression for R_V is obtained by

$$R_V(x', x) = 8\pi^2 \int_0^\pi R_V(x', x, \theta) \sin\theta d\theta \quad (3.17)$$

This function is computed using a highly accurate computer program developed by Mohan Rao et al. [44] based on the method described by Heinzl & Hubeny [25]. It is derived for an atom having lower and upper levels broadened by radiative broadening. The emission probability $R_V(x', x)/\phi(x')$ due to this redistribution function has been plotted in figure 3.2 with damping parameters $a_i = a_j = 10^{-3}$.

It is seen that a photon absorbed in the line wing has a high probability of being emitted at the line centre as well as in the wing. This is unlike the emission probability of R_{II} where, if a photon is absorbed in the line wing, it has the least probability of being emitted at the line centre. Also, R_V is less coherent than R_{II} in the line wing.

3.2.2 Choice of depth points N

The stellar envelope is divided into N depth points of equal radial thickness. These N depth points bound $N - 1$ spherical shells, each of equal radial thickness. n is the depth point counter that is taken to be increasing inwards and

$$1 \leq n \leq N \quad (3.18)$$

The outermost shell is bounded by $n = 1$ and $n = 2$; the innermost shell is bounded by $n = N - 1$ and $n = N$. T is the total optical depth of the atmosphere taken to be 10^4 . We set $N = 75$ in these computations. In selecting the value of $N = 75$, the dependence of the emergent flux profiles on this parameter has been investigated to ensure the accuracy of results. In order to find out which value of N is suitable for this study, test runs were made with $N = 10, 25, 50, 75$ and 100 and the emergent flux profiles were compared. Figure 3.3 shows the emergent flux profiles due to CRD, R_{II} and R_V for various values of N using exponential opacity distribution.

Figure 3.4 shows similar plots for power law r^{-2} opacity distribution.

These plots show the sensitivity of the emergent flux profiles to the number of depth points N . It is seen that there is a lot of difference between the results due to $N = 10$ and $N = 25$. This difference decreases for higher $N = 50$ and finally vanishes for $N = 75$ and 100 . This

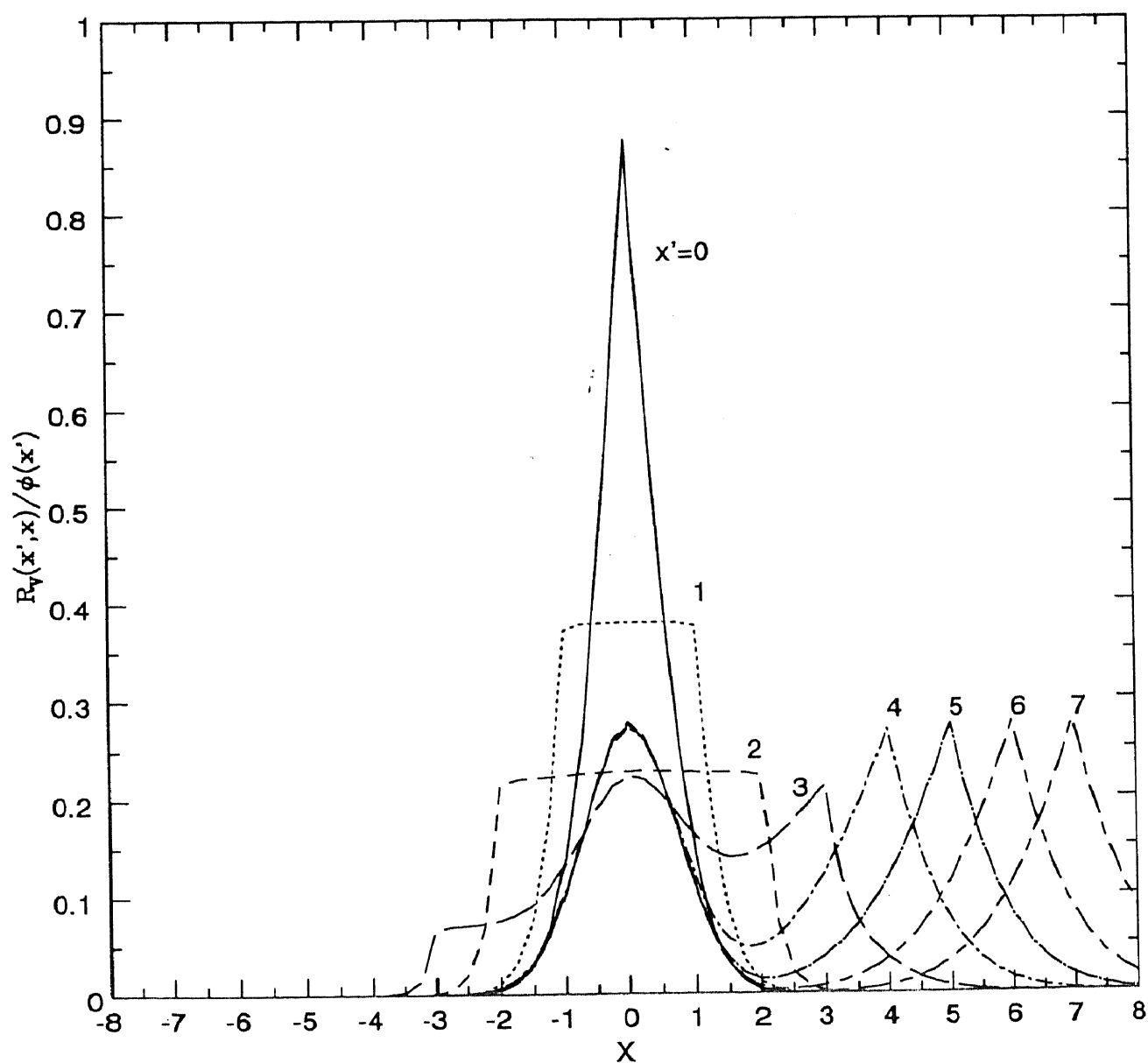


Figure 3.2: Plot of the emission probability ($R_V(x', x)/\phi(x')$) at frequency x per absorption, when the absorption is at frequency x' . Damping parameter $a = 2.0 \times 10^{-3}$. See P.Heinzel, 1981, JQSRT, 25, 483.

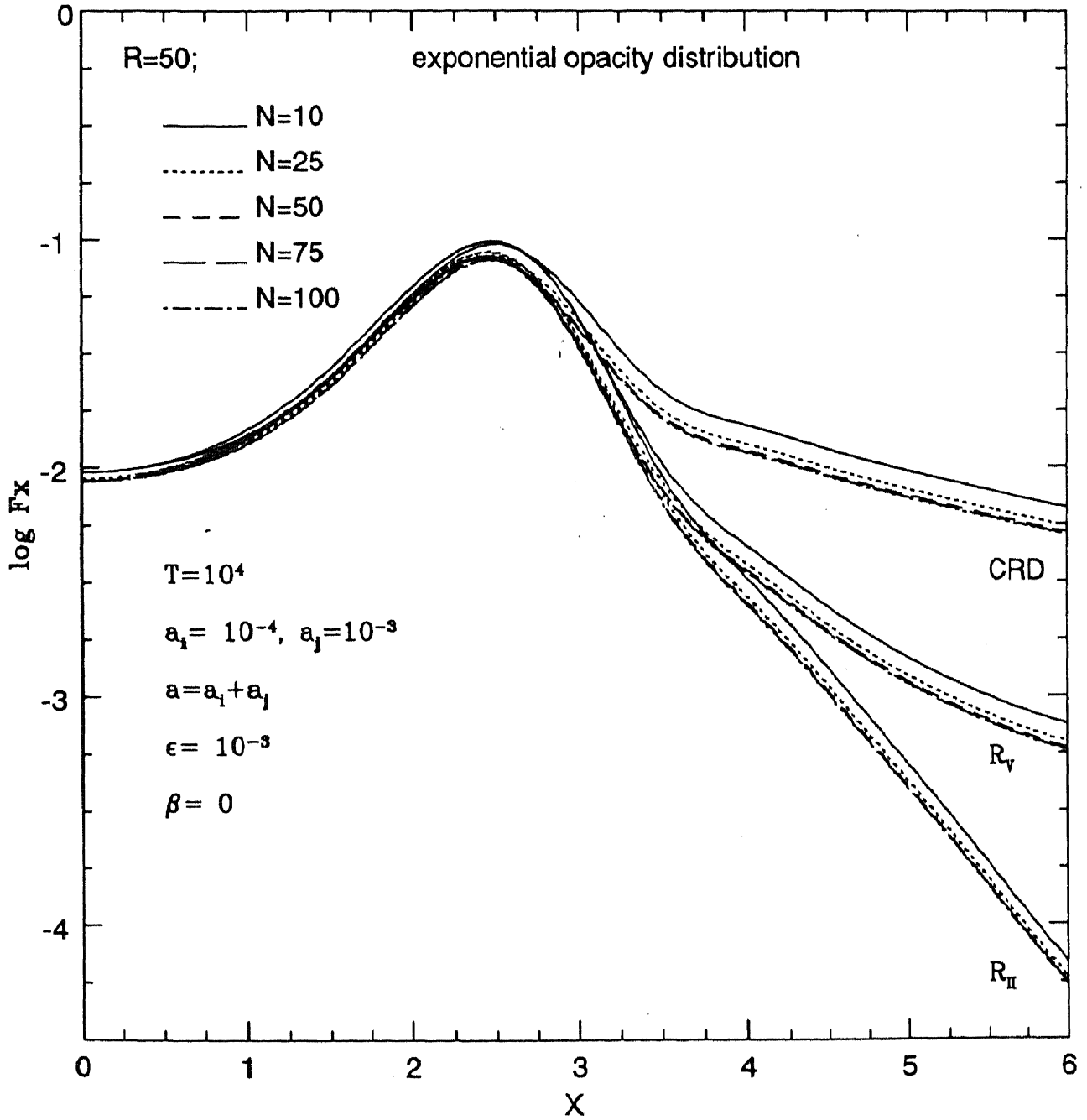


Figure 3.3: Sensitivity of emergent flux profiles to the number of depth points N using exponential opacity distribution.

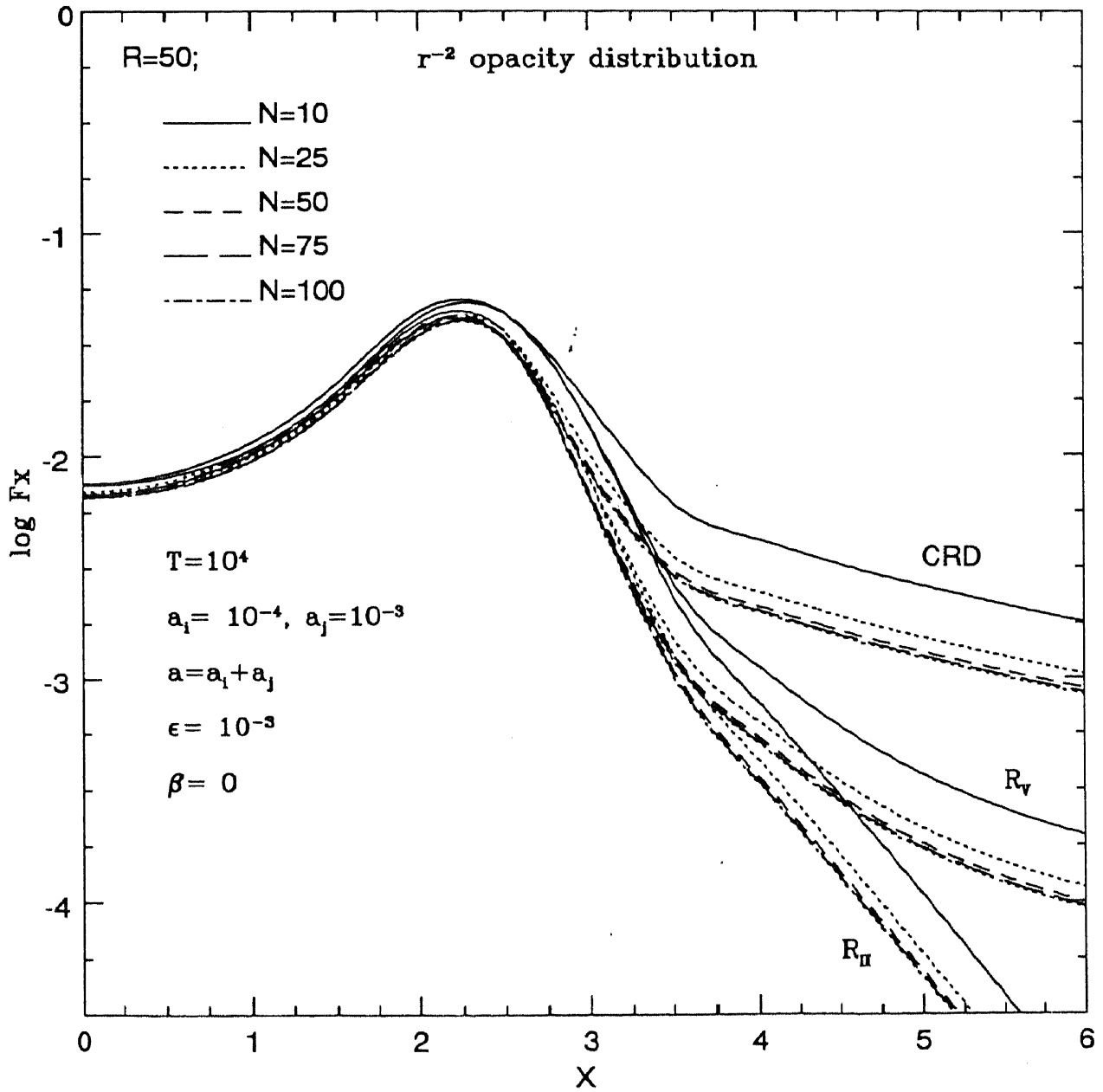


Figure 3.4: Sensitivity of emergent flux profiles to the number of depth points N using r^{-2} opacity distribution.

implies that, the resulting profiles are quite sensitive to the value of $N < 50$, and insensitive to the change in N beyond $N = 50$. Therefore, for the parameters used in this study, $N = 75$ is a suitable value.

3.2.3 Optical depth laws

For spherical atmospheres of fixed total optical thickness T , the optical depth variation ($\tau(r)$) in the atmosphere at radial points r is allowed to vary using

1. exponential opacity distribution, and
2. power law opacity distribution.

Both these laws are appropriate for spherical geometries: the former being more realistic for static media; latter for constant velocity winds. Let us define \mathfrak{R}_* to be the radius of the stellar photosphere. Further, let $\mathfrak{R}_* = 1$ to be the unit of length scale. Then, the extent of the atmosphere is defined in units of $\mathfrak{R}_* = 1$. The atmospheric extent has been denoted by a variable R . For example, $R = 1$ leads to plane-parallel approximation and $R = 50$ will mean that the atmosphere extends as far as 50 times the photospheric radius of the star. For plane-parallel cases the optical depth per layer is taken to be equal to be $2T/N$ (see Kunasz & Hummer [36]). For extended atmosphere the following laws have been used.

From the definition of optical depth, we have

$$\tau(r_n) = \int_{r_n}^R k(r) dr \quad (3.19)$$

where $k(r)$ is the opacity and r_n is radius (in units of \mathfrak{R}_*) at the depth point n .

Exponential opacity distribution

For an exponential opacity distribution, following expression is adopted in this study

$$k(r) = k_o e^{-\alpha(r-1)} \quad (3.20)$$

In this equation, α is a constant which controls the steepness of opacity variation. It is taken to be 0.1 in this study; k_o is a constant which is evaluated by integrating the equation 3.20 over whole radial length i.e. between r_1 and r_N , and setting the left-hand-side equal to T . It is found to be

$$k_o = T(e^{-\alpha(R-1)} - 1)^{-1} \quad (3.21)$$

Using the above relations, the optical depth of a shell bounded by n and $n+1$ has the following form

$$\tau(r_{n+1}) - \tau(r_n) = T(e^{-\alpha(R-1)} - 1)^{-1}(e^{-\alpha(r_n-1)} - e^{-\alpha(r_{n+1}-1)}) \quad (3.22)$$

Power law opacity distribution

For a power law opacity distribution we have (see Kunasz & Hummer [36])

$$k(r) = k_o r^{-m} \quad (3.23)$$

where $m = 0, 2, 3$. In the present study we set $m = 2$. k_o is a constant evaluated by integrating equation 3.20 (as done for exponential opacity distribution) over the whole radial extent of the atmosphere. It written as (with $m = 2$)

$$k_o = T(1 - R^{-1})^{-1} \quad (3.24)$$

The optical depth of a shell bounded by n and $n+1$ is given by the following expression

$$\tau(r_{n+1}) - \tau(r_n) = T(1 - R^{-1})^{-1}(r_{n+1}^{-1} - r_n^{-1}) \quad (3.25)$$

It is seen that for exponential opacity variation, the matter is far well spread out in the atmosphere, whereas for r^{-2} opacity distribution where the matter is concentrated in the innermost shells.

Following are the boundary conditions used for the transfer equation

$$U_1^+(x, \tau = 0, \mu) = 0 \quad \text{and} \quad U_{N+1}^-(x, \tau = T, \mu) = 0 \quad \text{if} \quad \epsilon > 0 \quad (3.26)$$

$$U_1^+(x, \tau = 0, \mu) = 0 \quad \text{and} \quad U_{N+1}^-(x, \tau = T, \mu) = 1 \quad \text{if} \quad \epsilon = 0 \quad (3.27)$$

where

$$U_n^\pm(x, \tau, \mu) = 4\pi r_n^2 I(x, \mu, \pm \tau(r_n)) \quad (3.28)$$

$I(x, \mu, \tau(r_n))$ being the specific intensity. $+$ specifies a ray directed towards the bottom of the envelope ($\tau = T$), and $-$ specifies a ray directed out of the envelope. The Planck's function has been set equal to 1 throughout the medium.

The above equations have been solved using the discrete space theory method described in chapter 2 of this thesis.

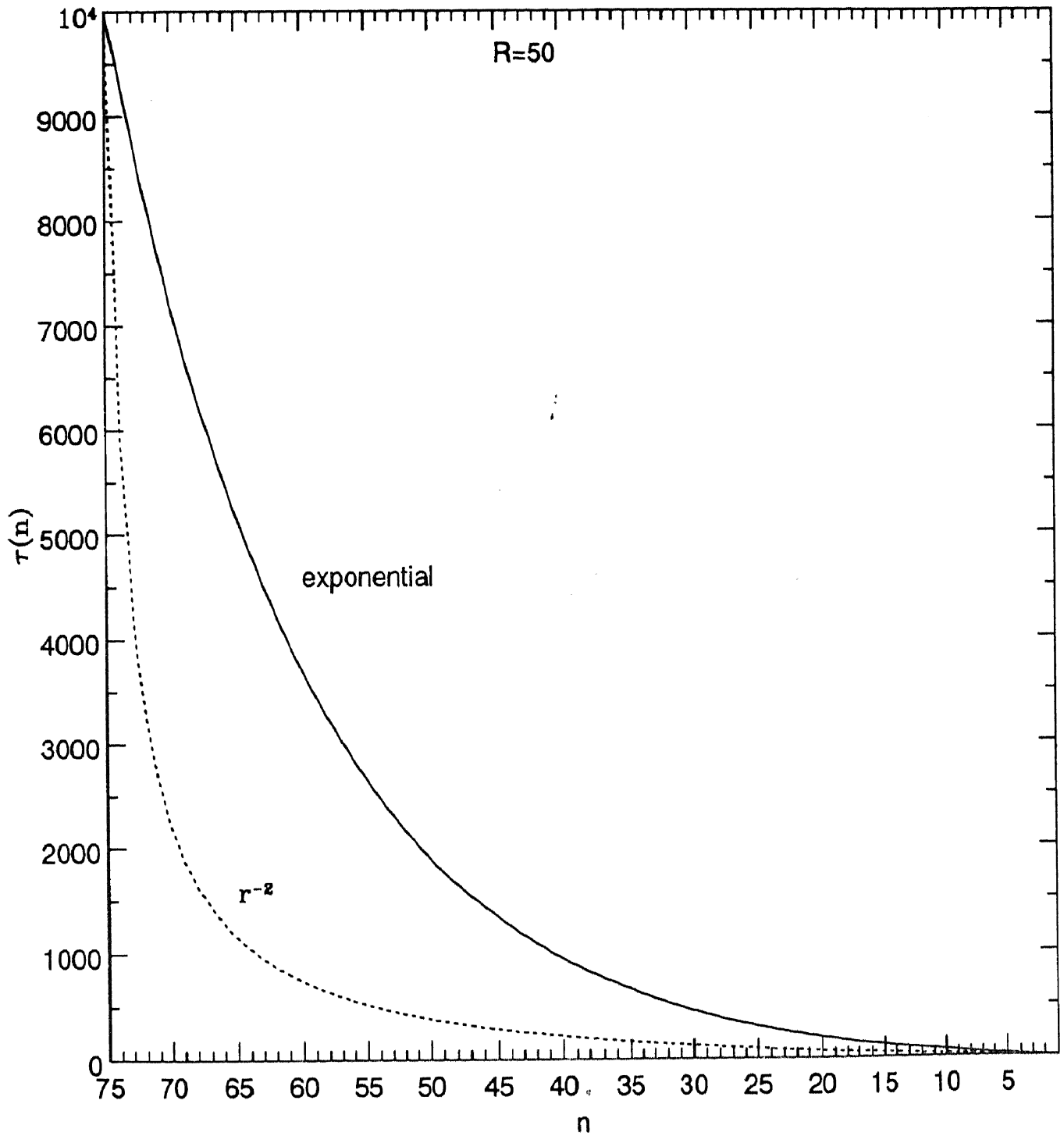


Figure 3.5: Optical depth variation versus depth points in a spherically symmetric atmosphere having $R = 50$. $n = 75$ denotes the innermost boundary and $n = 1$ denotes the boundary of the outermost layer of the atmosphere.

3.3 Results

The results are presented for two sets of calculations. In the first set, the exponential opacity distribution given above is used and in the second set $1/r^2$ variation of opacity given by equation 3.23 (by setting $m = 2$) is used. In each of these sets there are two subsets of calculations. In the first subset, the damping parameters for computing R_V are $a_i = a_j = 10^{-3}$ for the lower and upper level of the atom respectively, and in the second subset $a_i = 10^{-4}$ and $a_j = 10^{-3}$. The corresponding damping parameter for computing R_{II} and CRD is taken to be $a = a_i + a_j$. Thus, for the first subset $a = 2 \times 10^{-3}$ and for the second set $a = 1.1 \times 10^{-3}$. For convenience, the first set is called as 'model A' and the second set as 'model B'. Also, the first subset is named as 'model a' and the second subset as 'model b'. Using this nomenclature, the combinations are called as models 'Aa, Ab, Ba or Bb'.

Several test runs were made in order to ensure the accuracy of this code besides checking the dependence of the accuracy of results on N as described earlier (figures 3.3 & 3.4). This code is able to reproduce the same line profiles as given by Kunasz & Hummer [36] in figure 8 of their paper and those given by Hubeny & Heinzel [29] in figure 2 of their paper. Moreover, flux conservation is maintained to an accuracy of the order of 10^{-10} in double precision for a purely scattering medium i.e. when $\epsilon = 0$ (Peraiah [56]).

First, the results using exponential opacity distribution are presented. Figure 3.6 gives the line source functions of 'model Aa'.

The upper set of curves is for a plane-parallel atmosphere $R = 1$ and the lower set is for an extended atmosphere with $R = 50$. The line source functions S_x for the extended atmosphere lie much below those for a plane-parallel atmosphere. This is the effect of atmospheric extension which increases the effective escape probability of photons; and the major effect of increased photon escape is to decrease S_x . From this figure we see that for a plane-parallel atmosphere, the line source function due to CRD always lies below those due to PRD. This is not the case for extended atmosphere where S_x due to CRD lies above those due to PRD for $x \geq 4$. Also, it is seen that for $R = 50$, S_x due to R_V always lies between S_x due to CRD and R_{II} . It is not so for a planar atmosphere where S_x due to R_V lies above both R_{II} and CRD for $x \geq 4.5$.

Figure 3.7 gives the emergent flux profiles corresponding to the source functions given in figure 3.6.

An important result clearly seen is that in transition from a plane-parallel to an extended atmosphere the effects of R_{II} and R_V are significantly enhanced (note the log scale). It is also seen that the flux profile due to R_{II} is much more affected than that due to R_V . The emergent flux profiles for $R = 50$ follow the variation of the corresponding line source functions of figure 3.6, whereas it is not so for a plane-parallel atmosphere. The emergent flux profiles due to R_{II} and R_V lie below those due to CRD because both R_{II} and R_V are coherent in the line wings. Emergent flux due to R_{II} lies even below that due R_V because in the line wings R_{II} is much more coherent than R_V (see figures 3.1 & 3.2).

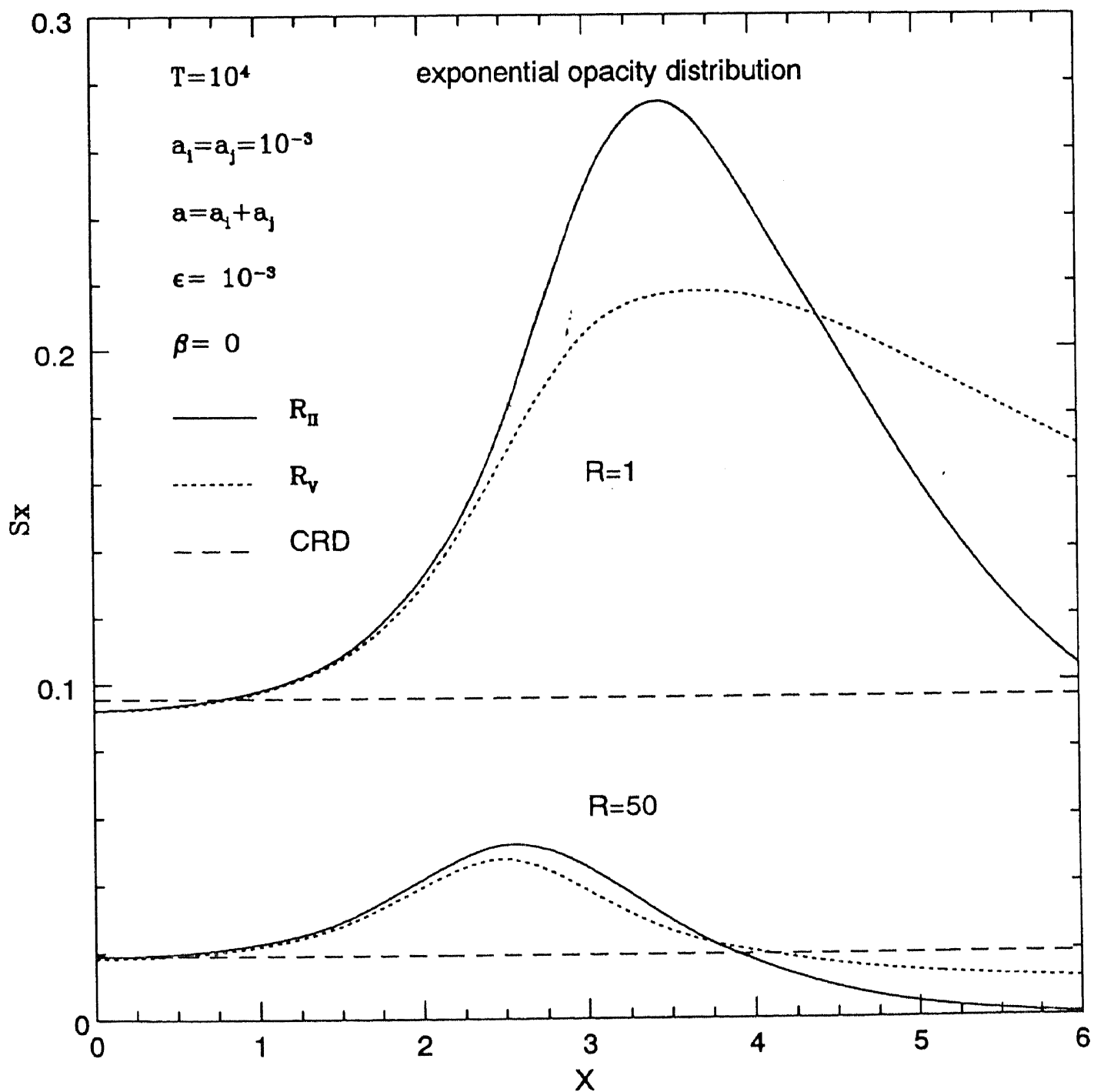


Figure 3.6: Emergent line source functions for the parameters shown in the figure.

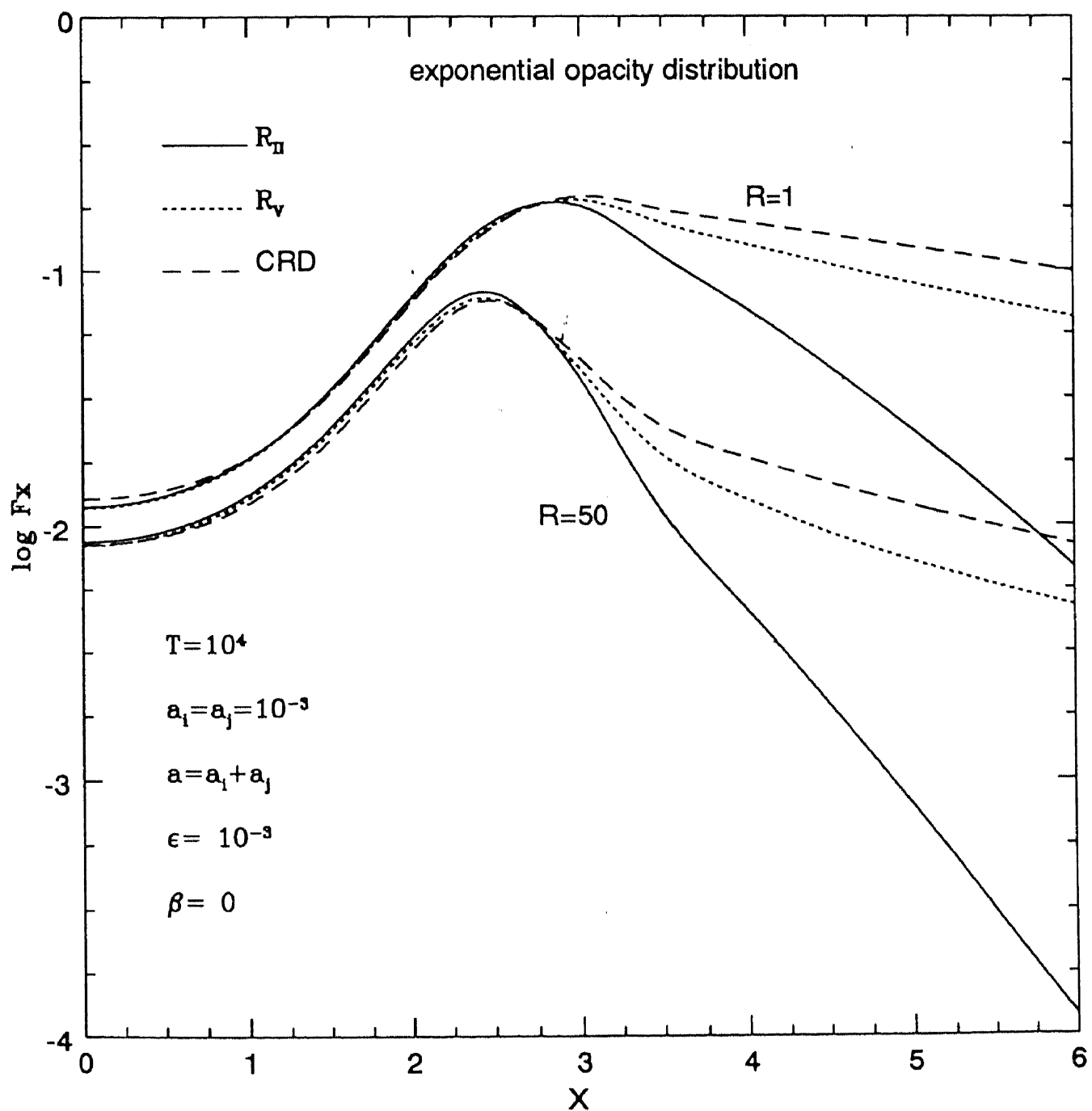


Figure 3.7: Emergent flux profiles corresponding to the source functions of fig.3.6.

Figure 3.8 gives the results of 'model Ab'. In this case, the lower level of the atom has been made ten times sharper (for R_V); from a value of $a_i = 10^{-3}$ to $a_i = 10^{-4}$.

There is a considerable change in the Sx curves due to R_V as compared to the curves given in figure 3.6. The values of Sx due to R_V have moved closer to the values of Sx due to R_{II} but have moved away from those of CRD. Thus the differences between the results due to R_V and CRD have increased. This is the consequence of making the lower level sharper and thus moving towards a condition for a resonance line where a_i tends to zero.

Figure 3.9 gives the emergent flux profiles corresponding to the source functions shown in figure 3.8.

First by looking at the plots for $R = 1$, it is seen that an increase in the ratio a_j/a_i from 1 in figure 3.7 to 10 in this case, has increased the departures between the emergent flux profiles due to R_V and CRD. This result is in qualitative agreement with the result of Hubeny & Heinzel [29]. In the line wings, the profiles due to R_V are closer to the profiles due to R_{II} than they were in figure 3.7. As mentioned above, this is the consequence of making the lower level sharper. Another noteworthy point is that these departures are enhanced by going from plane-parallel case ($R = 1$) to an extended spherically symmetric envelope having $R = 50$.

Now, the results using power law r^{-2} opacity are presented.

Figure 3.10 gives the results for 'model Ba'. Significant differences between the results of this figure and the corresponding results of figure 3.6 are not found, except that for $R = 50$ case the Sx curve due to R_V lies closer to that of R_{II} just outside the line core. Also in this figure $R = 50$ curves are much flatter than the corresponding ones in figure 3.6. This must be the effect of changing the opacity structure from exponential to r^{-2} form.

Figure 3.11 gives the emergent flux profiles corresponding to the source functions in figure 3.11. By comparing this figure with figure 3.7, the difference in the profile shapes for $R = 50$ are clearly seen. This is the effect of changing the opacity structure. But more *noteworthy* is the point that in the far line wing the departures between the PRD and CRD profiles are the same as for exponential opacity distribution. Therefore we can say that in the far wings of the emergent flux profiles, whereas the atmospheric extent is responsible for the departures between the solutions due to PRD and CRD; opacity structure is not. It only changes the line shape for the kind of atmospheres considered here.

Figure 3.12 gives the results of 'model Bb'. As compared to the results of figure 3.10, the line source function due to R_V lies closer to the Sx due to R_{II} . As in figure 3.8, this is again the consequence of making the lower level of the atom sharper by a factor of 10. As seen in figure 3.10, the curves for $R = 50$ are flatter than the corresponding curves (figure 3.8) using exponential opacity distribution.

Figure 3.13 gives the emergent flux profiles corresponding to the source functions given in figure 3.12. The effect of R_V is seen to be significantly enhanced as was the case in figure 3.9. Although the shape of the emergent profiles for $R = 50$ is conspicuously different from

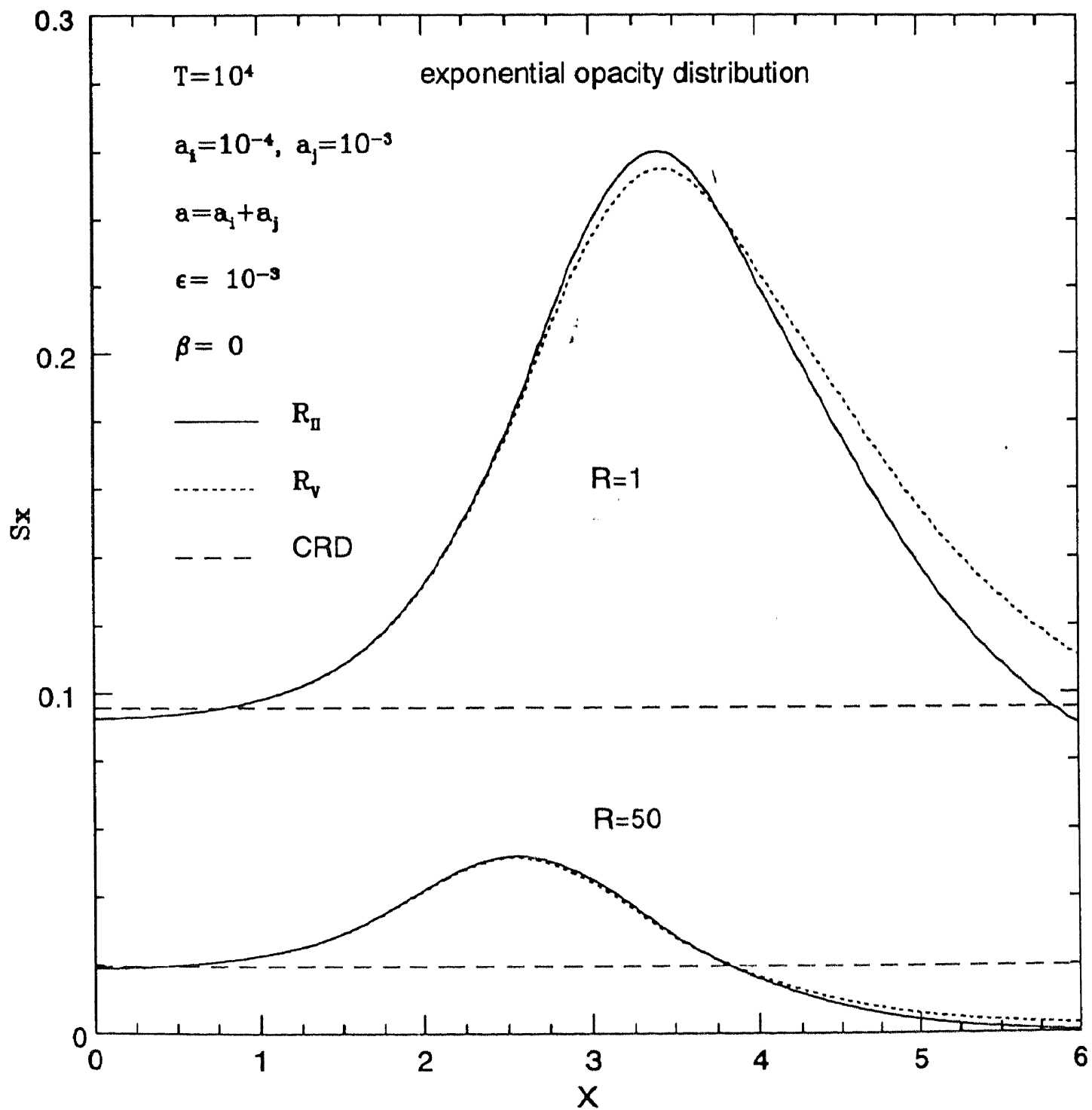


Figure 3.8: Same as fig. 4a but for $a_j/a_i = 10$.

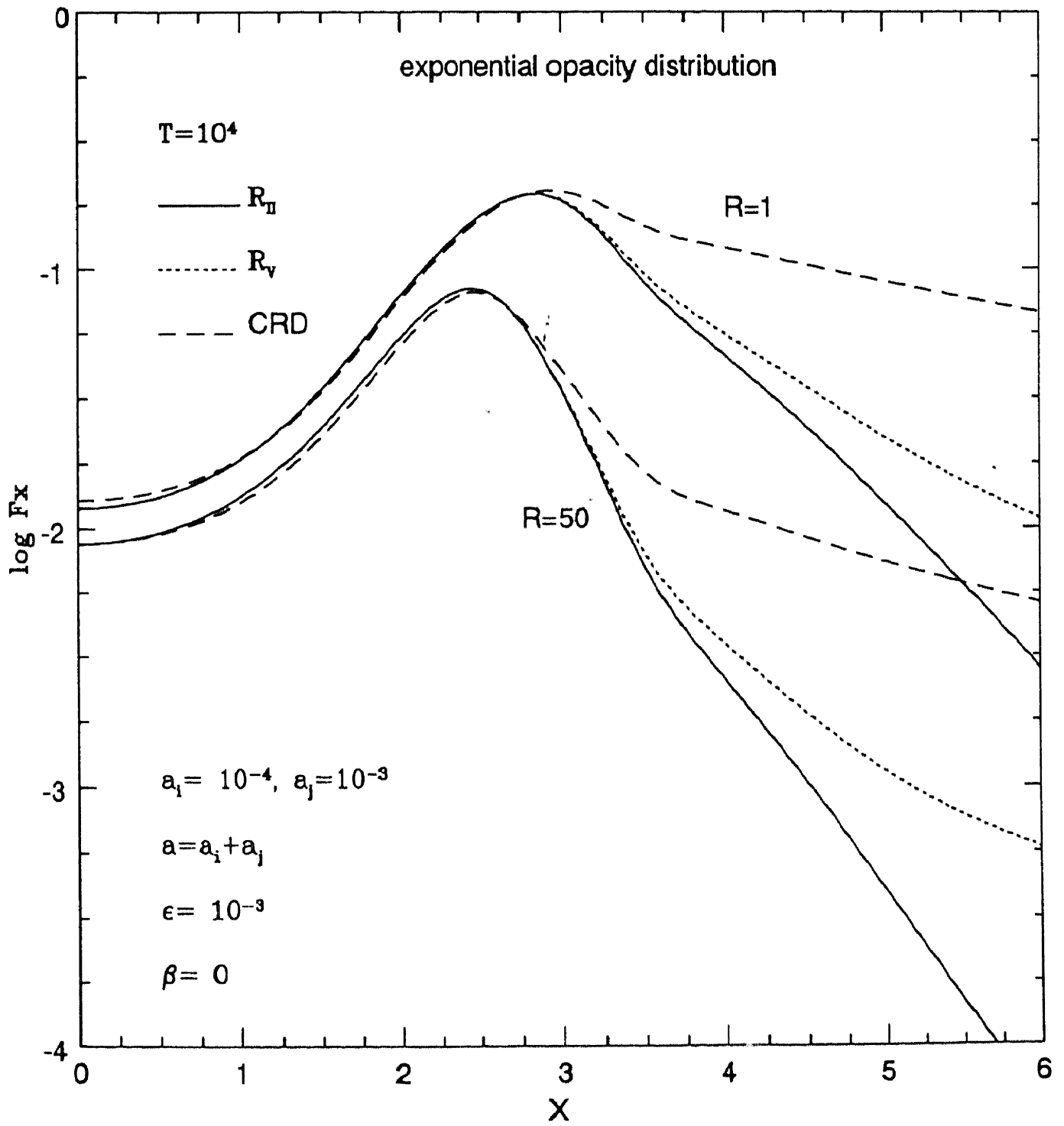


Figure 3.9: Emergent flux profiles corresponding to the line source functions of fig.3.8.

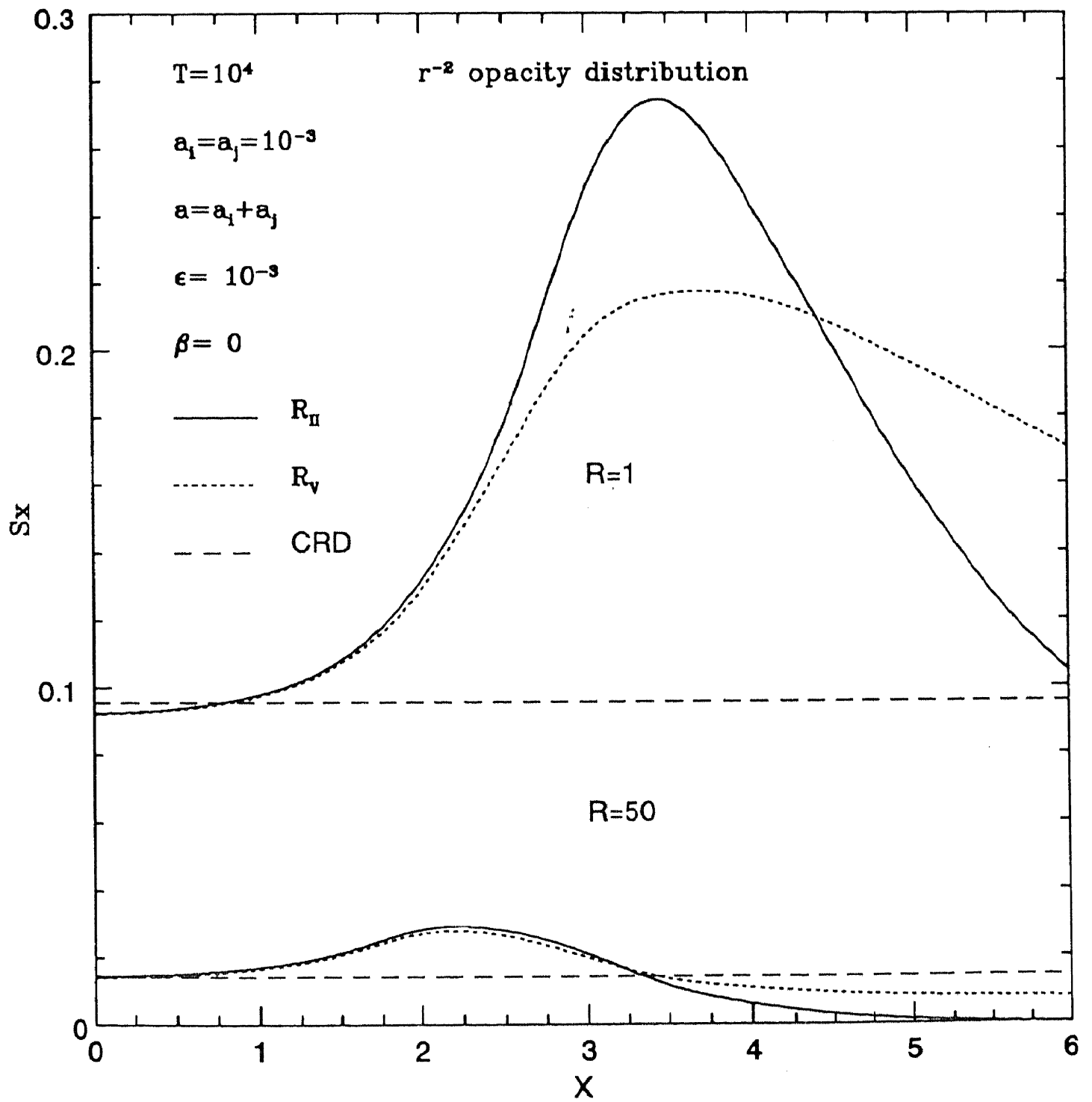


Figure 3.10: Same as fig.3.6 but for r^{-2} opacity distribution.

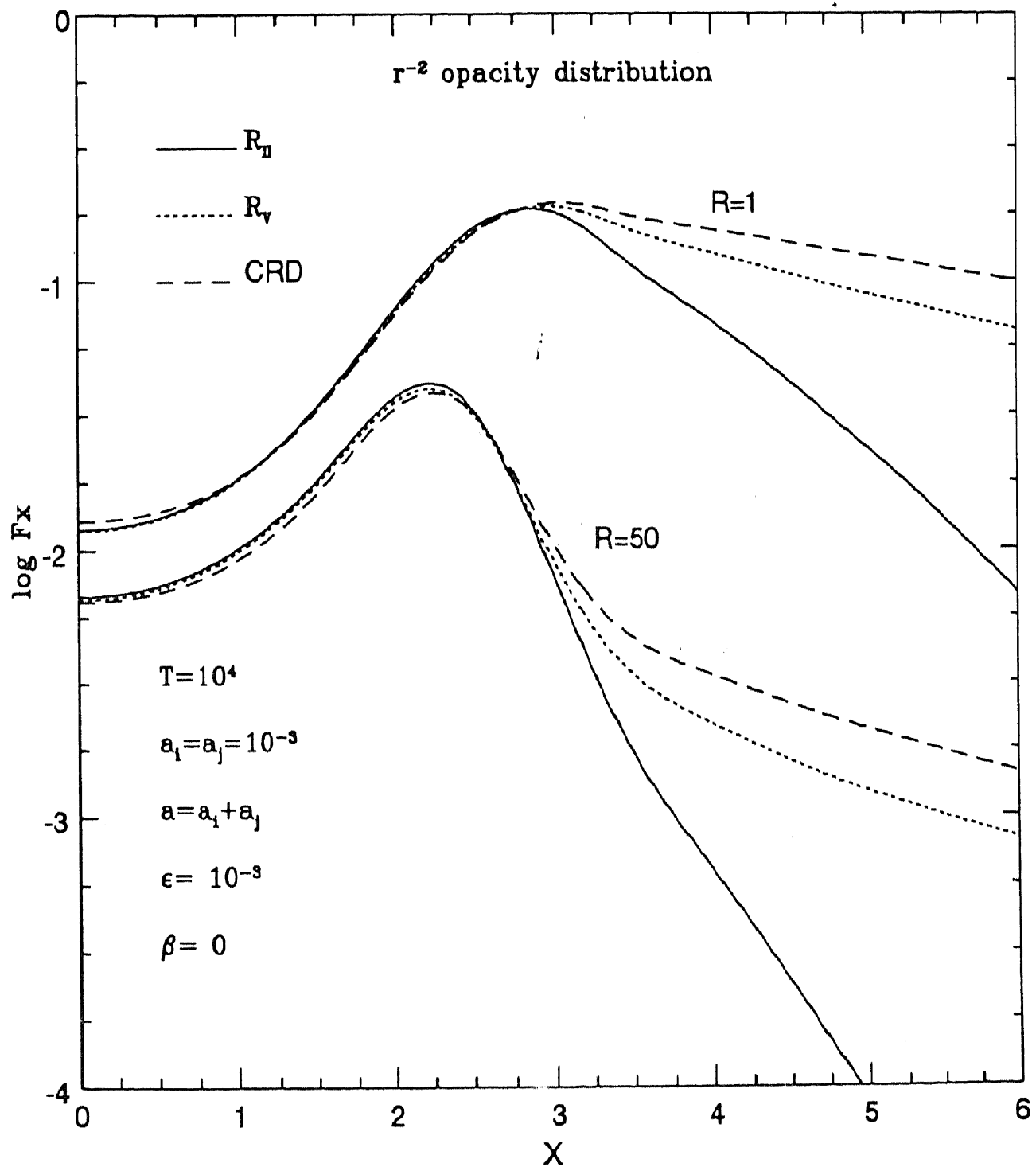


Figure 3.11: Emergent flux profiles corresponding to the line source functions of fig.3.10.

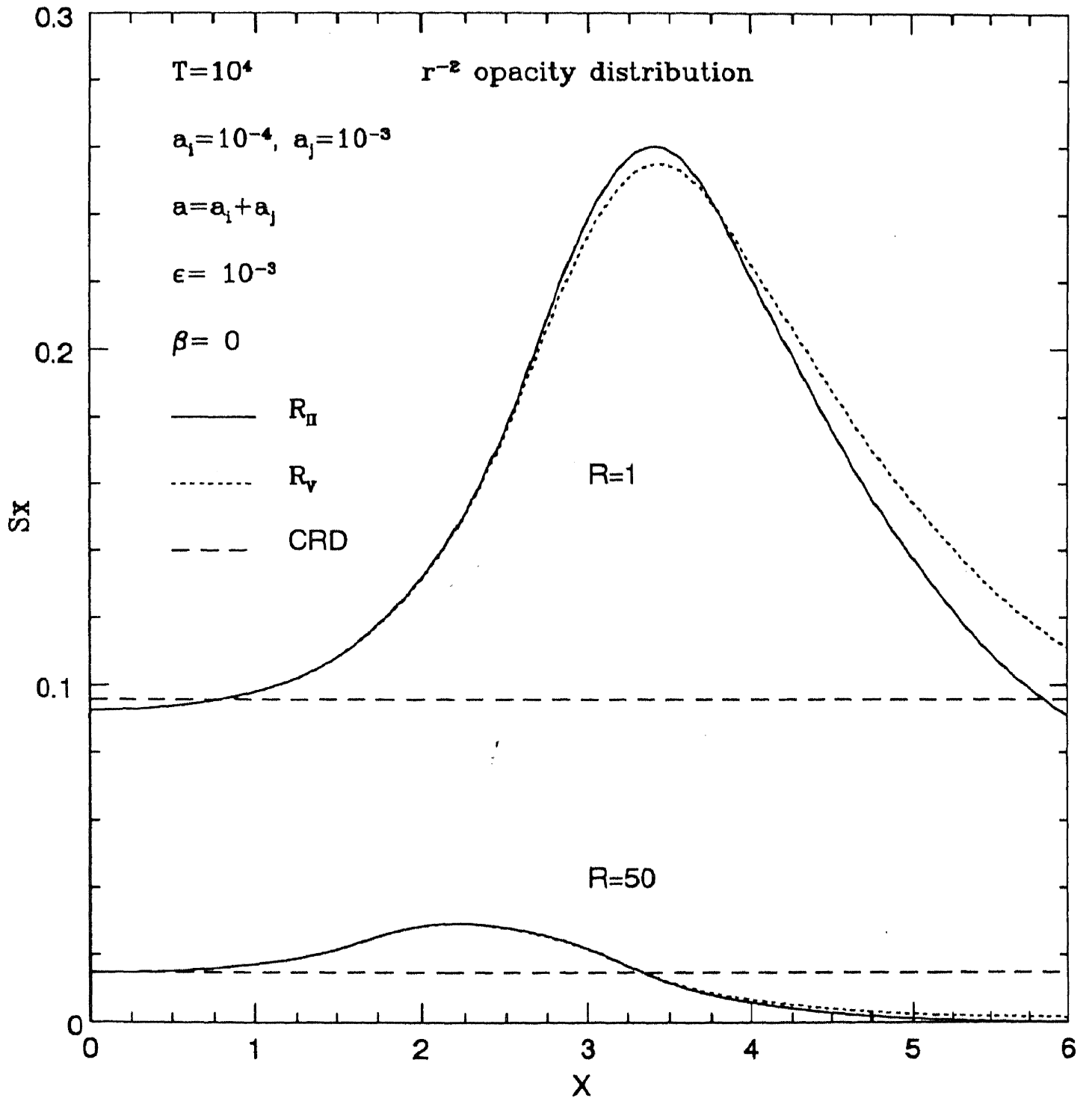


Figure 3.12: Same as fig.3.10 but for $a_j/a_i = 10$, $a = 1.1 \times 10^{-3}$.

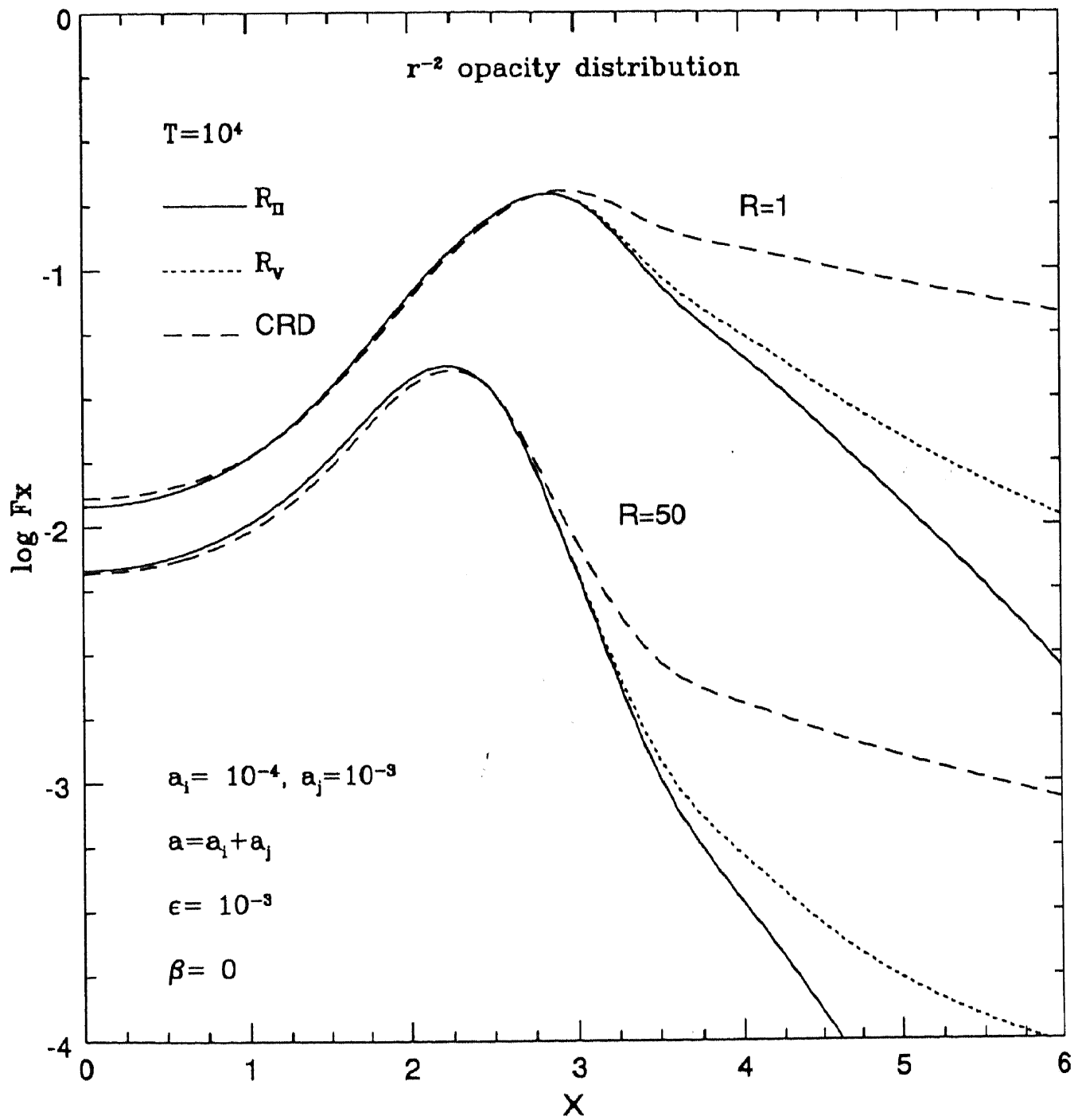


Figure 3.13: Emergent flux profiles corresponding to the line source functions of fig.3.12.

Table 3.1: Flux ratios showing the departures between the emergent fluxes due to PRD and CRD at $x = 4$, for different values of atmospheric extension R . $R = 1$ represents plane-parallel approximation, whereas $R > 1$ represents an extended and spherically symmetric atmosphere. These results are for $a_j/a_i = 1, 10$

R	$a_j/a_i = 1$			$a_j/a_i = 10$		
	$F_x(CRD)$	$\frac{F_x(CRD)}{F_x(R_{II})}$	$\frac{F_x(CRD)}{F_x(R_V)}$	$F_x(CRD)$	$\frac{F_x(CRD)}{F_x(R_{II})}$	$\frac{F_x(CRD)}{F_x(R_V)}$
1	0.154E+00	0.221E+01	0.122E+01	0.120E+00	0.261E+01	0.215E+01
5	0.517E-01	0.351E+01	0.141E+01	0.339E-01	0.407E+01	0.306E+01
10	0.290E-01	0.397E+01	0.146E+01	0.185E-01	0.456E+01	0.331E+01
50	0.691E-02	0.488E+01	0.153E+01	0.422E-02	0.547E+01	0.375E+01
100	0.440E-02	0.500E+01	0.154E+01	0.267E-02	0.558E+01	0.381E+01

Table 3.2: Same as above but for $x = 6$

R	$a_j/a_i = 1$			$a_j/a_i = 10$		
	$F_x(CRD)$	$\frac{F_x(CRD)}{F_x(R_{II})}$	$\frac{F_x(CRD)}{F_x(R_V)}$	$F_x(CRD)$	$\frac{F_x(CRD)}{F_x(R_{II})}$	$\frac{F_x(CRD)}{F_x(R_V)}$
1	0.987E-01	0.146E+02	0.152E+01	0.674E-01	0.242E+02	0.623E+01
5	0.249E-01	0.510E+02	0.173E+01	0.153E-01	0.730E+02	0.847E+01
10	0.134E-01	0.681E+02	0.176E+01	0.817E-02	0.921E+02	0.879E+01
50	0.298E-01	0.104E+02	0.178E+01	0.178E-02	0.126E+03	0.915E+01
100	0.187E-02	0.112E+02	0.179E+01	0.112E-02	0.132E+03	0.918E+01

the shape of corresponding profiles given in figure 3.9, the differences in the far wing between the PRD and CRD profiles do not seem to be different. Thus again, the change in opacity structure does not change the departures between PRD and CRD in far wings.

In order to further elucidate the above effects, the following three tables are presented. These tables give the ratios of the emergent fluxes due to CRD to the corresponding emergent fluxes due to PRD (R_{II} and R_V), indicating the departures of the results of PRD from those of CRD at $x = 4, 6$ and 8 for different values of the atmospheric extension R . Along with these ratios, CRD results are explicitly tabulated so that the ratios can be unravelled. Because the emergent flux profiles due to PRD and CRD are nearly the same in the line core ($x \in [0, 3]$), and most of the departures are in the line wings, we chose to present the emergent flux ratios only for $x = 4, 6$ and 8 in these tables. As defined earlier, $R = 1$ denotes the plane-parallel approximation, whereas, $R > 1$ denotes extended spherically symmetric atmospheres.

Tables 3.1, 3.2 and 3.3 gives the results at $x = 4$, $x = 6$ and at $x = 8$, respectively. The comparison is shown for the ratios $a_j/a_i = 1$ & $a_j/a_i = 10$. The effect of R_{II} is clearly more than the effect of R_V , both as a function of x and R . The given flux ratios are seen to increase much more sharply in going from $R = 1$ to 5 than in going from $R = 5$ to higher values, especially for R_{II} cases tabulated here for $x = 6$ and $x = 8$. Thus the geometry of the system

Table 3.3: Same as above but for $x = 8$

R	$a_j/a_i = 1$			$a_j/a_i = 10$		
	$F_x(CRD)$	$\frac{F_x(CRD)}{F_x(R_{II})}$	$\frac{F_x(CRD)}{F_x(R_V)}$	$F_x(CRD)$	$\frac{F_x(CRD)}{F_x(R_{II})}$	$\frac{F_x(CRD)}{F_x(R_V)}$
1	0.653E-01	0.149E+03	0.166E+01	0.417E-01	0.330E+03	0.857E+01
5	0.144E-01	0.706E+03	0.179E+01	0.868E-02	0.957E+03	0.960E+01
10	0.764E-02	0.815E+03	0.180E+01	0.458E-02	0.100E+04	0.968E+01
50	0.166E-02	0.789E+03	0.181E+01	0.988E-03	0.876E+03	0.973E+01
100	0.104E-02	0.781E+03	0.180E+01	0.602E-03	0.860E+03	0.972E+01

plays an important role for resonance line transfer in the far wings ($x > 6$). At frequencies $x = 4$ and 6 the departures between PRD and CRD results keep on increasing from $R = 1$ to 100, but at $x = 8$ the maximum departure occurs at $R = 10$ for R_{II} and at $R = 50$ for R_V for the physical parameters considered in this study. It is obvious from the results for the ratio $a_j/a_i = 10$, that the departures between PRD and CRD results are considerably more than those in the case where $a_j/a_i = 1$. Increase in R enhances these departures in the same trend as when $a_j/a_i = 1$.

3.4 Conclusions

The effects of angle-averaged R_V in spherically symmetric stellar atmospheres are investigated in comparison to the effects of angle-averaged R_{II} and complete redistribution approximation. This study establishes that for static and isothermal atmospheres, the partial frequency redistribution effects are significantly enhanced in transition from a plane-parallel to an extended spherically symmetric stellar atmosphere. In a comparative way, it has been shown that sphericity affects the solutions of R_{II} more than the solutions of R_V . The effect of R_V on the emergent flux profiles increases substantially by making the lower level of the atom sharper. This effect is found to get further enhanced in transition from a plane-parallel to an extended atmosphere case. These differences between the emergent flux profile due to PRD and CRD do not seem to vary by altering the opacity distribution in the atmosphere, at least for the exponential and r^{-2} forms used in this study. In the line wings, the departures between the results due to PRD and CRD increase much more rapidly for small atmospheric extensions than for larger extensions.

Chapter 4

Partial frequency redistribution effects of R_V and R_{II} in expanding spherically symmetric stellar atmospheres

4.1 Introduction

In the last chapter, we presented the comparative partial frequency redistribution effects of R_V and R_{II} on the spectral line formation in spherically symmetric *static* stellar atmospheres. In this chapter, we examine the same problem by including a constant velocity of expansion. In the previous chapter, the velocity fields were neglected in order to estimate the effect of *sphericity alone*. This chapter shows the combined effect of sphericity and velocity field, using the partial frequency redistribution functions R_V and R_{II} , in comparison to the effects of the assumption of complete redistribution (CRD). Thus this study inspite of being parametric, goes a step closer to a realistic situation of extended atmosphere and velocity of expansion. The atmosphere is assumed to be inhomogeneous and isothermal.

Mohan Rao et al. [45] examined the effects of R_{II} , R_{III} and R_V on the line source functions using *planar geometry* and *static* isothermal atmosphere. They showed that, for a purely scattering medium with frequency independent incident radiation, the frequency dependent source function $S_L(R_V)$, lies below $S_L(R_{III})$ but above $S_L(R_{II})$ in the line wings. Singh [66] investigated the comparative effects R_V , R_{II} and CRD on the emergent flux profiles, using a *spherically symmetric and static* stellar atmosphere. Hubeny & Heinzel [29] solved the transfer problem using R_V and R_{II} for isothermal finite and semi-infinite atmospheres. Besides these few works, it is difficult to find a comparative study in literature involving R_V , R_{II} and CRD. Therefore, in this chapter, we present, for the first time, a comparative study of the partial frequency redistribution functions R_V , R_{II} and CRD showing the combined effect of *sphericity and velocity fields*.

As highlighted in the previous chapters, this study is an interesting study of astrophysical relevance, because the PRD effects are expected to be pronounced in the extended atmospheres with low surface gravities. The physical parameters used in this study are characteristic of the atmospheres of *cool giants and supergiant stars*.

4.2 Equations and computational procedure

If x' and x are the frequency displacements from line center, in units of standard Doppler width, of the incident and scattered photons respectively, seen in the *rest frame*, then, the corresponding frequency displacements, seen in the *fluid frame* at radius r , are

$$X' = x' \pm V(r)\mu \quad (4.1)$$

$$X = x \pm V(r)\mu \quad (4.2)$$

where $\mu (\in [0, 1])$ is the cosine of the angle between the radius vector and the direction of propagation of the radiation, \pm stands for the oppositely directed beams of radiation, and $V(r)$ gives the macroscopic velocity at radius r . In this chapter we assume that the atmosphere expands with a uniform velocity, i.e., we neglect velocity gradient across the atmosphere. This kind of situation may arise in circumstellar shells where one can neglect the velocity gradients by assuming a constant wind velocity.

The equation of line transfer in spherical symmetry, rest frame and for a two-level atomic model is written as (Peraiah [52], Singh [65])

$$\pm \mu \frac{\partial I(x, \pm \mu, r)}{\partial r} \pm \frac{1 - \mu^2}{r} \frac{\partial I(x, \pm \mu, r)}{\partial \mu} = K_I [\beta + \phi(x, \pm \mu, r)] [S(x, \pm \mu, r) - I(x, \pm \mu, r)] \quad (4.3)$$

where \pm stands for the oppositely directed beams of radiation, $I(x, \pm \mu, r)$ represents specific intensity of the ray making an angle $\cos^{-1} \mu$ ($\mu \in [0, 1]$) with radius vector at the radial point r . $\phi(x, \pm \mu, r)$ represents the profile function, given as

$$\phi(x, \pm \mu, r) = \phi(X, r) = \int_{-\infty}^{+\infty} R_{II,V}(X', X) dX' \quad (4.4)$$

where angle-averaged partial frequency redistribution functions $R_{II,V}(X', X)$ have been stated and explained in the previous chapter (see equations 3.8 & 3.9 and figures 3.1 & 3.2).

Redistribution function R_V is derived for subordinate line scattering and assumes an atom having both the upper level and the lower level broadened by radiative and collisional damping. R_{II} envisions an atom having a sharp lower level and a radiatively broadened upper level.

$S(x, \pm\mu, r)$ is the total (line plus continuum) source function which is written as

$$S(x, \pm\mu, r) = \frac{\phi(X, r)S_l(x, \pm\mu, r) + \beta S_c(r)}{\phi(X, r) + \beta} \quad (4.5)$$

where $\beta = K_c/K_l$ (continuum to line opacity, S_c is the continuum source function set equal to 1 in this computation. $S(x, \pm\mu, r)$ represents the line source function, which is given by the following expression

$$S_l(x, \pm\mu, r) = \frac{1}{2} \frac{1 - \epsilon}{\phi(X, r)} \int_{-\infty}^{+\infty} dx' \int_{-1}^{+1} d\mu' R_{II,V}(X', X) I(x', \pm\mu, r) + \epsilon B(r) \quad (4.6)$$

where ϵ is the probability per scatter that a photon is destroyed by collisional de-excitation. The procedure to compute ϵ for the chosen resonance lines has been given above in section 5.3.

Under the assumption of complete redistribution, the line source function is written as

$$S_l(r) = \frac{1 - \epsilon}{2} \int_{-\infty}^{+\infty} dx \int_{-1}^{+1} d\mu \phi(X, r) I(x, \pm\mu, r) + \epsilon B(r) \quad (4.7)$$

where $\phi(X, r)$ is taken to be a Voigt profile with damping parameter set equal to the sum of the damping parameters (for R_{II} and CRD) of the upper and lower levels of an atom causing subordinate line scattering.

The normalization condition for the profile function at each radial point is

$$\int_{-\infty}^{+\infty} dx \phi(X, r) = 1 \quad (4.8)$$

In a differentially expanding medium, due to the presence of velocity gradients, one has to compute, at all radial points all the four redistribution functions appearing in the scattering integral viz

$$\begin{aligned} &R_{II,V}(x' + V(r)\mu, x + V(r)\mu) \\ &R_{II,V}(x' - V(r)\mu, x - V(r)\mu) \\ &R_{II,V}(x' + V(r)\mu, x - V(r)\mu) \\ &R_{II,V}(x' - V(r)\mu, x + V(r)\mu) \end{aligned}$$

in order to evaluate the diffuse radiation field (see chapter 2 & Peraiah [52, 55]).

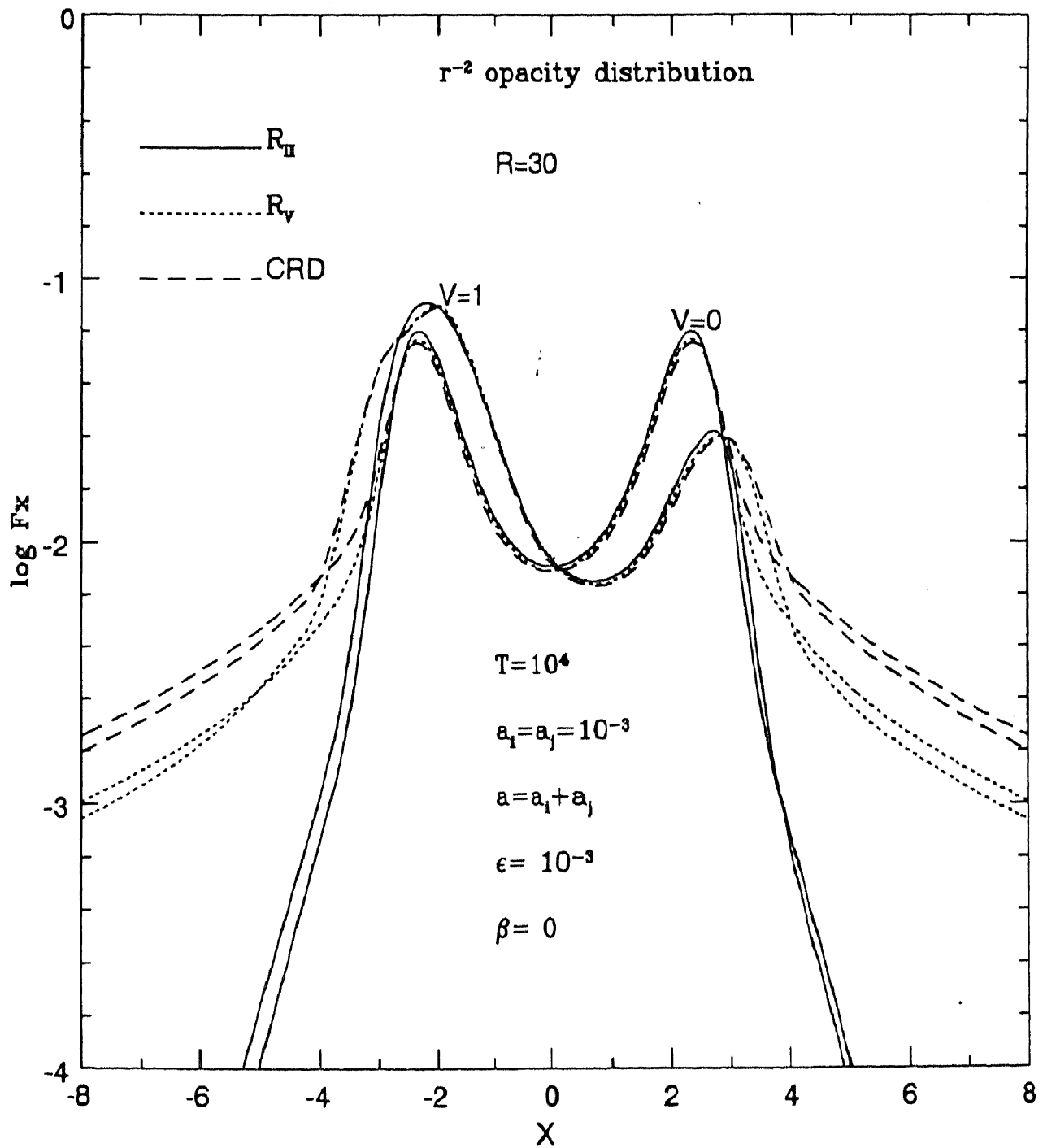


Figure 4.1: Emergent flux from an expanding atmosphere having the velocity of expansion $V = 1$ in units of thermal velocity; $R = 1$ denotes plane-parallel case and $R = 30$ denotes the extended atmosphere having an extension 30 times the stellar radius (set equal to 1).

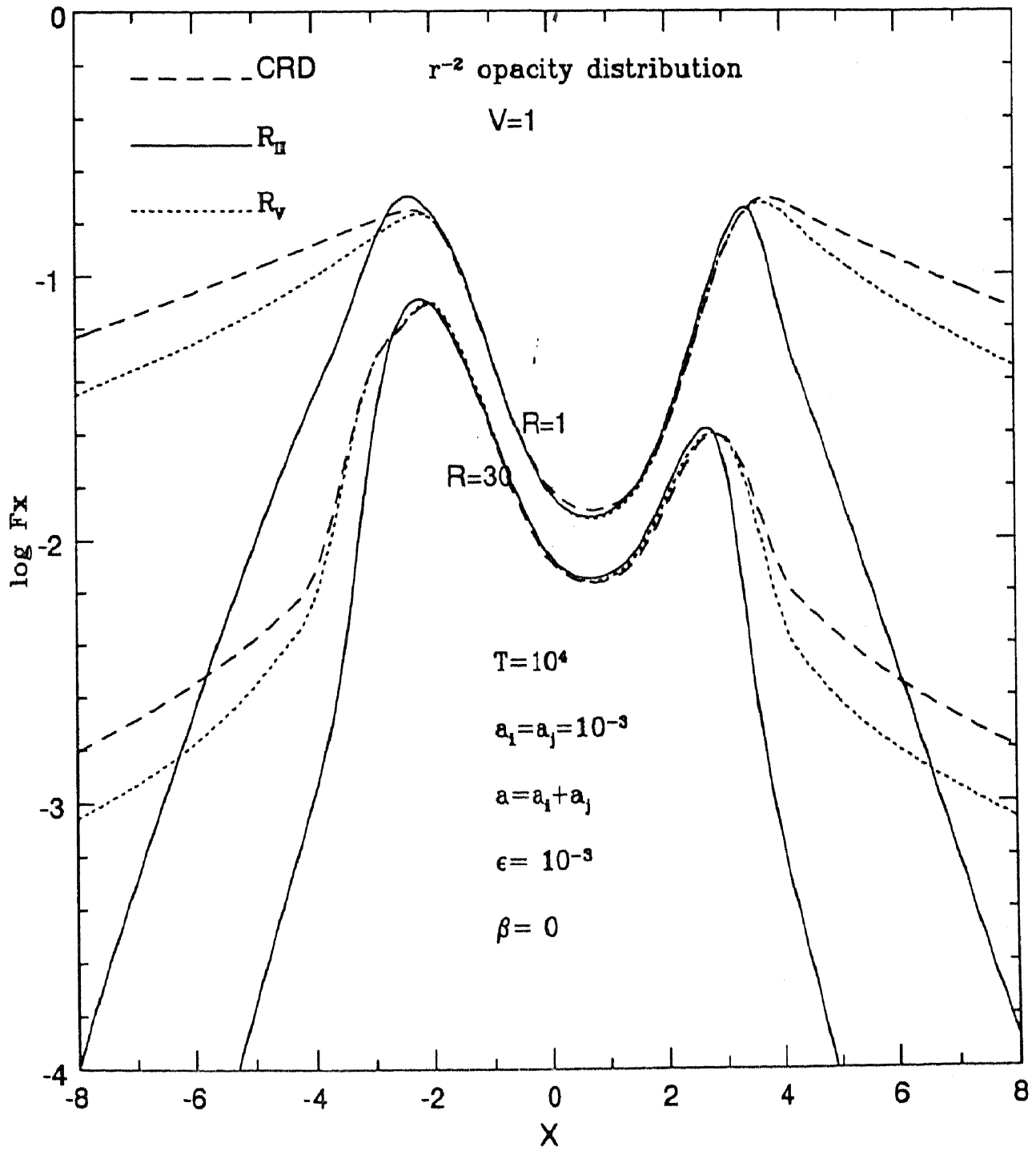


Figure 4.2: The effect of expansion velocity $V = 1$ in comparison to static case $V = 0$ for an extended atmosphere $R = 30$.

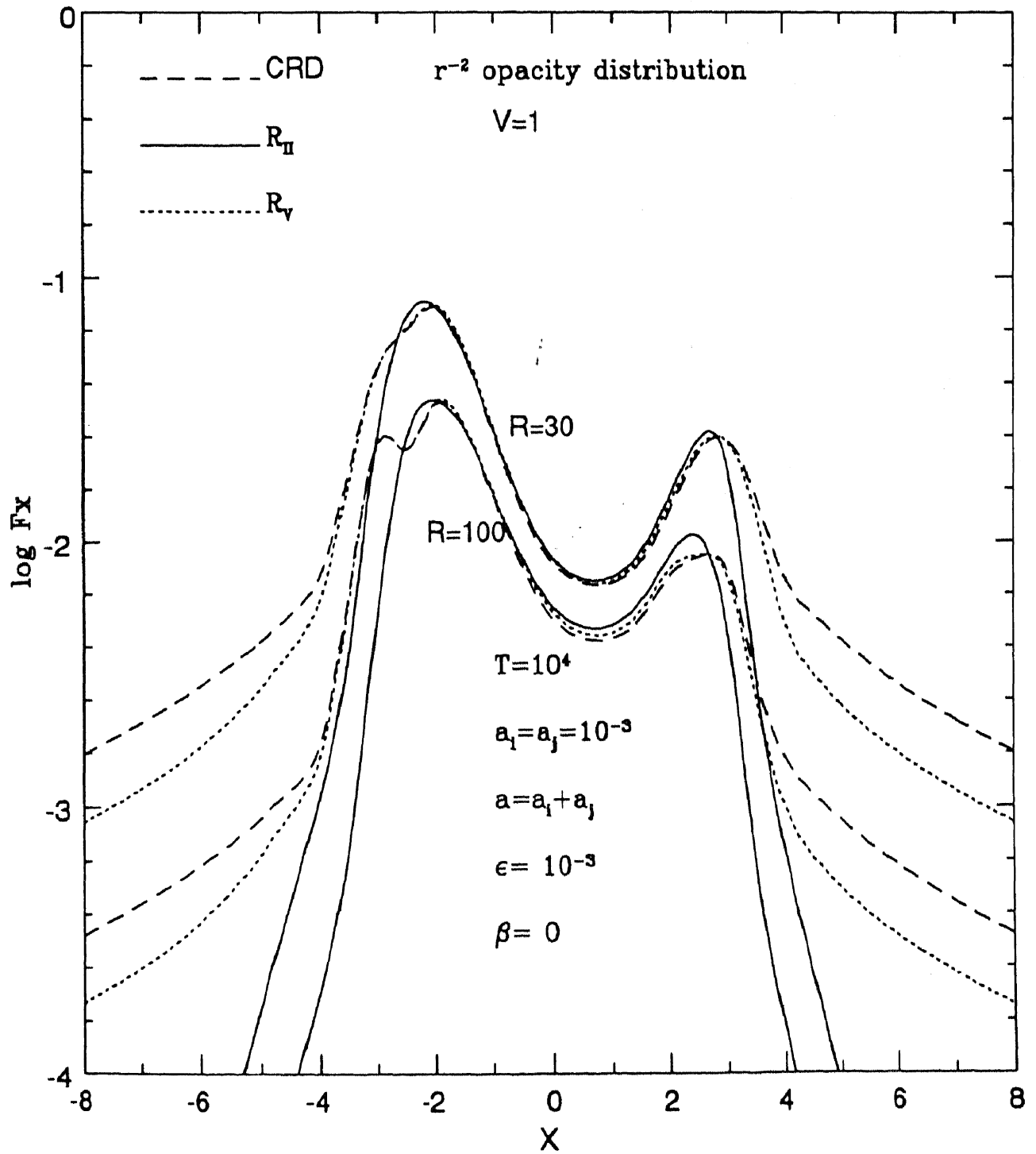


Figure 4.3: The effect of increasing the atmospheric extension from $R = 30$ to $R = 100$ for an atmosphere with constant velocity of expansion $V = 1$.

In this work since we assume a constant expansion velocity, we do not have velocity gradients across the atmosphere. This assumption is valid for expanding circumstellar shells; and reduces the computational time of the R_V and R_{II} matrices enormously. The above written redistribution functions are computed at one depth point in the atmosphere, and the other corresponding redistribution functions at other depth points are equal to these. As is known from the works of Bernat [11] Sanner [63] and several other authors, the ratio of expansion velocity to the turbulent velocity for cool giants and supergiants lies between 0.5 and 2.0. Therefore, in this study for all the cases the value of this ratio has been chosen to be equal to 1.0 at all depth points of the atmosphere. The envelope is divided into n shells, $n = 1$ defines the outermost shell and $n = N$ defines the innermost shell. The total optical depth, T , of the medium has been set equal to 10^4 . The total number of shells have been taken equal to 25 in this study. The sensitivity of the results for static cases has been discussed in detail in the previous chapter section 3.2.2. Because at this stage, we are interested only in the departures between the solutions due to various redistribution functions, rather than modeling any specific spectral line, the choice of $N = 25$ is justified.

Ideally, for moving media calculations, one should use *angle-dependent* redistribution functions, because the frequency-angular coupling effects could be important in anisotropic radiation field. By employing angle-averaged redistribution functions, we have neglected the angular effects (which are of secondary importance to this study) but have *fully accounted for frequency redistribution effects*. Also, it has been shown by Vardavas [73] that for planar geometries and differentially expanding medium, the differences between the results due to angle-dependent and angle-independent redistribution functions are below 10%. Moreover we have considered only *constant* velocity of expansion leading to the absence of velocity gradients, therefore, it is justified to use angle-independent redistribution functions.

Following boundary condition has been used for the transfer equation

$$U_{n=1}^+(x, \mu) = 0 \quad \text{and} \quad U_{N+1}^-(x, \mu) = 0 \quad (4.9)$$

where

$$U_n^\pm(x, \mu) = 4\pi r_n^2 I(x, \mu) \quad (4.10)$$

$I(x, \mu)$ being the specific intensity. $+$ specifies a ray directed towards the bottom of the envelope ($\tau = T$), and $-$ specifies a ray directed out of the envelope.

To solve the line transfer equation the **discrete space theory** method described in chapter 2 of this thesis has been used.

4.3 Results

Figure 4.1 shows the differences between the PRD and CRD results for a plane-parallel and extended atmosphere expanding with a constant velocity of $V = 1$ (in terms of thermal velocity). The differences are substantial for both the cases. Closer look at the profiles shows that the differences are slightly more for the extended atmosphere. Recalling the results of the previous chapter, we know, that sphericity enhances the PRD effects. It is also known from earlier works (e.g. see Hempe [26]) that increasing velocity decreases the PRD effects. In the present case, where both extension and velocity is present, the effects cancel out and the differences remain more or less the same for $R = 1$ and for $R = 30$.

Figure 4.2 shows the effect of introducing a constant wind velocity $V = 1$ (in thermal-velocity units) into an extended atmosphere $R = 30$. Asymmetry in the profile shape introduces enhanced departures between corresponding PRD and CRD results just outside the line core $x \approx \pm 3$. Overall differences remain significant.

Figure 4.3 shows the effect of increasing the extension from $R = 30$ to (over three times) $R = 100$. Differences are still found to be substantial. Another effect well known effect of increasing the extension is seen in this figure. The central absorption becomes shallower. This is because the effective emitting area increases in the line core by increasing the atmospheric extent.

4.4 Conclusion

The role of partial frequency redistribution functions R_V and R_{II} on the emergent flux profiles has been presented in a comparative way. Extended atmosphere and constant wind velocity has been assumed. It is shown by this study, that for the parameters used here, *the effects of partial frequency redistribution are substantial* for all cases discussed here. These results clearly demonstrate the importance of partial frequency redistribution functions in spectral line formation in the atmospheres of *cool giant and supergiant stars*.

Chapter 5

Effects of angle-averaged R_{III} on spectral line formation in expanding spherically symmetric stellar atmospheres

5.1 Introduction

After having explored the *combined effects* of sphericity and velocity fields on the spectral line formation, using partial frequency redistribution functions R_V and R_{II} , we now consider the redistribution function R_{III} *alone*. The *motivation* behind doing so is the following. Most often the limiting case of complete redistribution (CRD) is taken to be an adequate representation of the partial frequency redistribution (PRD) function R_{III} in radiative transfer problems to study spectral line formation in stellar atmospheres. The works of Finn [16] and Vardavas [71, 72] have shown that for plane parallel (static and moving) stellar atmospheres the differences between the emergent intensities due to R_{III} and CRD are below 20%. But, with the advent of very high resolution stellar spectroscopy (resolving power $\sim 10^5 - 2.10^5$), highly accurate line profiles (e.g. for bright giants and supergiants see Sanner [63] are available, therefore, even small differences between CRD and PRD profiles could be important in a quantitative analysis of stellar spectra e.g. in stellar winds and mass loss phenomenon in giants and supergiants (Hempe [26]). Also, the combined effect of sphericity and macroscopic velocity on these differences cannot be estimated *a priori*.

So far, there is no paper in literature showing the effects of R_{III} alone on spectral line formation in *spherically symmetric and differentially expanding* stellar atmospheres. Therefore, this paper has considered a parametrized spherically symmetric and differentially expanding stellar envelope to study the effects angle-averaged R_{III} on spectral line formation. Line transfer equation has been solved in the rest frame of the star assuming two-level atom model.

This work we have also examines the behaviour of emergent mean intensity profiles (J_x), the source function (S) and the emergent flux profiles (F_x) as a function of atmospheric extension (b/a = outer/inner stellar radius), maximum velocity of expansion (V_b) and the thermalization parameter (ϵ). The results are in aggrement with the earlier known results of Kunasz and Hummer [36] and Mihalas [38]. The mean intensity profiles due to $R_{III}(x', x)$ and CRD are compared. Here x' and x are the frequency displacements from the line centre in Doppler units of the incident and scattered photons respectively.

5.2 Basic equations and computational procedure

If x' and x are the frequency displacements from line centre, in units of standard Doppler width, of the incident and scattered photons respectively, seen in the *rest frame*, then, the corresponding frequency displacements, seen in the *fluid frame* at radius r , are

$$X' = x' \pm V(r)\mu \quad (5.1)$$

$$X = x \pm V(r)\mu \quad (5.2)$$

where $\mu (\in [0, 1])$ is the cosine of the angle between the radius vector and the direction of propagation of the radiation, \pm stands for the oppositely directed beams of radiation, and $V(r)$ gives the macroscopic velocity at radius r .

The line transfer equation for spherical geometry in the rest frame for a two-level atom model has the following form (Peraiah citeperl b)

$$\pm \mu \frac{\partial I(x, \pm \mu, r)}{\partial r} \pm \frac{1 - \mu^2}{r} \frac{\partial I(x, \pm \mu, r)}{\partial \mu} = K_l [\beta + \phi(x, \pm \mu, r)] [S(x, \pm \mu, r) - I(x, \pm \mu, r)] \quad (5.3)$$

where \pm stands for the oppositely directed beams of radiation, $I(x, \pm \mu, r)$ represents specific intensity of the ray making an angle $\cos^{-1} \mu$ ($\mu \in [0, 1]$) with radius vector at the radial point r . $\phi(x, \pm \mu, r)$ represents the profile function, given as

$$\phi(x, \pm \mu, r) = \phi(X, r) = \int_{-\infty}^{+\infty} R_{III}(X', X) dX' \quad (5.4)$$

where angle-averaged partial frequency redistribution function $R_{III}(X', X)$ has the following form (Mihalas [38])

$$\begin{aligned} R_{III}(X', X) &= \pi^{-5/2} \int_0^\infty \left[\tan^{-1}\left(\frac{X' + u}{a}\right) - \tan^{-1}\left(\frac{X' - u}{a}\right) \right] \\ &\times \left[\tan^{-1}\left(\frac{X + u}{a}\right) - \tan^{-1}\left(\frac{X - u}{a}\right) \right] du \end{aligned} \quad (5.5)$$

where a is the damping parameter set equal to 10^{-3} in this calculation. $S(x, \pm \mu, r)$ is the total (line plus continuum) source function which is written as

$$S(x, \pm \mu, r) = \frac{\phi(X, r) S_l(x, \pm \mu, r) + \beta S_c(r)}{\phi(X, r) + \beta} \quad (5.6)$$

where $\beta = K_c/K_l$ (continuum to line opacity, S_c is the continuum source function set equal to 1 in this computation. $S(x, \pm\mu, r)$ represents the line source function, which is given by the following expression

$$S_l(x, \pm\mu, r) = \frac{1}{2} \frac{1 - \epsilon}{\phi(X, r)} \int_{-\infty}^{+\infty} dx' \int_{-1}^{+1} d\mu' R_{III}(X', X) I(x', \pm\mu, r) + \epsilon B(r) \quad (5.7)$$

where ϵ is the probability per scatter that a photon is destroyed by collisional de-excitation written as

$$\epsilon = \frac{C_{21}}{C_{21} + A_{21}[1 - \exp(-\frac{h\nu}{k\theta})]^{-1}} \quad (5.8)$$

where C_{21} is the rate of collisional de-excitation from level 2 to 1, A_{21} is Einstein's spontaneous emission probability for transition $2 \rightarrow 1$, h is the Planck's constant, ν is the photon frequency, k is the Boltzmann's constant and θ is the temperature.

Under the assumption of complete redistribution, the line source function is written as

$$S_l(r) = \frac{1 - \epsilon}{2} \int_{-\infty}^{+\infty} dx \int_{-1}^{+1} d\mu \phi(X, r) I(x, \pm\mu, r) + \epsilon B(r) \quad (5.9)$$

where $\phi(X, r)$ is taken to be a Voigt profile with damping parameter set equal to 10^{-3} .

The normalization condition for the profile function at each radial point is

$$\int_{-\infty}^{+\infty} dx \phi(X, r) = 1 \quad (5.10)$$

In a differentially expanding medium, due to the presence of velocity gradients, one has to compute, at all radial points all the four redistribution functions appearing in the scattering integral (equation 5.9) viz

$$\begin{aligned} &R(x' + V(r)\mu, x + V(r)\mu), \\ &R(x' - V(r)\mu, x - V(r)\mu), \\ &R(x' + V(r)\mu, x - V(r)\mu) \text{ and} \\ &R(x' - V(r)\mu, x + V(r)\mu) \end{aligned}$$

in order to evaluate the diffuse radiation field (Peraiah [52, 55])

In this work, a linear velocity law given in Peraiah [52] has been used, which gives a radially increasing velocity, with minimum velocity (V_a) at the innermost boundary and maximum velocity of expansion (V_b) at the outer boundary of the stellar envelope. The envelope is divided into n shells, each of equal radial thickness, $n = 1$ defines the outermost shell ($\tau = 0$) and $n = N$ defines the innermost shell ($\tau = T$). Total optical depth (T) of the envelope has been taken to be 10^3 and we have set $N = 10$ in these computations. Optical depth (τ) through the envelope varies as r^{-2} . V_b has been set equal to 1 and 2 in units of mean thermal velocity of the gas. Rest frame calculation is limited to low expansion velocities due to numerical difficulties. Following are the boundary conditions used for the transfer equation

$$U_1^+(x, \tau = 0, \mu) = 0 \text{ and } U_{N+1}^-(x, \tau = T, \mu) = 0 \text{ if } \epsilon > 0 \quad (5.11)$$

$$U_1^+(x, \tau = 0, \mu) = 0 \text{ and } U_{N+1}^-(x, \tau = T, \mu) = 1 \text{ if } \epsilon = 0 \quad (5.12)$$

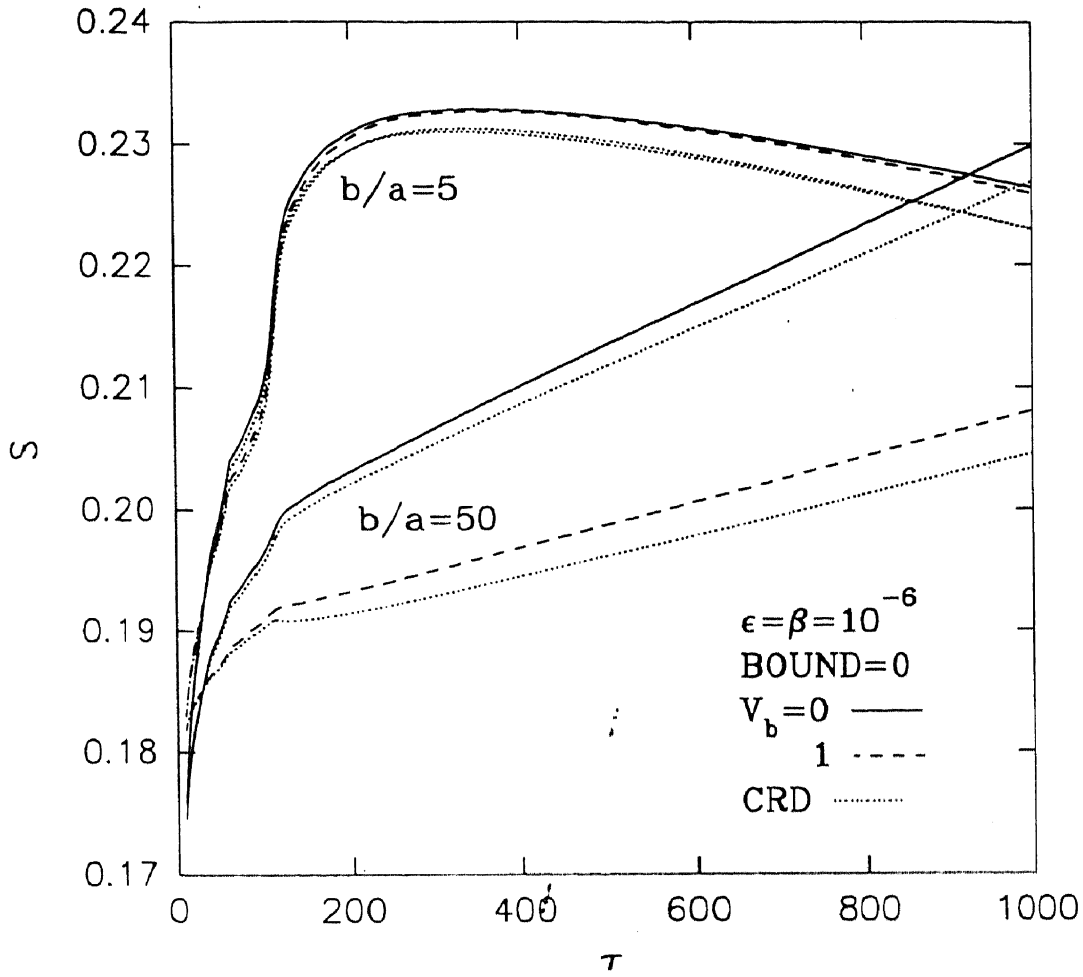


Figure 5.1: Source function S versus optical depth τ through spherically symmetric and differentially expanding envelope having $b/a = 5, 50$; $V_b = 0, 1$; and $T = 10^3$. Corresponding CRD results are shown by dotted (....) lines.

where

$$U_n^\pm(x, \tau, \mu) = 4\pi r_n^2 I(x, \mu, \tau(r_n)) \quad (5.13)$$

$I(x, \mu, \tau(r_n))$ being the specific intensity. + specifies a ray directed towards the bottom of the envelope ($\tau = T$), and - specifies a ray directed out of the envelope. The Planck's function has been set equal to 1 throughout the medium. Flux conservation has been maintained accurate to the order of 10^{-10} in double precision for purely scattering medium i.e. when $\epsilon = 0$ (Peraiah [56]).

To solve the above equations the *discrete space theory method* described in chapter 2 of this thesis has been used.

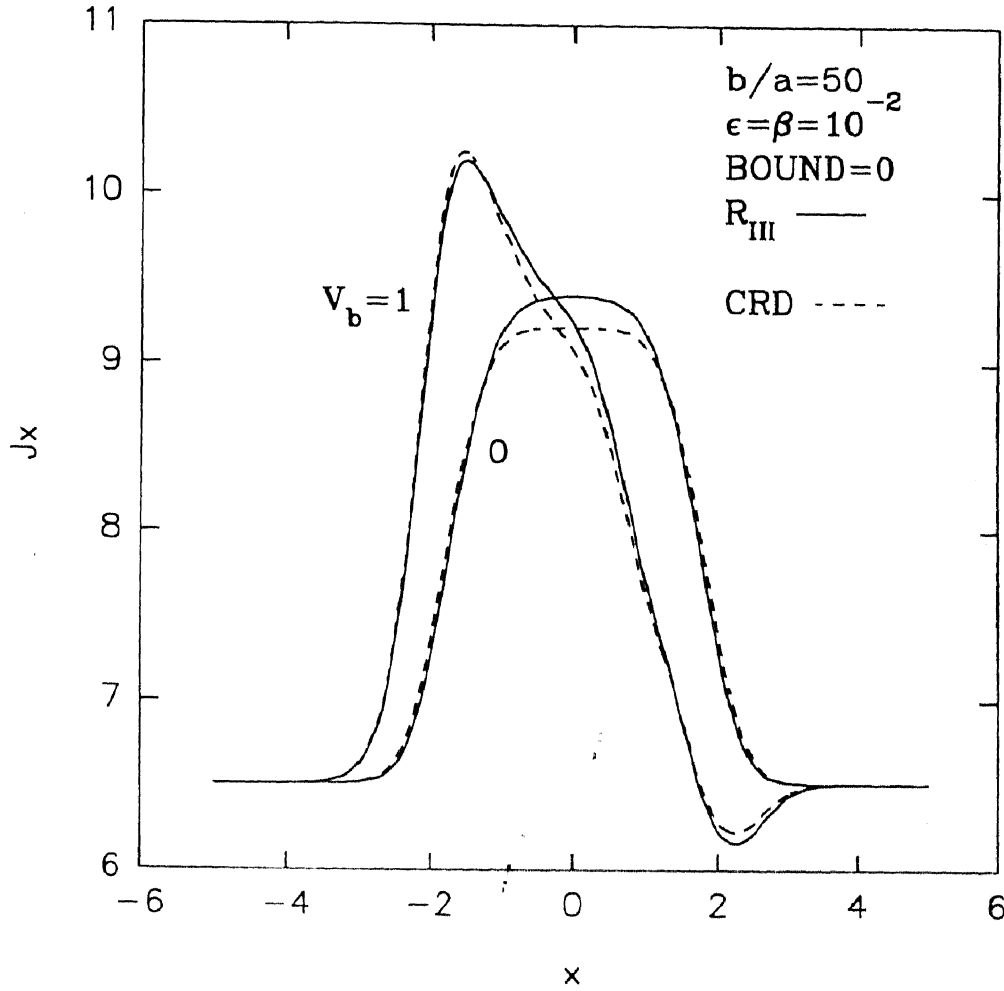


Figure 5.2: Emergent mean intensities J_x in the line versus x , corresponding to source functions of figure 1. $x = (\nu - \nu_0)/w$; w being standard Doppler width.

5.3 Results

Figure 5.1 gives the run of the source function S as a function of optical depth τ through a spherically symmetric and differentially expanding envelope where $\epsilon = \beta = 10^{-6}$. We recover the known results that the increase in velocity and extension suppresses the source functions. We also see that the effect of expansion velocity is more at larger extension. The source functions due to CRD are less than those due to R_{III} .

Figure 5.2 gives the mean intensity profiles J_x corresponding to the source functions shown in figure 1. We see that at any given velocity of expansion the mean intensity in the line is lower for larger extension. The profiles are asymmetric for $V_b = 1$ (expressed in mean thermal velocity of the gas). *More important is the result* that the difference between the CRD and R_{III} profiles is below 5% near the line centre and negligible at the wings. This is much smaller than reported for planar geometries by Finn [16] and Vardavas [71, 72].

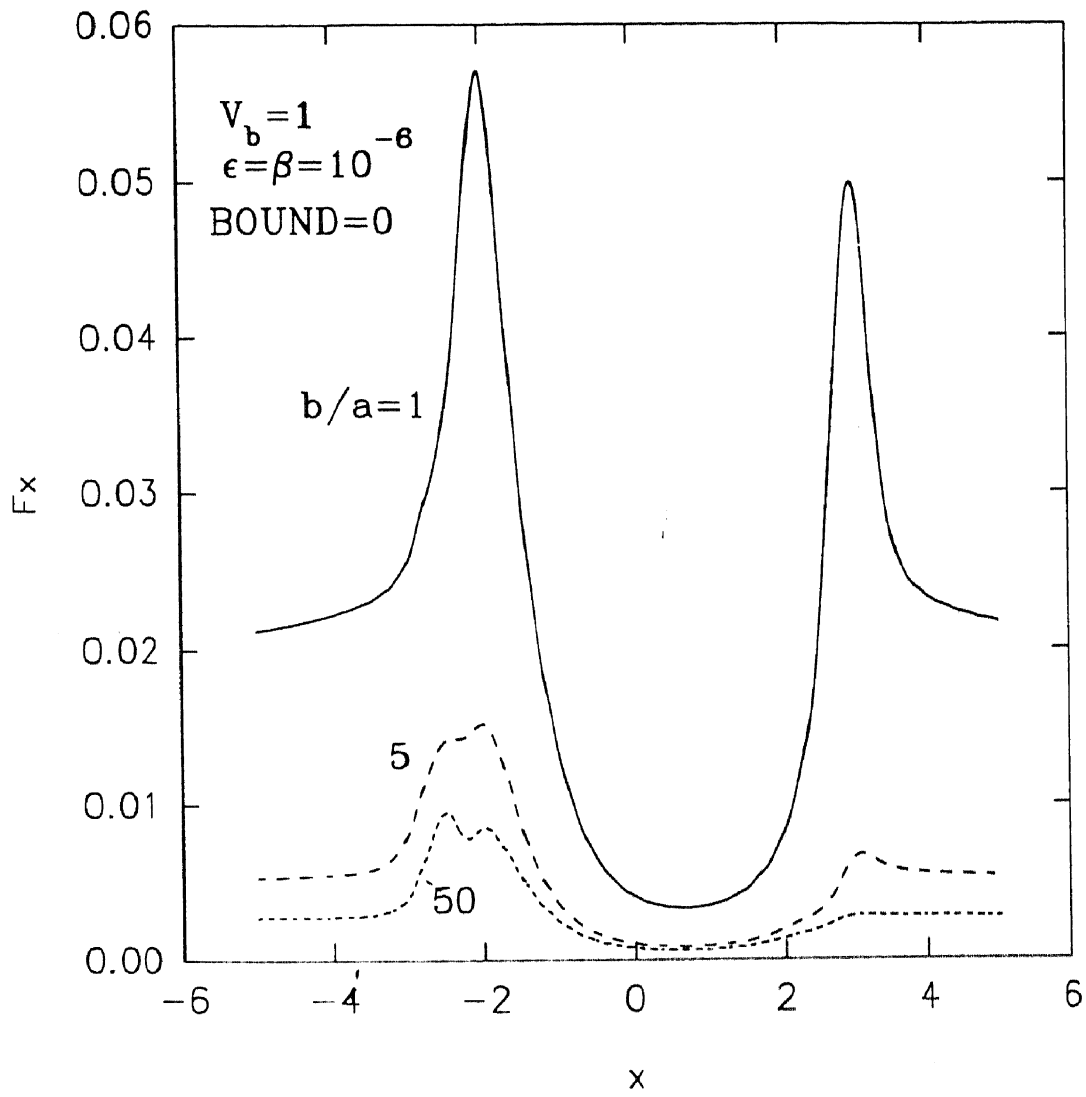


Figure 5.3: Emergent line flux F_x versus x at $V_b = 1$; $\epsilon = \beta = 10^{-6}$; $b/a = 1$ (plane-parallel atmosphere), 5, 50 and $T = 10^3$.

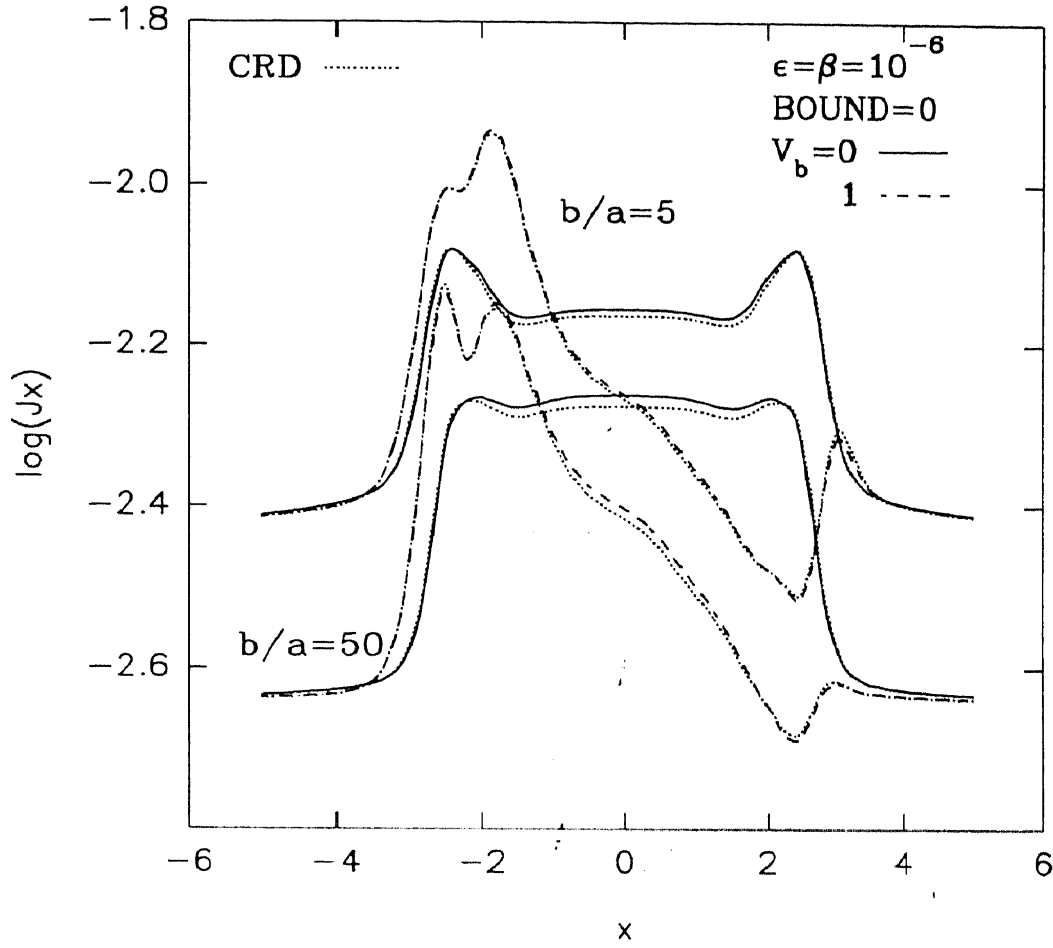


Figure 5.4: Emergent mean intensity profiles J_x versus x for a spherically symmetric envelope having extension $b/a = 50$; expansion velocity $V_b = 0$ (static case) and 1; and $\epsilon = \beta = 10^{-2}$.

In figure 5.3 emergent flux profiles are shown for a differentially expanding ($V_b = 1$) envelope at different values of extension. Emergent line flux from a plane-parallel ($b/a = 1$) atmosphere is considerably higher than from spherically symmetric extended ($b/a = 5, 10$) atmospheres. Again, the known result is recovered that higher the extension, lower is the emergent line flux.

In figure 5.4 a comparison is made between the emergent mean intensity (J_x) profiles due to CRD and R_{III} for a static ($V_b = 0$) and differentially expanding ($V_b = 1$) spherically symmetric envelope having extension $b/a = 50$ and $\epsilon = \beta = 10^{-2}$. Although, the differences between CRD and R_{III} profiles are slightly more than what they were in fig. 2 where a lower value of $\epsilon = \beta = 10^{-6}$ was used, still, the differences are within 5%, again, much lower than those reported for planar geometries by Finn [16] and Vardavas [71, 72].

Figure 5.5 shows the effects of ϵ and β on emergent flux (F_x) profiles due to R_{III} for a static and differentially expanding spherically symmetric and extended envelope. It is found that the profiles have deeper absorption depths and more asymmetry at lower value of ϵ and β . The

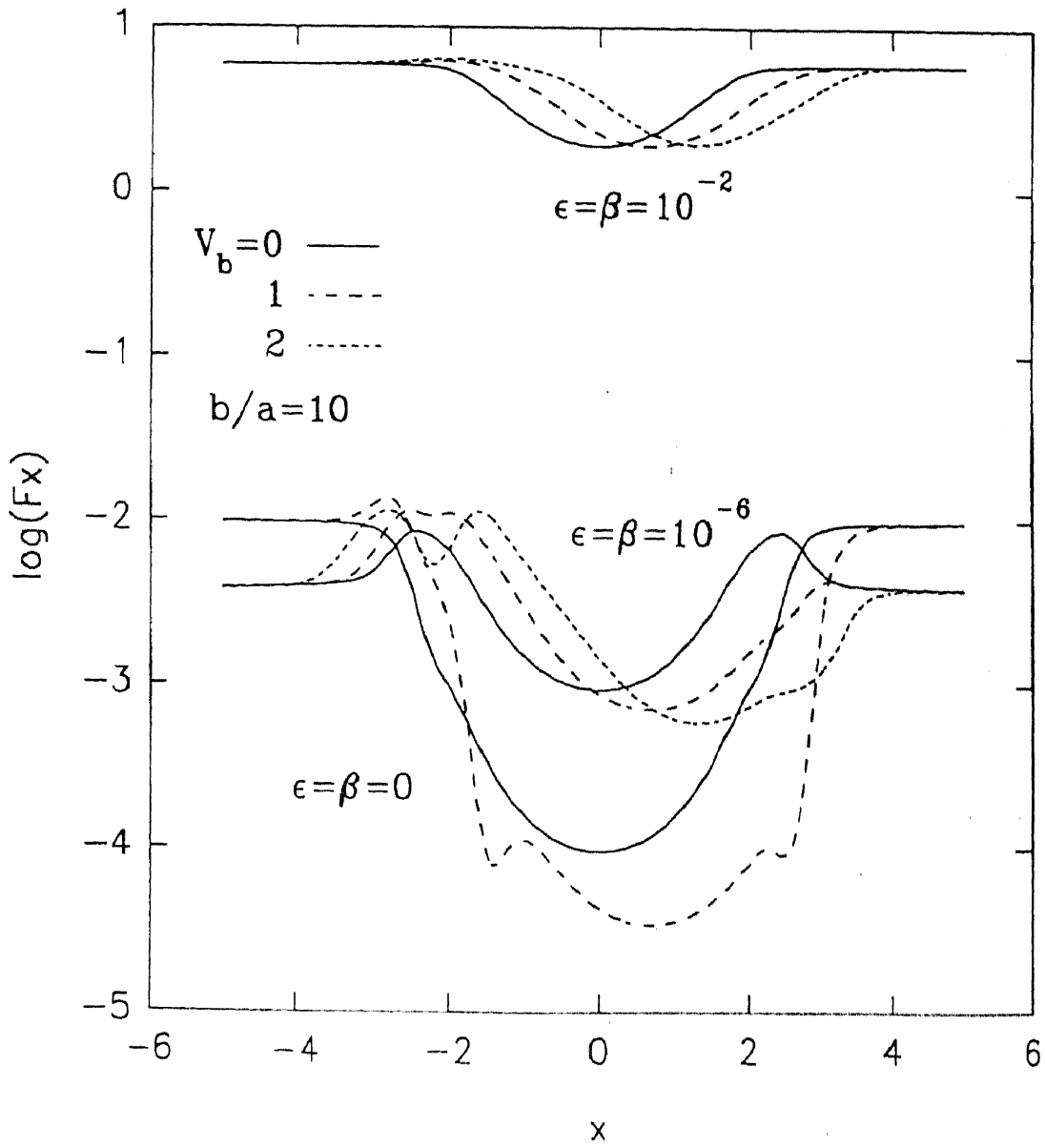


Figure 5.5: $\text{Log}(F_x)$ versus x for $b/a = 10$, at $V_b = 0, 1, 2$ for different values of $\epsilon = \beta = 0, 10^{-6}, 10^{-2}$.

same is also true for CRD as shown by Kunasz and Hummer [36].

5.4 Conclusion

The differences between the emergent mean intensity profiles due to complete redistribution and angle-averaged R_{III} are found to be much smaller in spherically symmetric and differentially expanding stellar atmospheres than those reported for plane-parallel (static and moving) atmospheres.

Chapter 6

Partial frequency redistribution effects on observed resonance lines using model atmospheres of cool stars

6.1 Introduction

After considering the parameterized atmospheres of cool stars in the previous chapters, this chapter employs realistic computed model atmospheres of late type giants and supergiants to study PRD effects on some of the observed spectral lines. The spectral lines chosen for this study are the three strong resonance lines Si II $\lambda 1818$, C II $\lambda 1335$ and Ba II $\lambda 4554$. Out of these, the first two spectral lines have been observed in the cool supergiant star α -Orionis, spectral type M2 Ia-Ib, with very high resolution from the Hubble Space Telescope (see Carpenter et al. [12]) using the Goddard High Resolution Spectrograph (GHRS). The observed high resolution profiles of Ba II $\lambda 4554$ have been presented by Sanner [63]. The *motivation* behind this study is that *PRD effects are expected to become important in the extended tenuous atmospheres of cool giants and supergiants*. This is an interesting study of astrophysical relevance because it shows the model dependence of the differences between the results due to PRD and CRD in observed spectral lines. The knowledge of these departures could be useful to the modellers of stellar atmospheres and for quantitative analysis of the stellar spectra.

As mentioned in the review of the related work (section 1.4), several researchers have made attempts, with varying degree of success, to model the chromospheres of late-type stars based on the matching of observed and computed PRD profiles. Most of these works have neglected velocity fields and atmospheric extension. In the present study both the atmospheric extension of the chromospheres and velocity fields have been taken into account. This study aims at highlighting the differences between the solutions of PRD and CRD and the dependence of these differences on the adopted model atmospheres.

6.2 Adopted model atmospheres

In this study two kinds of model atmospheres of cool giants and supergiants have been adopted :

- atmospheres without chromospheres; and
- atmospheres with chromospheres.

The atmospheres without chromospheres have been taken from Plez [58]; and to study PRD effects in atmospheres with chromospheres, the extended chromospheric model of α -Orionis (M2 Ia-Ib) given by Hartmann and Avrett [22] has been adopted.

The model atmospheres without chromospheres are the spherical opacity sampling models for M-giants and supergiants (Plez [58]) covering the range $3000 \text{ K} \leq T_{eff} \leq 4000 \text{ K}$, $-0.5 \leq \log(g) \leq 1.5$ for 1, 2 and 5 M_{\odot} . These assume hydrostatic equilibrium, spherical symmetry, LTE and homogeneity. Out of these given models, the models having the following parameters have been adopted in this study:

1. $T_{eff} = 4000 \text{ K}$; $\log g = 0$; $M/M_{\odot} = 1.0$; $R/R_{\odot} = 166.0$; and $\log L = 3.804$.
(T_{eff} , g , M , R and L are the effective temperature, surface gravity, mass, radius and luminosity, respectively).
2. $T_{eff} = 3000 \text{ K}$; $\log g = 0$; $M/M_{\odot} = 1.0$; $R/R_{\odot} = 166.0$; and $\log L = 3.304$.

The run of the gas pressure P_g , the electron pressure P_e and the temperature T for the first model has been plotted in figure 6.1, and the same parameters for the second model have been plotted in figure 6.2. Hereafter we will call them as *model1* and *model2*. These parameters have been plotted against the variable n which is the depth point counter in the atmosphere. $n = 1$ refers to the outer most boundary and $n = 25$ refers to the innermost boundary of the atmosphere.

The main difference in the two adopted models is that *model1* is cooler ($T_{eff} = 3000 \text{ K}$), than the *model2* ($T_{eff} = 4000 \text{ K}$). This choice has been made to study the effect of different temperature structure on the differences between the CRD and PRD results. *Model1* and *model2* *do not* have chromospheric temperature structure.

The third model atmosphere, hereafter *model3*, chosen for this study is the extended *chromospheric model* of the supergiant star α -Orionis (popularly known as *Betelgeuse*, spectral type M2 Ia-Ib, given by Hartmann & Avrett [22]. This model has been constructed by a desire to explain cool winds observed from a wide variety of giants. The authors have used a schematic wave-driven wind theory to compute the density, temperature and velocity structure of the wind. The run of the hydrogen number density $n_H \text{ cm}^{-3}$, the electron number density $n_e \text{ cm}^{-3}$ and the temperature T have been plotted versus $z = r/R_*$ in figure 6.3. $z = 30$ refers to the

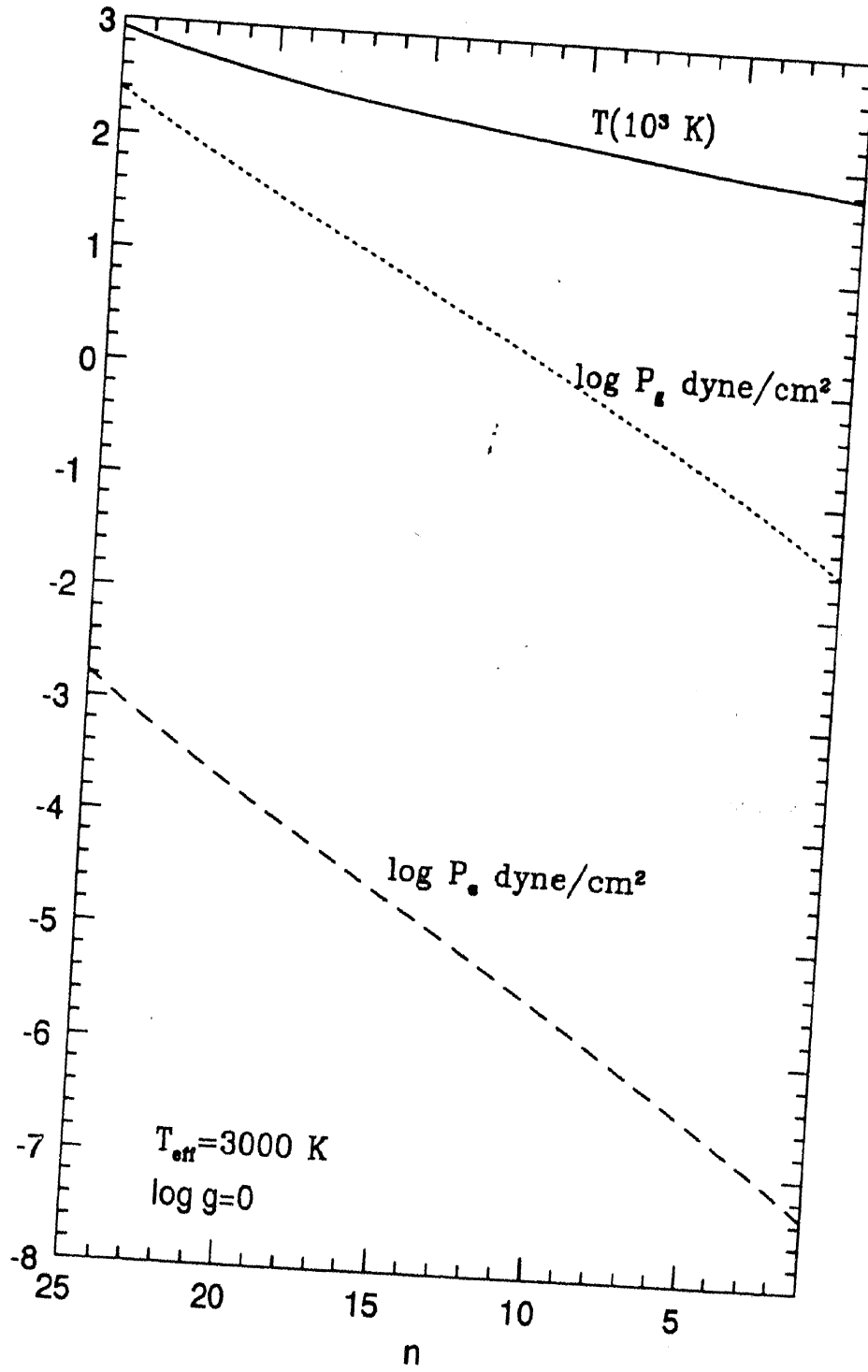


Figure 6.1: Model1: Variation of the gas pressure P_g , the electron pressure P_e and the temperature T inside the adopted model atmosphere (Plez (1992)).

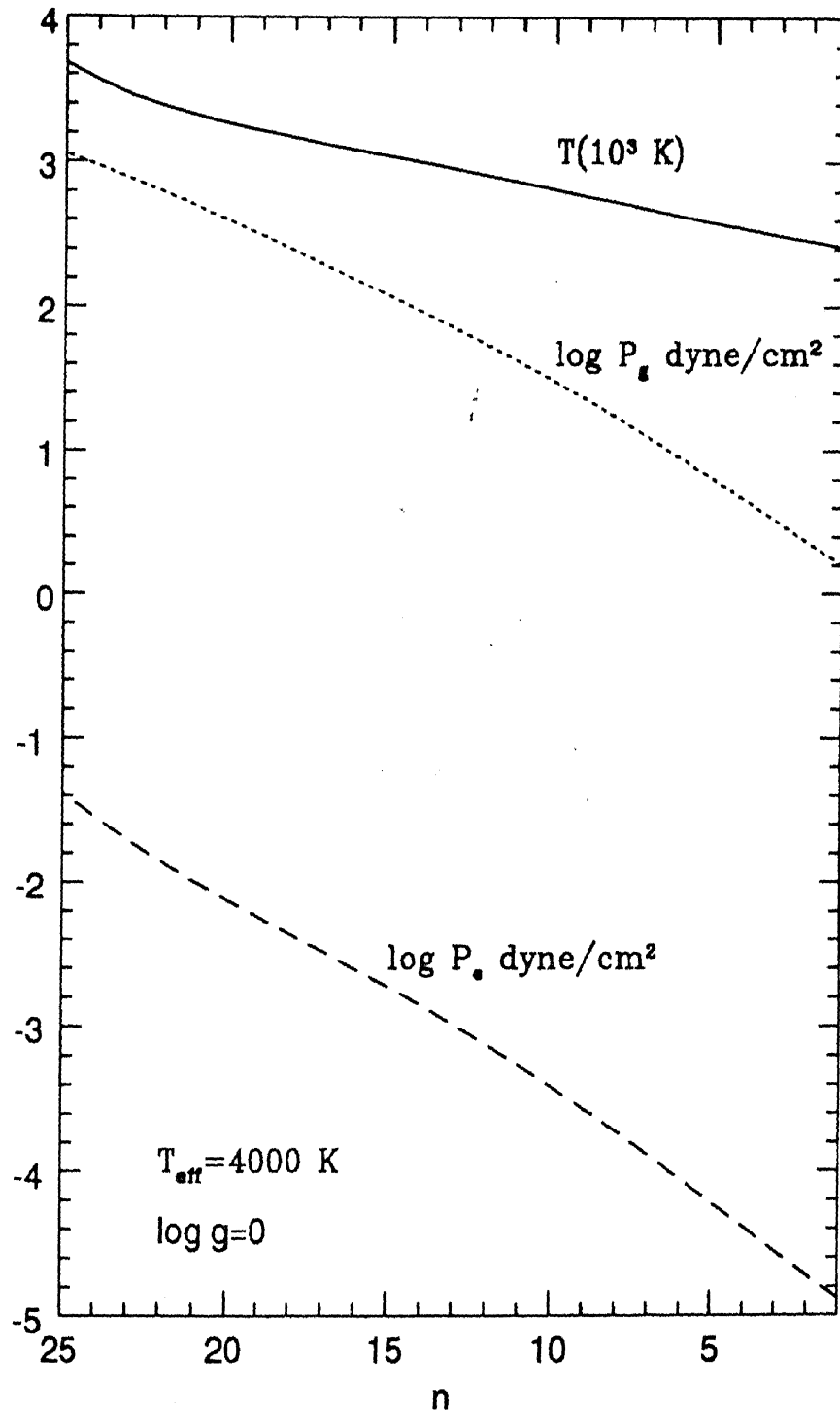


Figure 6.2: Model2: Variation of the gas pressure P_g , the electron pressure P_e and the temperature T inside the adopted model atmosphere (Plez (1992)).

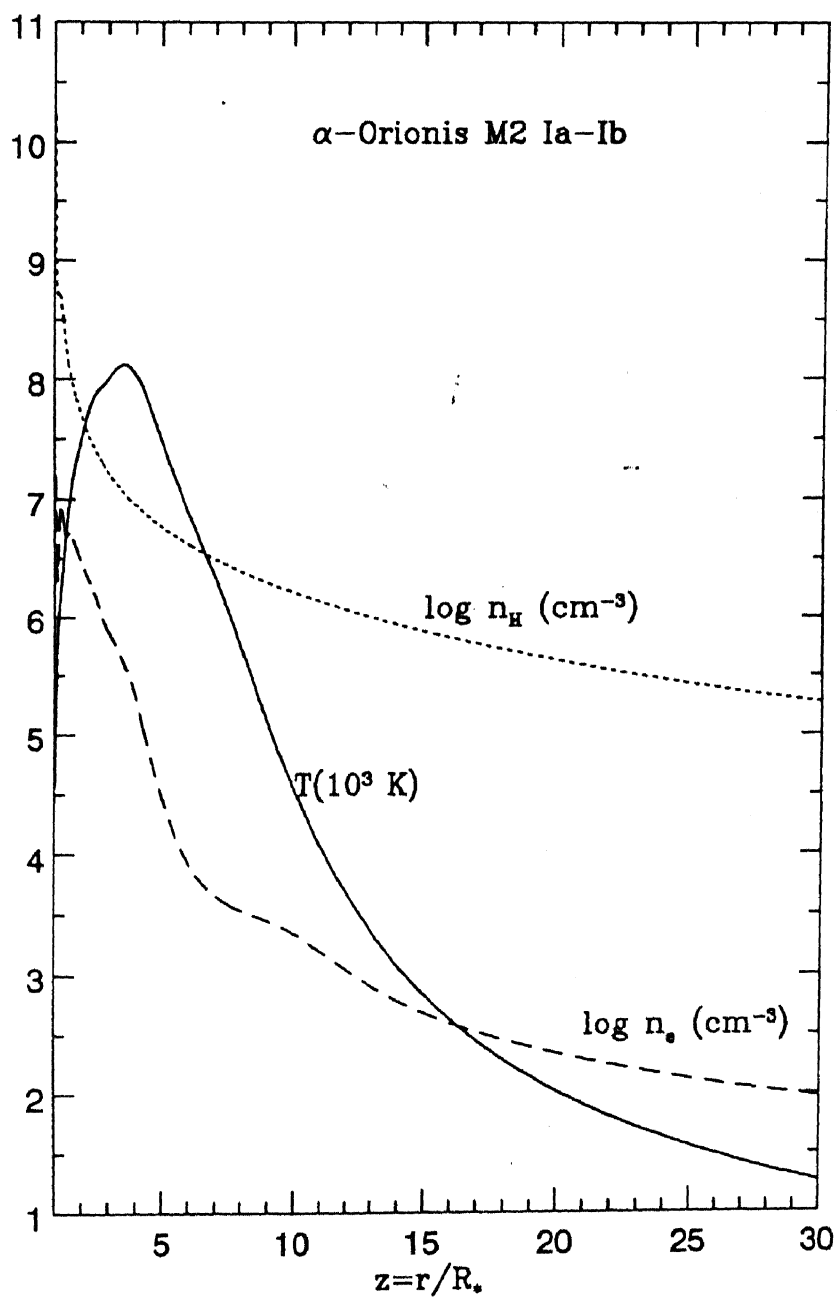


Figure 6.3: Model3: Chromospheric model of α -Orionis (Hartmann & Avrett (1984)).

point 30 stellar radii away from $z = 1$. In this model stellar radius, $R_* = 1350 R_\odot$ and stellar mass, $M_* = 10 M_\odot$.

In order to compute the emergent flux profiles using the above model atmospheres, one requires to solve the equation of line transfer; and to solve the transfer equation one needs to compute the *thermalization parameter* ϵ and the *line center optical depth* τ_0 , at all the radial points r inside the atmosphere. In the next three sections, it is explained that how one proceeds to achieve that.

6.3 Calculation of thermalization parameter ϵ

The thermalization parameter ϵ is defined as the probability per scattering that a photon will be destroyed by collisional de-excitation. As seen in earlier chapters, the line source function has two terms, the first term with coefficient $(1 - \epsilon)$ is the *noncoherent scattering* term, (see equation 3.7), followed by a *thermal source* term ϵB_ν . The line source function will depart from being a Planckian (B_ν) if $\epsilon \neq 1$. In such cases the assumption of local thermodynamic equilibrium (LTE) does not hold. In virtually all situations of astrophysical interest, $\epsilon \ll 1$ in regions of line formation. Only very close to the photosphere, one finds that $\epsilon \rightarrow 1$, and only in such regions the condition of LTE prevails. Thus, when $\epsilon \ll 1$, the noncoherent scattering dominates the line source function, and the partial frequency redistribution (PRD) effects should be important. The expression to calculate the thermalization parameter at radial point r is written as

$$\epsilon(r) = \frac{C_{21}(r)}{C_{21}(r) + A_{21}[1 - \exp\left[\frac{-h\nu_0}{kT(r)}\right]]^{-1}} \quad (6.1)$$

where C_{21} is the rate of collisional de-excitation from level 2 to 1 at each radial point r , A_{21} is Einstein's spontaneous emission probability for transition $2 \rightarrow 1$, h is the Planck's constant, ν_0 is the line center frequency, k is the Boltzmann's constant and $T(r)$ is the temperature at radius r . In this study, $C_{21}(r)$ and $T(r)$ are depth dependent. $T(r)$ at each depth is taken from the respective model, and $C_{21}(r)$ is computed from the following expression given by Van Regemorter [70]

$$C_{21}(r) = 20.60 \lambda_{cm}^3 N_e(r) \sqrt{T_e(r)} P\left(\frac{\Delta E}{kT(r)}\right) \quad (6.2)$$

where $N_e(r)$ is the electron number density (cgs units) at radial point r , taken from the respective model at each depth point, ΔE is the energy of the transition and k is the Boltzmann's constant. The function $P(\frac{\Delta E}{kT(r)})$ is interpolated from table 2 of Van Regemorter [70].

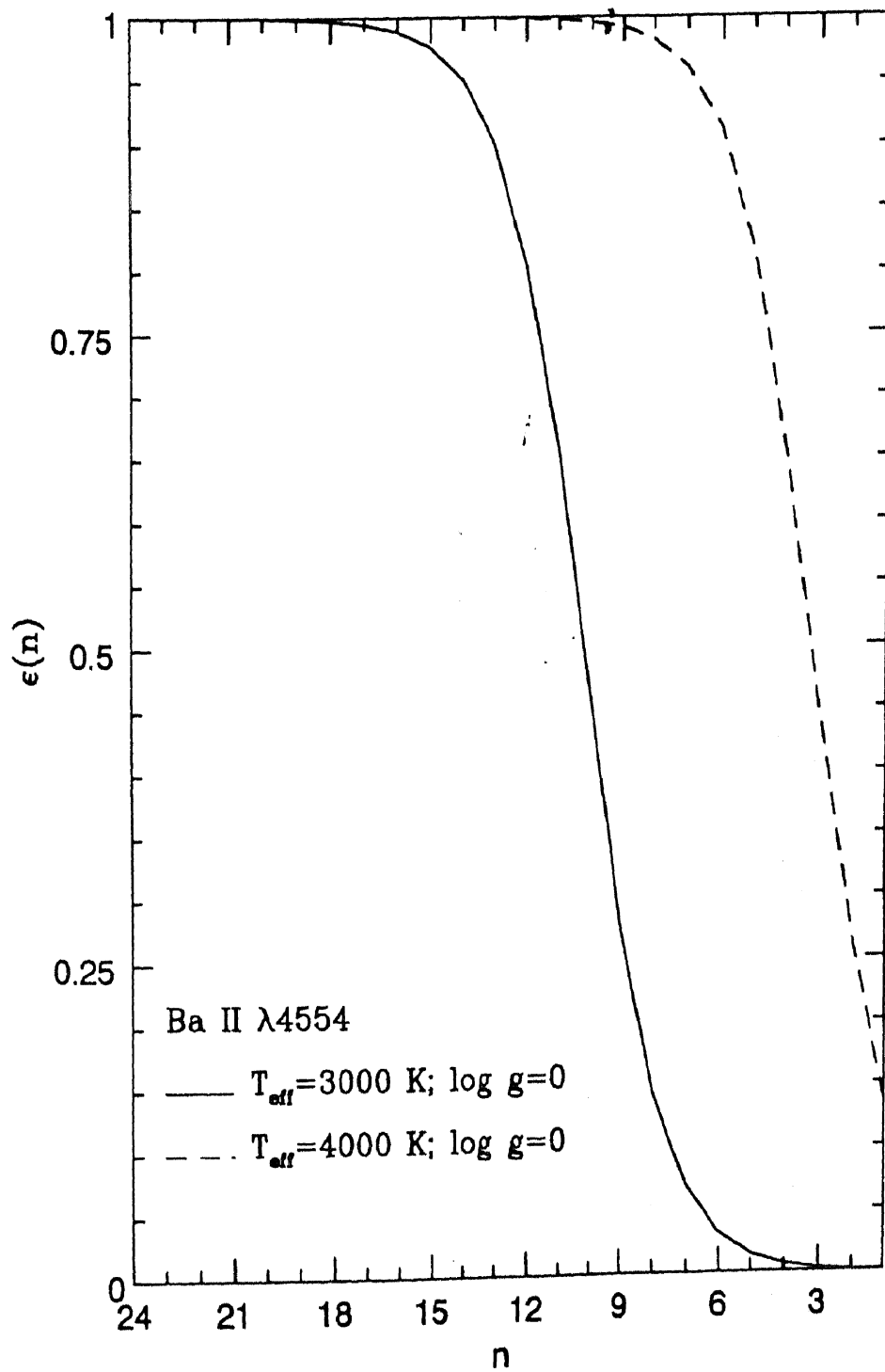


Figure 6.4: Variation of thermalization parameter ϵ versus depth point counter n for Ba II λ 4554, plotted for model1 ($T_{\text{eff}} = 3000 \text{ K}$) and for model2 ($T_{\text{eff}} = 4000 \text{ K}$).

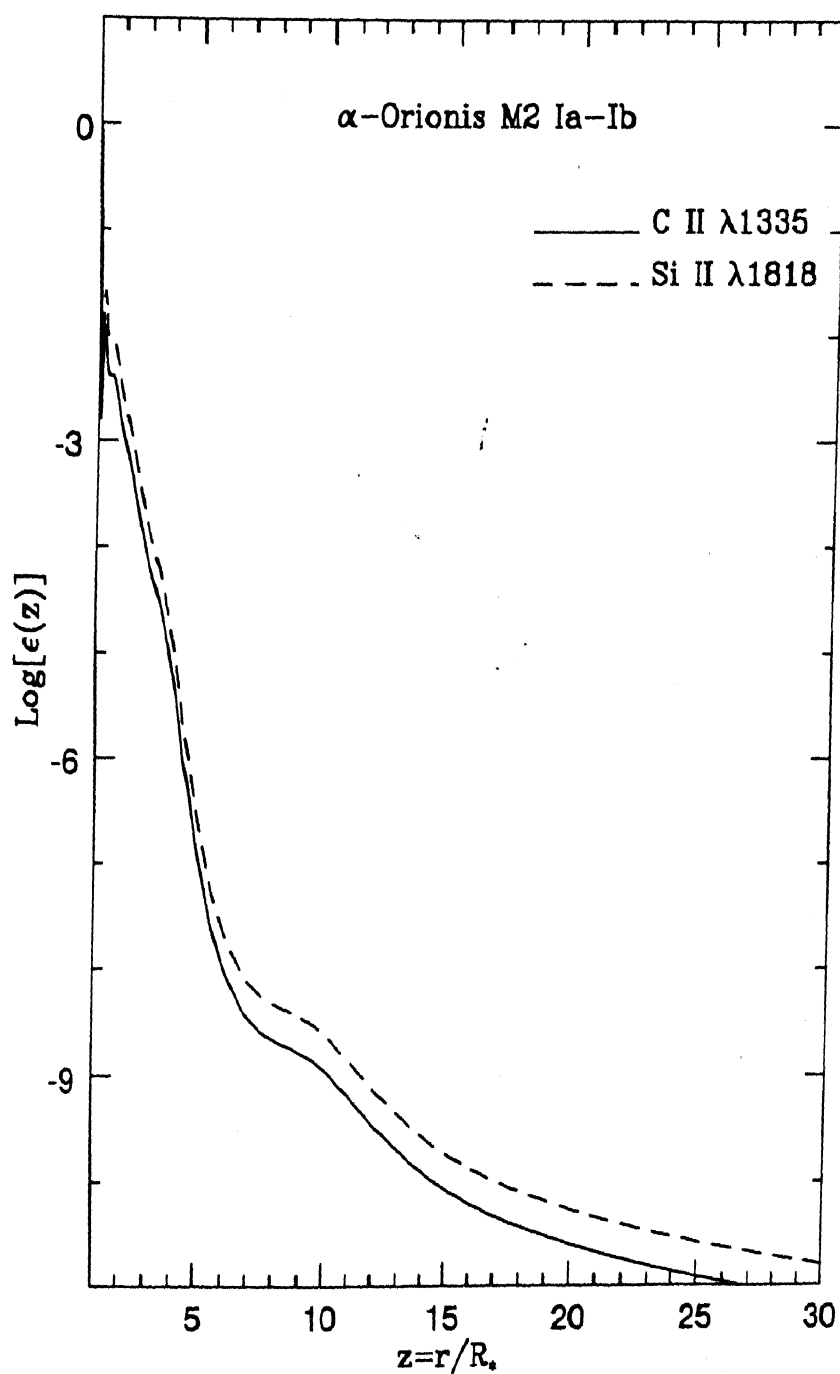


Figure 6.5: Variation of thermalization parameter ϵ versus the atmospheric extent z for C II $\lambda 1335$ and Si II $\lambda 1818$, plotted for model3 (α -Orionis).

Figure 6.4 shows the variation of thermalization parameter ϵ versus depth point counter n for Ba II λ 4554, plotted for model1 ($T_{eff} = 3000$ K) and for model2 ($T_{eff} = 4000$ K). It is seen that $\epsilon < .25 < 1$ in the outer layers of model1 and model2. In these regions the noncoherent scattering dominates the line source function..

Figure 6.5 shows the variation of thermalization parameter ϵ versus the atmospheric extent z for C II λ 1335 and Si II λ 1818, plotted for model3 (α -Orionis). From this plot it is clear that for $z > 1$, $\epsilon \ll 1$. This is the effect of the chromospheric temperature structure and the large extension of the atmosphere. For most of this atmosphere, the situation is highly non-LTE. In principle, as compared to model1 and model2, the effects of non-coherent scattering will be larger.

6.4 Calculation of line center optical depth τ_0

another important ingredient required for solving the line transfer equation is the line center optical depth τ_0 . The expression to compute the line center absorption coefficient at radial points r in the transition between levels i and j is written as

$$\chi_{\nu_0}(r) = \frac{\sqrt{\pi} e^2}{m_e c} \frac{N_i(r) f_{ij} (1 - e^{-[\frac{h\nu_0}{kT(r)}]})}{\Delta\nu_D(r)} \quad (6.3)$$

Consider a shell bounded by radii r and $r + \Delta r$. If we assume that χ_{ν_0} does not have a steep variation through this shell of thickness Δr , then $\tau_0(r)$ will be given as

$$\tau_0(r) = \chi_{\nu_0}(r) \times \Delta r \quad (6.4)$$

where

$$\begin{aligned} m_e &= 9.1094 \times 10^{-28} g \\ c &= 2.9979 \times 10^{10} cm/s \\ k &= 1.3807 \times 10^{-16} erg/deg(K) \end{aligned}$$

are the mass of an electron, speed of light in vacuum and the Boltzmann's constant respectively; N_i is the number density of absorbers in level n computed by solving the Saha's ionization equation and assuming solar abundances taken from Allen [1]; f_{ij} is the oscillator strength for the transition between i and j ; ν_0 is the line center frequency; $\Delta\nu_D(r)$ is the Doppler width, which is written as

$$\Delta\nu_D = \frac{\nu_0}{c} \sqrt{\frac{2kT(r)}{m_A}} \quad (6.5)$$

where m_A is the mass of the particular atom.

Using the expressions given above, the line center optical depth is calculated for Ba II λ 4554, C II λ 1335 and Si II λ 1818. To study PRD effects in non-chromospheric atmospheres given by model1 and model2, Ba II λ 4554 has been chosen. The line center optical depth structure through the atmosphere of model1 ($T_{eff} = 3000$ K) and model2 ($T_{eff} = 4000$ K) is plotted in figure 6.6. It is seen that τ_0 for model2 is higher than it is for model1. This is because of higher temperatures there are more number of singly ionized barium (Ba II) atoms in the atmosphere of model2.

Figure 6.7 shows the variation of line center optical depths C II λ 1335 & Si II λ 1818 versus the atmospheric extension z in the chromospheric atmosphere of α -Orionis (model3). It is seen that τ_0 of C II λ 1335 remains significantly above the unit optical depth and drops to $\tau_0 = 1$ at large extension $z \sim 20$. This structure will have a bearing on the emergent flux causing a deep absorption self-reversal. The τ_0 variation of Si II λ 1818 exhibits a plateau with $\tau_0 \approx 10$ at $z \approx 11$ slowly falling to a value of $\tau_0 \approx 1$ at $z \approx 18$.

6.5 The equation of line transfer

With the thermalization parameter ϵ and the line optical depth τ_0 computed, one goes ahead to solve the equation of line transfer. Since strong resonance line are chosen for this study, the partial frequency redistribution function $R_{II}(x', x)$ given by equation 3.8 and plotted in figure 3.1 of this thesis, is appropriate and has been used. This redistribution applies to an atom having radiation damping in the upper state and coherence in the atom's rest frame. The results due to $R_{II}(x', x)$ are compared with the results due to complete redistribution (CRD) approximation.

Here, x' and x are the frequency displacements from line centre, in units of standard Doppler width, of the incident and scattered photons respectively, seen in the *rest frame*. Then, the corresponding frequency displacements, seen in the *fluid frame* at radius r , are

$$X' = x' \pm V(r)\mu \quad (6.6)$$

$$X = x \pm V(r)\mu \quad (6.7)$$

where $\mu(\in [0, 1])$ is the cosine of the angle between the radius vector and the direction of propagation of the radiation, \pm stands for the oppositely directed beams of radiation, and $V(r)$ gives the macroscopic velocity at radius r .

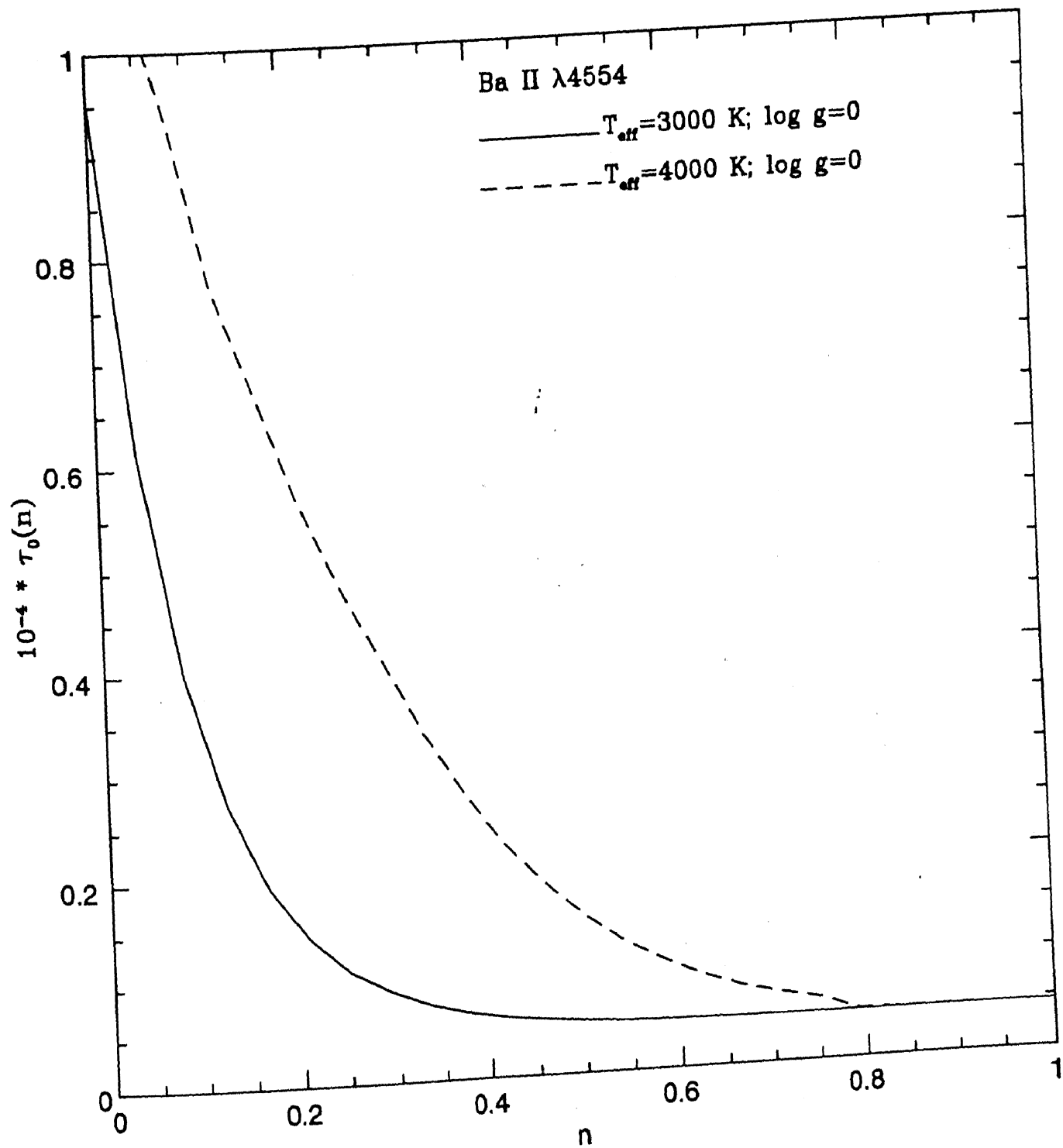


Figure 6.6: Variation of line center optical depth of Ba II $\lambda 4554$ versus the depth point counter n in the atmospheres of model1 ($T_{\text{eff}} = 3000 \text{ K}$) and model2 ($T_{\text{eff}} = 4000 \text{ K}$).

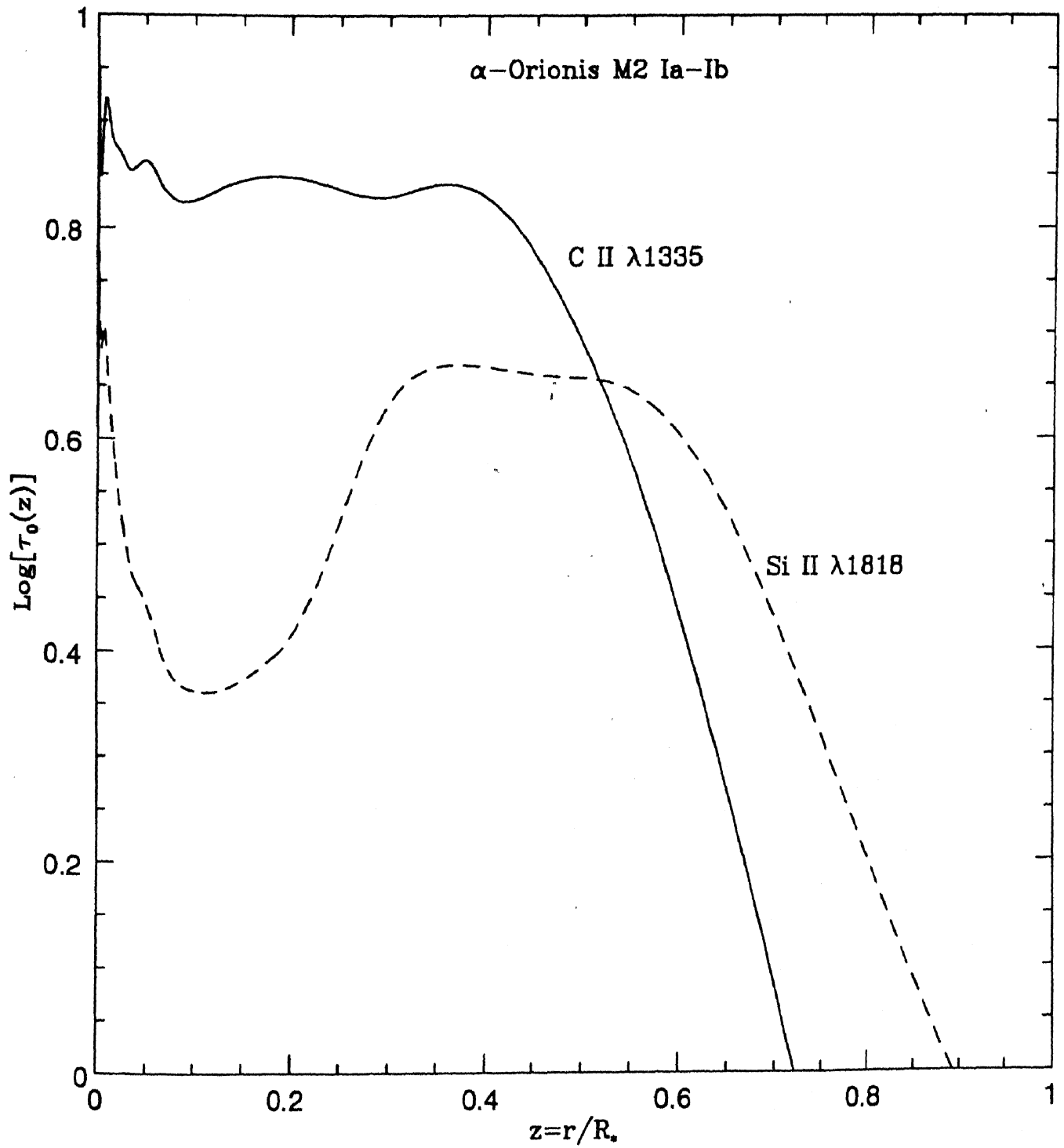


Figure 6.7: Variation of line center optical depths of C II λ 1335 & Si II λ 1818 versus the atmospheric extension z in the chromospheric atmosphere of α -Orionis (model3).

The equation of line transfer in spherical symmetry, rest frame and for a two-level atomic model is written as (Peraiah [52], Singh [65])

$$\pm\mu \frac{\partial I(x, \pm\mu, r)}{\partial r} \pm \frac{1-\mu^2}{r} \frac{\partial I(x, \pm\mu, r)}{\partial \mu} = K_l[\beta + \phi(x, \pm\mu, r)][S(x, \pm\mu, r) - I(x, \pm\mu, r)] \quad (6.8)$$

where \pm stands for the oppositely directed beams of radiation, $I(x, \pm\mu, r)$ represents specific intensity of the ray making an angle $\cos^{-1}\mu$ ($\mu \in [0, 1]$) with radius vector at the radial point r . $\phi(x, \pm\mu, r)$ represents the profile function, given as

$$\phi(x, \pm\mu, r) = \phi(X, r) = \int_{-\infty}^{+\infty} R_{II}(X', X) dX' \quad (6.9)$$

where angle-averaged partial frequency redistribution function $R_{II}(X', X)$ has the following form (Mihalas [38])

$$R_{II}(x', x) = \pi^{-3/2} \int_{\frac{|x'-x|}{2}}^{\infty} e^{-u^2} [\tan^{-1}(\frac{x+u}{a}) - \tan^{-1}(\frac{\bar{x}-u}{a})] du \quad (6.10)$$

where $\bar{x} = \max(|x|, |x'|)$ and $\underline{x} = \min(|x|, |x'|)$; a is the damping parameter.

R_{II} envisions an atom having a sharp lower level and a radiatively broadened upper level. The above expression has been derived assuming isotropic phase function. Figure 3.1 of this thesis gives the plot of the emission probability ($R_{II}(x', x)/\phi(x')$) at frequency x per absorption, when the absorption is at frequency x' . Damping parameter $a = 2.0 \times 10^{-3}$.

$S(x, \pm\mu, r)$ is the total (line plus continuum) source function which is written as

$$S(x, \pm\mu, r) = \frac{\phi(X, r)S_l(x, \pm\mu, r) + \beta S_c(r)}{\phi(X, r) + \beta} \quad (6.11)$$

where $\beta = K_c/K_l$ (continuum to line opacity, S_c is the continuum source function set equal to 1 in this computation. $S(x, \pm\mu, r)$ represents the line source function, which is given by the following expression

$$S_l(x, \pm\mu, r) = \frac{1}{2} \frac{1-\epsilon}{\phi(X, r)} \int_{-\infty}^{+\infty} dx' \int_{-1}^{+1} d\mu' R_{II}(X', X) I(x', \pm\mu, r) + \epsilon B(r) \quad (6.12)$$

where ϵ is the probability per scatter that a photon is destroyed by collisional de-excitation. The procedure to compute ϵ for the chosen resonance lines has been given above in section 5.3.

Under the assumption of complete redistribution, the line source function is written as

$$S_I(r) = \frac{1-\epsilon}{2} \int_{-\infty}^{+\infty} dx \int_{-1}^{+1} d\mu \phi(X, r) I(x, \pm\mu, r) + \epsilon B(r) \quad (6.13)$$

where $\phi(X, r)$ is taken to be a Voigt profile with damping parameter set equal to 10^{-3} .

The normalization condition for the profile function at each radial point is

$$\int_{-\infty}^{+\infty} dx \phi(X, r) = 1 \quad (6.14)$$

As explained in the previous chapters, in a differentially expanding medium, due to the presence of velocity gradients, one has to compute, at all radial points all the four redistribution functions appearing in the scattering integral (equation 5.12) viz

$$\begin{aligned} R_{II}(x' + V(r)\mu, x + V(r)\mu) \\ R_{II}(x' - V(r)\mu, x - V(r)\mu) \\ R_{II}(x' + V(r)\mu, x - V(r)\mu) \\ R_{II}(x' - V(r)\mu, x + V(r)\mu) \end{aligned}$$

in order to evaluate the diffuse radiation field (see chapter 2 & Peraiah [52, 55]).

In this work, a linear velocity law given in Peraiah [52] has been used, which gives a radially increasing velocity, with minimum velocity (V_a) at the innermost boundary and maximum velocity of expansion (V_b) at the outer boundary of the stellar envelope. For the model3, one could have computed the ratio of expansion velocity to the turbulent velocity from the values given in the table 2 of Plez [58]. It has not been done as the values of expansion velocities given are larger by a factor of two to three. As is known from the works of Bernat [11] Sanner [63] and several other authors, the ratio of expansion velocity to the turbulent velocity for cool giants and supergiants lies between 0.5 and 2.0. Therefore, in this study for all the models the value of this ratio has been chosen to be equal to 2.0 at the outermost layer and decreasing towards the bottom of the atmosphere according to the linear velocity law mentioned above. The envelope is divided into n shells, each of equal radial thickness, $n = 1$ defines the outermost shell and $n = N$ defines the innermost shell. The total number of shells have been chosen according to the number of depth points given in the respective model atmospheres adopted for this study. The line center optical depth is computed as explained in section 5.4. Following boundary condition has been used for the transfer equation

$$U_{n=1}^+(x, \mu) = 0 \quad \text{and} \quad U_{N+1}^-(x, \mu) = B_{\nu_0}(T(n=1)) \quad (6.15)$$

where

$$U_n^\pm(x, \tau, \mu) = 4\pi r_n^2 I(x, \mu, \tau(r_n)) \quad (6.16)$$

$I(x, \mu, \tau(r_n))$ being the specific intensity. $+$ specifies a ray directed towards the bottom of the envelope ($\tau = T$), and $-$ specifies a ray directed out of the envelope. $B_{\nu_0}(T(n=1))$ is the Planck function at line center frequency ν_0 and at temperature T at $n=1$.

To solve the line transfer equation the discrete space theory method described in chapter 2 of this thesis has been used.

6.6 Results

In this section, the emergent flux profiles due to partial frequency redistribution function $R_{II}(x', x)$ are presented in comparison to those due to the assumption of complete redistribution (CRD), in order to show the departures between the two.

First the results due to the formation of Ba II λ 4554 in non- chromospheric models, model1 and model2, are presented. Figure 6.8 shows the emergent flux profile of Ba II λ 4554 using model1 having $T_{eff} = 3000$ K. The profiles due to PRD (R_{II}) and CRD hardly differ from one another, except for negligible departure in the far wing on the red side.

Figure 6.9 shows the emergent flux profiles of Ba II λ 4554 using model2 having $T_{eff} = 4000$ K. We see $\approx 10\%$ differences between the profiles due to PRD and CRD. As compared to figure 6.8, the departures between PRD and CRD are more in this case because the star is hotter and that leads to more number of singly ionized Ba atoms.

Figure 6.9 shows the emergent flux profiles of Ba II λ 4554 using model2 having $T_{eff} = 4000$ K. We see $\approx 10\%$ differences between the profiles due to PRD and CRD. As compared to figure 6.8, the departures between PRD and CRD are more in this case because the star is hotter and that leads to more number of singly ionized Ba atoms. This can be seen from figure 6.6, where throughout the atmosphere, the line center optical depth of Ba II is more for the hotter star. Thus, for this line, hotter the star, more will be the differences, with the upper limit being decided by the ionization potential of barium.

Figure 6.10 shows the emergent flux profiles of Si II λ 1818 due to PRD and CRD in the chromospheric atmosphere of α -Orionis. These profile exhibit enormous difference in the wings between PRD and CRD profiles. This is a collisionally dominated line and exhibits the typical absorption self-reversal. One can clearly see how the assumption of CRD can lead to significantly different (and erroneous) results. The assymetry in peaks is due to the presence of velocity fields. One can also notice that, as expected in the line core, there are no differences between the results due to CRD and PRD.

Figure 6.11 shows the emergent flux profiles of C II λ 1335 from the chromospheric atmosphere of α -Orionis, due to PRD and CRD. One immediately notices the striking differences between

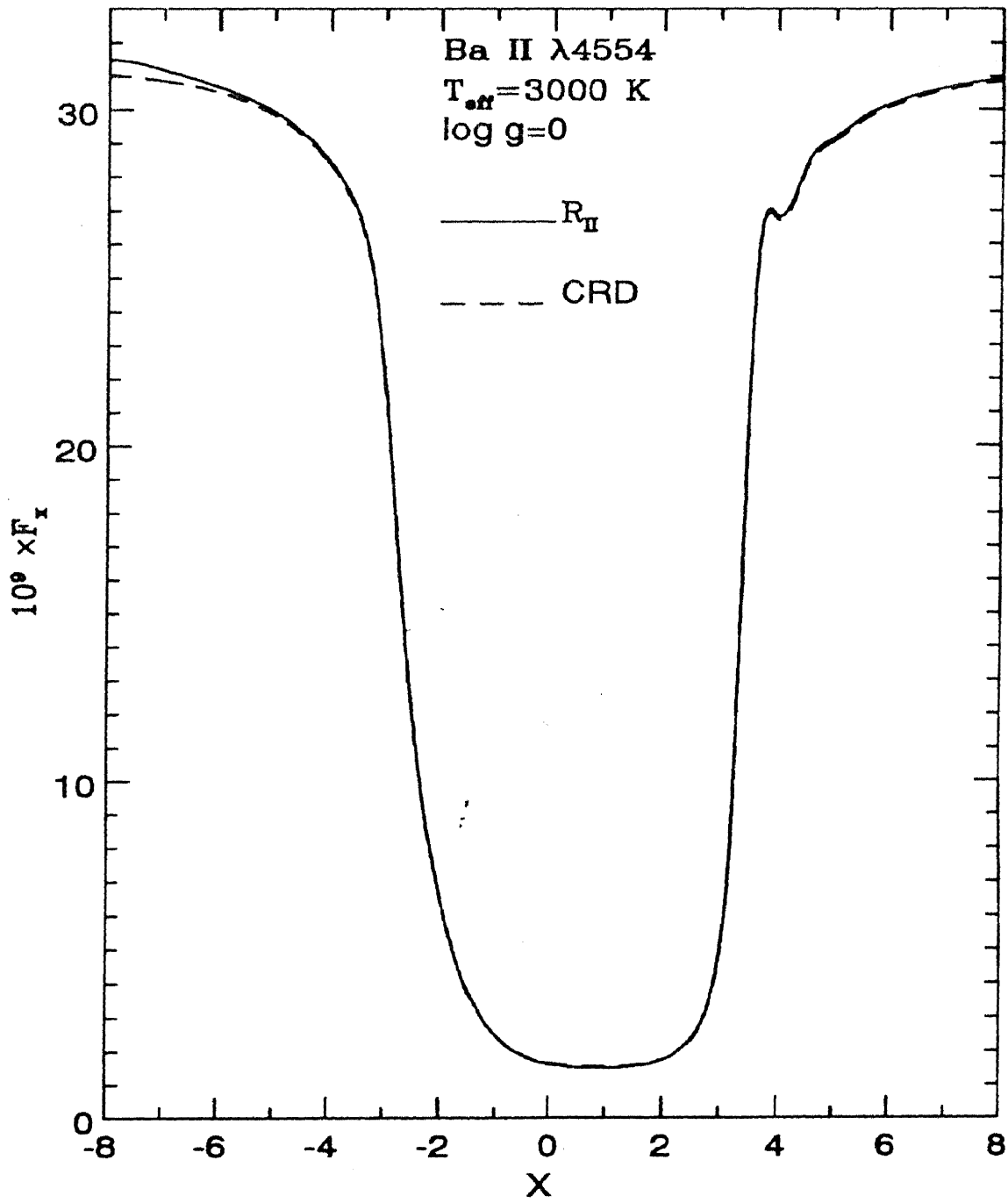


Figure 6.8: Emergent flux profiles of Ba II λ 4554 for model 1.

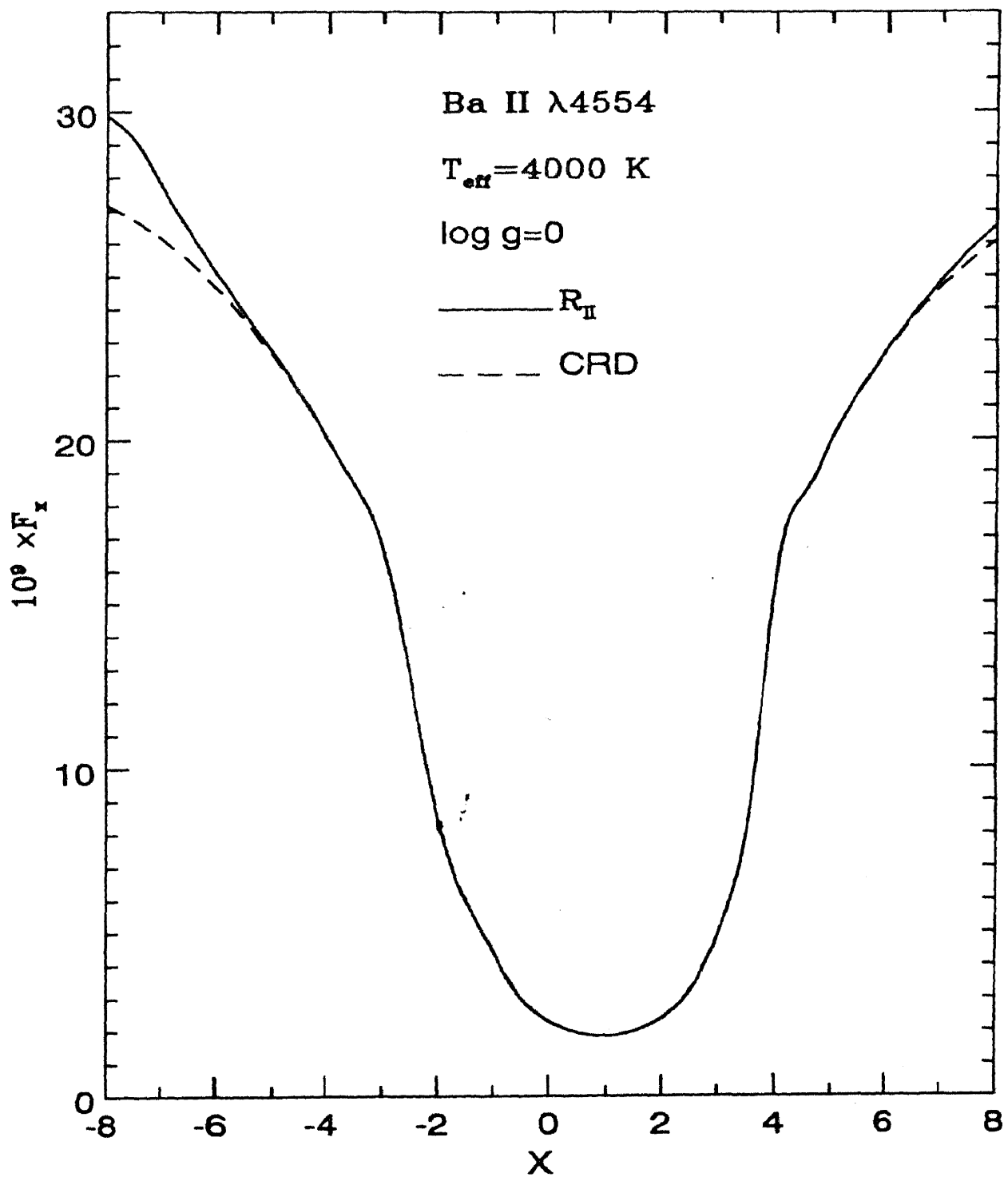


Figure 6.9: Emergent flux profiles of Ba II λ 4554 for model2.

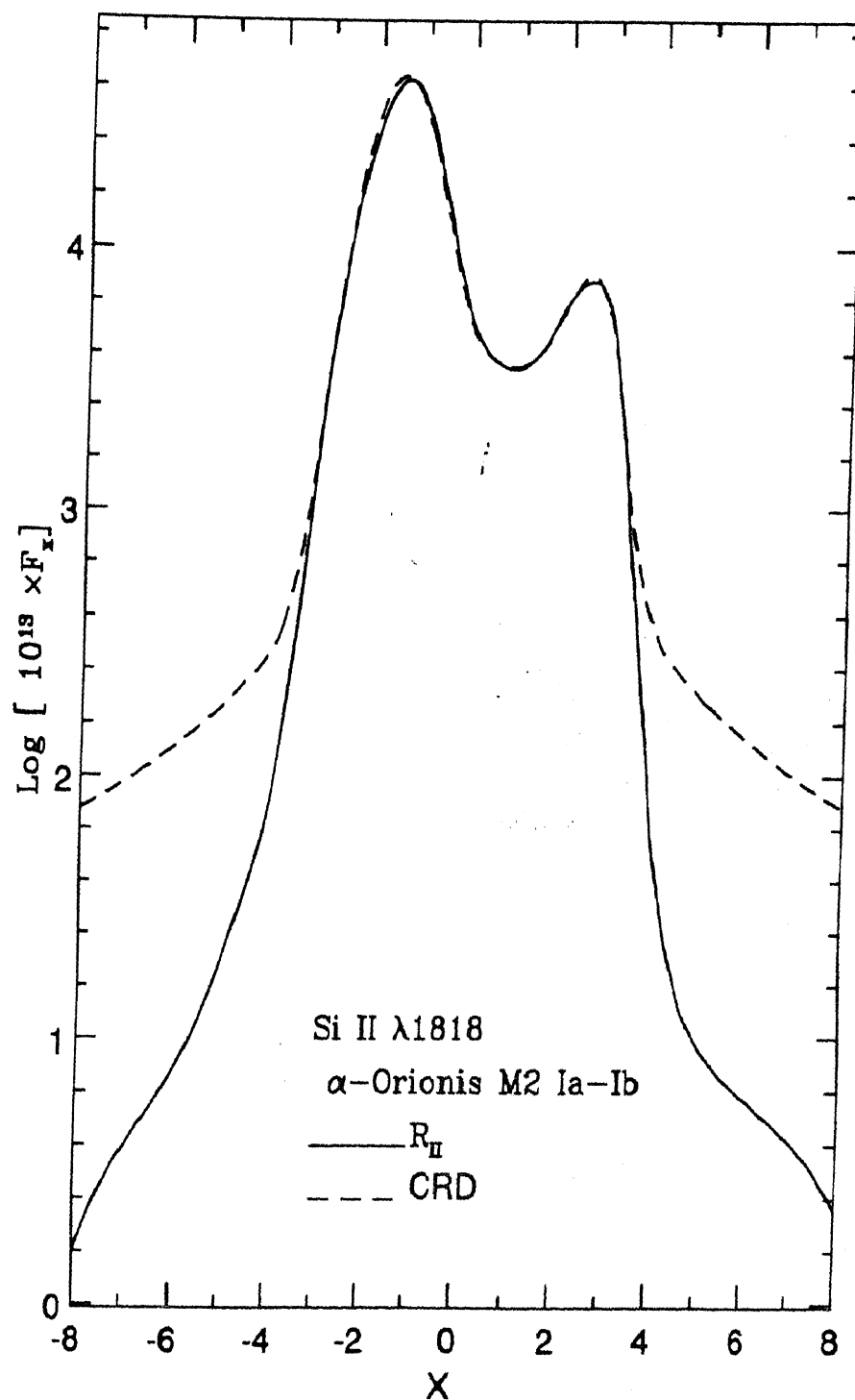


Figure 6.10: Emergent flux profile of Si II λ 1818 from the chromospheric atmosphere of α -Orionis, model3, due to PRD and CRD.

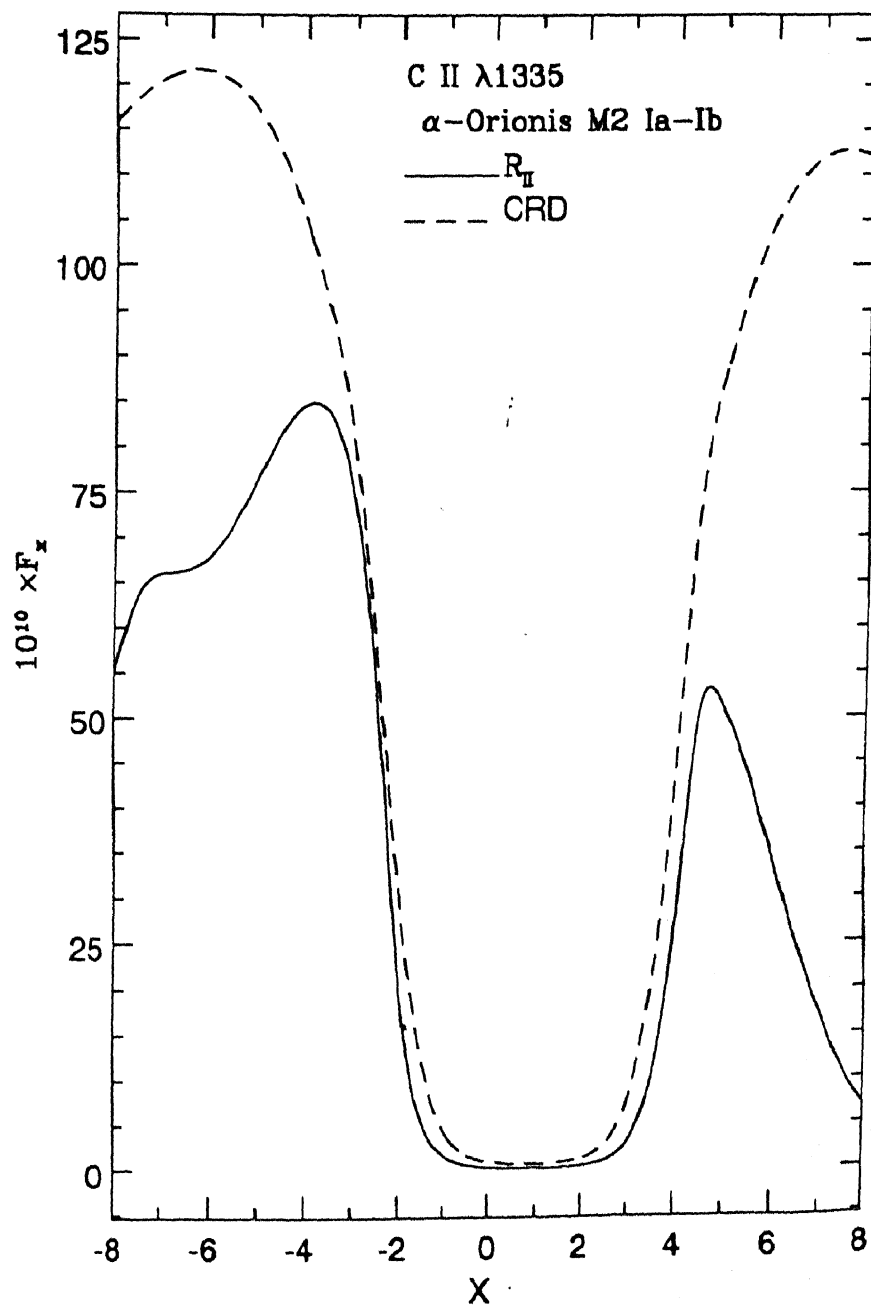


Figure 6.11: Emergent flux profile of C II $\lambda 1335$ from the chromospheric atmosphere of α -Orionis, model3, due to PRD and CRD.

the results due to PRD and CRD in the line wings. Also as compared to the Si II profiles, the absorption in the line core is much deeper. Again, one can see that how much lowering of the line profile in the wings of this strong resonance line takes place by employing partial frequency redistribution function R_{II} . This is because, this function is strongly coherent in the line wings. In the process of quantitative analysis of stellar spectra, these substantial differences between PRD and CRD can lead to incorrect temperature structure and hence incorrect estimates of the quantities dependent on temperature. It can be emphasized, on the basis of these results, that for line modeling and for computing synthetic spectra of chromospheric atmospheres of cool giants and supergiant stars, the assumption of complete redistribution should be relaxed.

6.7 Conclusion

The study of the differences between CRD and PRD emergent flux profile of strong resonance lines Ba II λ 4554, Si II λ 1818 and C II λ 1335, from the atmospheres of cool giant and supergiant stars has been presented. Atmospheres *with* chromospheres and *without* chromospheres have been considered. The differences between PRD and CRD are found to be highly model dependent. For *non-chromospheric* type atmospheres, the overall differences between the PRD and CRD profiles of Ba II λ 4554 are within 10% for the hotter star having $T_{eff} = 4000$ K, and negligible for cooler star having $T_{eff} = 3000$ K. For the *chromospheric* model of cool supergiant star α -Orionis (M2 Ia-Ib), there are substantial differences between the PRD and CRD results for Si II λ 1818 & C II λ 1335 emergent flux profiles. On the basis of these results, it is recommended that the assumption of CRD should be relaxed for quantitative analysis of spectra of cool giants/supergiants having chromospheres.

Chapter 7

Concluding Remarks

7.1 In retrospect

In the last six chapters we reported on the effects of partial frequency redistribution functions on the emergent flux profiles against the background of relevant literature. The availability of high resolution spectral data from satellites like the Hubble Space Telescope, EUV Explorer and many others is making this an important area of study for the accurate quantitative analysis of spectra. This thesis is presented as a modest contribution to the efforts in that direction.

Besides "true absorption", scattering of radiation is one of the important physical processes in the stellar atmospheres. In very extended and tenuous *atmospheres of cool giants and supergiant stars*, where the rates of collisions are low, scattering of photons is the dominating factor in transport of radiation. Early works on radiative transfer assumed that scattering is either strictly coherent or that the photons are completely redistributed over the line profile. Neither of these limits is achieved exactly in stellar atmospheres, and it becomes necessary to use partial frequency redistribution functions. Due to the difficulties in tackling the scattering integral employing exact partial frequency redistribution functions, the numerical solutions of the transfer equation had to wait till modern times with their effective computational tools. The progress of studies in this direction is now rapid with varying degrees of success. It is important to be aware of the departures of the emergent flux profiles due to partial frequency redistribution from those due to complete redistribution.

This thesis is an attempt to locate the various scenarios in the atmospheres of cool stars, where the effects of partial frequency redistribution functions R_{II} , R_{III} and R_V (as compared to CRD) could be important and to present these effects in a comparative manner using spherical geometry. The study using parameterized stellar atmospheres provides an insight into the role of single or combined effects of physical variables like the atmospheric extension, velocity fields and the thermalization parameter. The study involving realistic model atmospheres and

observed strong resonance lines is an important step further in investigating the role of partial frequency redistribution functions on spectral line formation in cool giants and supergiants.

The present work

The assumption of complete redistribution is expected to fail in extended stellar atmospheres where low gravities and hence low collision rates prevail. In this thesis, with a clear objective of bringing out the departures between the solutions due to PRD and CRD in various situations in the atmospheres of cool giants and supergiants, the understanding has been developed in stages, starting with spherically symmetric static atmospheres, then including the velocity fields and finally considering realistic temperature and density structures to explore PRD effects in observed resonance lines. This systematic approach has resulted in considerable success in generating useful information and enhancing the understanding of the PRD effects on spectral line formation in cool giant and supergiant stars.

- Chapter one explains the need to investigate this problem and presents the layout of the thesis.
- Chapter two, describes the solution of equation of radiative transfer in the frame-work of the discrete space theory of radiative transfer using Peraiah-Grant formalism.
- In chapter three, the effects of angle-averaged R_V and R_{II} on emergent flux profiles in static spherically symmetric stellar envelopes have been examined. The equation of transfer for spherical symmetry in the rest frame is solved for a two-level atom. Initially, to bring out the effects of geometrical extension alone, velocity fields have been neglected. A constant value of the thermalization parameter has been assumed and the Planck's function is set equal to unity throughout the atmosphere. The background continuum is neglected. This study establishes that sphericity enhances PRD effects. It has also shown that the effect of spherical extension is much more on the emergent flux profiles resulting from R_{II} than on those resulting from R_V when the damping parameters of the lower and upper levels of an atom are comparable. The effect of R_V (as compared to CRD) on emergent flux profiles increases by making the lower level sharper than the upper level. This effect is further enhanced by increasing the spherical extension.
- In chapter four, a step further is taken to include velocity of expansion in order to explore the *combined* effects of sphericity and expansion on the emergent flux profiles resulting from R_{II} and R_V , as compared to CRD. An atmosphere having geometrical extension and small velocity of expansion is considered which is characteristic of the atmospheres of cool giants and supergiants. It is assumed that there is no background continuum; Planck's function is set equal to unity and a constant value of the thermalization parameter is chosen at all depths in the atmosphere. This study shows that there are substantial differences between the emergent flux profiles resulting from PRD (R_{II} and R_V) and CRD.

- In chapter five, the PRD effects of R_{III} alone on the emergent line profiles in an expanding spherically symmetric stellar atmosphere are explored. This is because, the limiting case of complete redistribution is usually taken to be an adequate representation of R_{III} in radiative transfer problems to study the spectral line formation in stellar atmospheres. However, the combined effect of sphericity and macroscopic velocity cannot be estimated a priori. Only low velocity regime is considered which is appropriate for the *atmospheres of cool giants and supergiants*. This problem is treated in the rest frame formalism. In this work it is established that the differences between the emergent mean intensity profiles resulting from CRD and R_{III} are much smaller in expanding spherically symmetric stellar atmospheres than reported previously for plane-parallel atmospheres.
- Chapter six presents the study of the differences between CRD and PRD emergent flux profile of strong resonance lines Ba II λ 4554, Si II λ 1818 and C II λ 1335, from the atmospheres of cool giant and supergiant stars. Atmospheres *with* chromospheres and *without* chromospheres have been considered. The differences between PRD and CRD are found to be highly model dependent. In non-chromospheric type atmospheres, the overall differences between the PRD and CRD profiles of Ba II λ 4554 are within 10% for the hotter star having $T_{eff} = 4000$ K, and negligible for cooler star having $T_{eff} = 3000$ K. There are found to be substantial differences between the PRD and CRD results for Si II λ 1818 & C II λ 1335 profiles computed using the chromospheric model of cool supergiant star α -Orionis (M2 Ia-Ib). On the basis of these results, it is recommended that the assumption of CRD should be relaxed for quantitative analysis of spectra of cool giants/supergiants having chromospheres.

...and its limitations

Although the foregoing achievement is significant, still we must look at the limitations of the currently achieved success, particularly with a view to plan future line of action. In the present phase of work, we were eager to explore the frequency redistribution effects on the spectral line formation in the atmospheres of cool giants and supergiants. Even within the scope of employing exact forms of the redistribution functions R_{II} , R_{III} and R_V , small velocity fields, atmospheric extension, use of computed model atmospheres to examine PRD effects on observed resonance lines of Ba II λ 4554, Si II λ 1818 and C II λ 1335, we restricted ourselves in many directions. For instance, we considered only angle-averaged redistribution functions in this study. By doing so, we accounted fully for the frequency redistribution effects but sacrificed information on angular effects, which could be important when the radiation field is anisotropic. We assumed a two-level atomic model for all cases of study. Thus we neglected extra channels of excitation or decay. But since only strong resonance lines are considered, we could afford to neglect this aspect. We did not take up the modeling of these observed lines, but aimed at highlighting the differences between the PRD and CRD results using realistic model atmospheres. We did not adopt the velocity structure given by the model atmospheres, but employed a linearly increasing velocity field. The value of this velocity field matches the

values derived from the observational data. Considering the uncertainties in the model values, it is justified to employ the velocity structure used in this study.

7.2 In prospect

Further possibilities for exploring the partial frequency redistribution effects on spectral line formation are many and most of them can be handled by the techniques developed and employed in the present work. Some of these are listed as follows:

1. The radiation field in the tenuous atmospheres can be anisotropic where the angular effects on the emergent profiles could be significant. This would require the use of *angle-dependent* partial frequency redistribution functions.
2. Keeping in mind the availability of very high resolution spectroscopic data for stellar atmospheres the assumption of an isolated line may fail. One has to consider the use of multilevel radiative transfer employing angle-dependent redistribution functions derived for multilevel atoms.
3. Modeling of chromospheric lines must relax the assumption of complete redistribution, and exact angle-dependent forms of redistribution functions should be employed. Attention needs to be devoted to the study of the combined effects of partial frequency redistribution, velocity fields and the geometry along with other physical phenomena.

Some of these questions have been partially resolved, but much work remains to be done before a completely satisfactory understanding of spectral line formation in the presence of partial redistribution effects is achieved.

A journey of thousand miles begins with a single step.

— Chinese proverb

Bibliography

- [1] Allen, C., 1973, *Astrophysical Quantities*, 3rd ed. London: Athlone Press.
- [2] Ambartsumian, V.A., 1943, Dokl. Akad. Nauk., SSR, 38, 229.
- [3] Avrett, E.H., Johnson, H.R., 1984, in *Cool Stars, Stellar Systems and the Sun*, ed. S.L. Baliunas, L. Hartmann (Berlin: Springer-Verlag), p.330.
- [4] Ayres, T.R., 1979, *Astrophys. J.*, 228, 509.
- [5] Ayres, T.R. , 1984, preprint.
- [6] Ayres, T.R., Linsky, J.L., Shine, R.A., *Astrophys. J. Lett.*, 195, L121.
- [7] Ayres, T.R., Linsky, J.L., 1975, *Astrophys. J.*, 200, 660.
- [8] Baliunas, S.L., Avrett, E.H., Hartmann, L., Dupree, A.K., 1979, *Astrophys. Letts.*, 233, L129.
- [9] Basri, G.S. , *Ph.D. Thesis*, Uni. of Colorado at Boulder, 1979.
- [10] Basri, G.S., Linsky, J.L., Eriksson, K., 1981, *Astrophys. J.*, 251, 162.
- [11] Bernat, Andrew P., 1977, *Astrophys. J.*, 213, 756.
- [12] Carpenter, Kenneth G., Robinson, Richard G., Wahlgren, M., Linsky, Jeffrey L., Brown, Alexander, 1994, *Astrophys. J.*, 428, 329.
- [13] Chandrasekhar, S., 1950, *Radiative Transfer*, Oxford.
- [14] Drake, S.A., in *Progress in Stellar Spectral Line Formation Theory*, 1985, ed. J.E. Beckman, L. Crivellari, D. reidel Publishing Company, p351.
- [15] Eriksson, K., Linsky, J.L., Simon, T., 1983, *Astrophys. J.*, 272, 665.
- [16] Finn, G.D. , 1967, *Astrophys. J.*, 147, 1085.
- [17] Grant, I.P., 1963, *MNRAS*, 125, 417.
- [18] Grant, I.P., Hunt, G.E., *MNRAS*, 141, 27.
- [19] Grant, I.P., Hunt, G.E., *Proc. Roy. Soc. Lond.*, A 313, 183.
- [20] Grant, I.P., Hunt, G.E., *Proc. Roy. Soc. Lond.*, A 313, 199.
- [21] Grant, I.P., Peraiah, A., 1972, *MNRAS*, 160, 239.
- [22] Hartmann, L., Avrett, E.H., 1984, *Astrophys. J.*, 284, 238.
- [23] Heinzel, P. , 1981, *JQSRT*, 25, 483.

- [24] Heinzel, P. , Hubeny, I. , 1982, JQSRT, 27, 1.
- [25] Heinzel, P. , Hubeny, I. , 1983, JQSRT, 30, 77.
- [26] Hempe, K. , 1984, in *Progress in Stellar Spectral Line Formation Theory*, ed. Beckman, John E. and Crivellari, L., NATO ASI Series.
- [27] Henyey, L.G. , 1941, Proc. Nat. Acad. Sci., 26, 50.
- [28] Holstein, T., 1947, Phys. Rev., 72, 1212.
- [29] Hubeny, I., Heinzel, P. , 1984, J.quant.Spectrosc.radiat.Transfer, 32, 159.
- [30] Hulst, Van-de, 1965, A new look at multiple scattering, NASA Institute for Space Studies, New York.
- [31] Hummer, D.G. , 1962, MNRAS, 125, 21.
- [32] Hummer, D.G. , 1969, MNRAS, 145, 95.
- [33] Jefferies, J.T., White, O.R., 1960, Astrophys. J., 132, 767.
- [34] Kelch, W.L., Linsky, J.L., Basri, G.S., Chiu, H.-Y. Chang, S.H., Maran, S.P., Furenlid, I., 1978, Astrophys. J., 220, 962.
- [35] Kneer, F., 1975, Astrophys. J., 200, 367.
- [36] Kunasz, P.B. , Hummer, D.G. , 1974, MNRAS, 166, 19.
- [37] Matta, F. , Reichel, A. , 1971, Math.Comput., 25, 339.
- [38] Mihalas, D. , 1978, *Stellar Atmospheres*, 2nd Edn., W.H. Freeman, San Fransisco.
- [39] Milkey, R.W., Ayres, T.R., Shine, R.A., 1975, Astrophys. J., 197, 143.
- [40] Milkey, R.W. , Mihalas, D. , 1973a, Astrophys. J., 175, 185.
- [41] Milkey, R.W. , Mihalas, D. , 1973b, Solar Phys., 32, 709.
- [42] Milkey, R.W. , Mihalas, D. , 1974, Astrophys. J., 192, 361.
- [43] Milkey, R.W., Shine, R.A., Mihalas, D., Astrophys. J., 1979, 202, 250.
- [44] Mohan Rao, D., Rangarajan, K.E., 1993, Astron. Astrophys., 274, 993.
- [45] Mohan Rao, D. , Rangarajan, K.E. , Peraiah, A. , 1984, J. Astrophys. Astr., 5, 169.
- [46] Nagendra, K.N., Rangarajan, K.E., Mohan Rao, D., 1993, MNRAS, 262, 855.
- [47] Nagendra, K.N., 1994, Astrophys. J., 432, 274.
- [48] Nagendra, K.N., 1995, MNRAS, 274, 523.
- [49] Omont, A., Smith, E.W., Cooper, J., 1972, Astrophys. J, 175, 185.
- [50] Peraiah, A., 1975, Astron. Astrophys., 40, 75.
- [51] Peraiah, A. , 1978a, Astrophys. Sp. Sc., 58, 189.
- [52] Peraiah, A. , 1978b, Kodiakanal Obs. Bull. Ser. A, 2, 115.
- [53] Peraiah, A., 1978c, Astrophys. & Space Sc., 58, 189.
- [54] Peraiah, A., Wehrse, R., 1978d, Astron. Astrophys., 70, 213.
- [55] Peraiah, A. , 1979, Kodiakanal Obs. Bull. Ser. A, 2, 203.

- [56] Peraiah, A. , 1984, in *Numerical Methods in Radiative Transfer*, ed. W. Kalkofen, (Cambridge: Cambridge Univ. Press).
- [57] Peraiah, A., Grant, I.P., 1973, *J. Inst. Math. Applc.*, 12, 75.
- [58] Plez, B., 1994, *Astron. Astrophys. Suppl. Ser.* 94, 527.
- [59] Preisendorfer, R.W., 1965, *Radiative Transfer on Discrete Spaces*, Sections 24, 25 & 47.
- [60] Rangarajan, K.E. , Mohan Rao, D. , Peraiah, A. , 1990, *Astron. Astrophys.*, 235, 305.
- [61] Redheffer, R.M., 1962, *J. Math. Phys.*, 41, 1.
- [62] Roussel-Dupré, D., 1983, *Astrophys. J.*, 272, 723.
- [63] Sanner, F. , 1976, *Astrophys Suppl. Ser.*, 32, 115.
- [64] Shine, R.A., Milkey, R.W., Mihalas, D., 1975, *Astrophys. J.*, 199, 724.
- [65] Singh, P. , 1994, *MNRAS*, 269, 441.
- [66] Singh, P. , 1994, *Submitted to MNRAS*.
- [67] Sobolev, V.V., 1955, *Vestn. Leningr. Univ.*, No. 5, 85.
- [68] Stokes, Sir George, 1862, *Proc. Roy. Soc.*, 11, 545.
- [69] Unno, W., 1952, *Publ. Astron. Soc. Japan.*, 4, 100.
- [70] Van Regemorter, H., 1962, *Astrophys. J.*, 136, 906.
- [71] Vardavas, I.M. , 1976 a, *JQSRT*, 16, 1.
- [72] Vardavas, I.M. , 1976 b, *JQSRT*, 16, 715.
- [73] Vardavas, I.M. , 1976 c, *JQSRT*, 16, 781.
- [74] Vernazza, J.E., 1972, *Ph. D. Thesis*, Harvard University.
- [75] Vernazza, J.E., Avrett, E.H., Loeser, R., 1973, *Astrophys. J.*, 184, 605.
- [76] Warwick, J.W., 1955, *Astrophys. J.*, 121, 190.

Publications from this work :

- Prabhjot Singh, 1994, *em A radiative transfer calculation using R_{III} in an expanding spherically symmetric stellar atmosphere*, *MNRAS*, 269,441-446.
- Prabhjot Singh, 1994, *Non-coherent subordinate line scattering in static spherically symmetric stellar atmospheres*, Presented at the XVI Meeting of the ASI.
- Prabhjot Singh, 1995, *A radiative transfer calculation using R_V and R_{II} in a static spherically symmetric stellar atmosphere*, Submitted to *MNRAS*.

Notes